Study on Structure and Properties of Organic Substance with the Nanomatrix Structure

Lina Fukuhara

2015

A Table of Contents

Chapter 1

General Introduction

Electron microscopy is widely recognized to be a powerful technique to observe morphology of the organic materials, which is related to mechanical properties of the materials. For instance, nanomatrix structure, discovered for natural rubber, is hypothesized to play an important role in viscoelastic properties of the rubber. In order to elucidate the relationship between the morphology and the properties, more exactly, it is necessary to develop a sophisticated technique to observe the morphology of the materials, which possess complicated nano-structure.

In the present study, 3D imaging techniques, newly developed[1-5], were applied to precise observations of the nano-structure in order to investigate the relationship between the morphology and the properties. For instance, the nanomatrix structure was carefully observed by electron tomography technique[6] and focused ion beam - scanning electron microscopy (FIB-SEM)[6,7]. The procedure to form the continuous nanomatrix and discontinuous nanomatrix was also investigated: that is, the removal of proteins from natural rubber, graft-copolymerization of vinyl monomer onto natural rubber and sulfonation of the grafted natural rubber.

1.1 3D observation of the morphology

Transmission electron microscopy (TEM) has been applied to the observation of the morphology of organic materials as a long standing powerful technique. Recently, however, a serious problem on the TEM observation was suggested on the basis of computer simulation and observation of the phase separated structure of a block-copolymer through electron tomography technique[1]. The electron beam transmitted throughout an ultra-thin section made an apparent 2D image, which was different from a real object, because of a thickness of the section[8,9]. In order to obtain the real image of the phase separated structure, therefore, it is necessary to perform the 3D observation for the nanomatrix structure. Furthermore, attention must be paid in a diameter of the dispersoid of the nanomatrix structure, which is about a micro-meter in diameter. Since the thickness of the ultra-thin

section is less than several hundred nm, the 3D image is not obtained for the nanomatrix structure as long as electron tomography observation is performed; that is, the electron tomography image is similar to the 2D TEM image. To observe the nanomatrix structure in a range of nano- and micro-metric scales, thus, one may apply not only electron tomography but also dual beam electron microscopy, i.e. field-emission scanning electron microscopy equipped with focused ion beam, FIB-SEM[1,10,11]. Using these techniques, a relationship between the 3D structure and properties may be investigated for the nanomatrix structured material.

There are preliminary observations of the nanomatrix structure through FIB-SEM and electron tomography techniques. Figure 1-1 shows the FIB-SEM image of the nanomatrix structure, after alignment of the observed images of surfaces of DPNR-*graft*-PS. At this low magnification, the bright domains appear well connected to each other in all directions. The natural rubber particles are dispersed in the nanomatrix of polystyrene. Figure 1-2 shows the electron tomography image. The natural rubber particles of various dimensions were randomly dispersed in the polystyrene matrix, reflecting a broad distribution of the particle dimension, i.e. 50 nm - 3 μm in volume mean particle diameter[12].

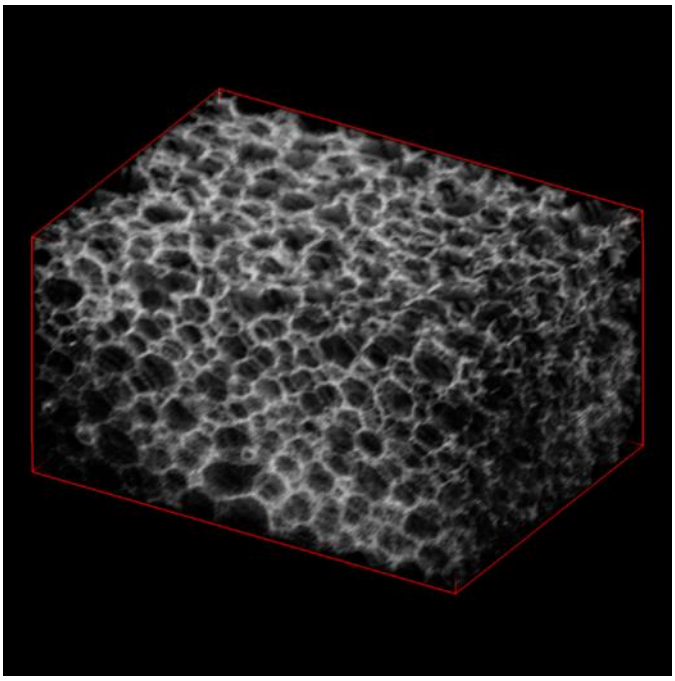

Figure 1-1 FIB-SEM image of DPNR-*graft*-PS with the nanomatrix structure before annealing.

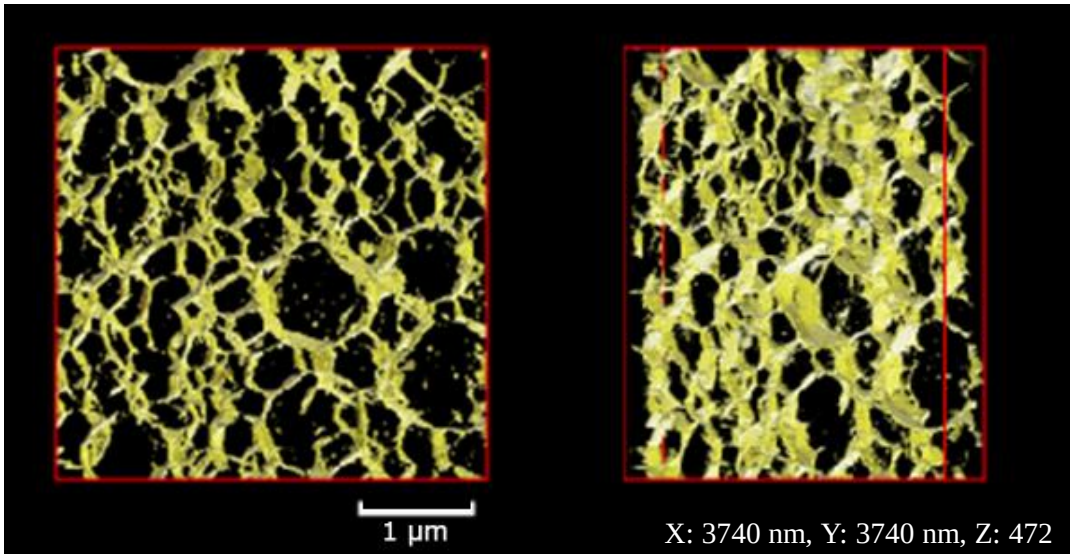

Figure 1-2 3D TEM images for DPNR-*graft*-PS. The film was stained with RuO_4. Transparent domains represent natural rubber and light yellow domains represent polystyrene.

Based on the preliminary observations, it is obvious that the FIB-SEM and electron tomography technique is indispensable for precise observations of the nanomatrix structure.

1.2 Nanomatrix structure

Organic material with the nanomatrix structure[13] may have unique properties, since the structure consists of dispersoid of major component and the matrix of minor component[6]. It is distinguished from ordinary soft materials with the island-matrix structure[14], which consists of dispersoid of minor component and matrix of major component. The properties of the organic material may, thus, be easily tuned by precise design of the nanomatrix structure[15], since the nanomatrix may change from continuous to discontinuous or *vice versa*. It is possible to achieve not only the dispersoid's properties but also the matrix's properties, based on the empirical rule that the major component and the matrix component govern the properties of the organic material[16]. Thus, the nanomatrix structure may possess a potential to bring about a breakthrough against dilemma fallen into by the ordinary organic materials, in which the properties of the dispersoid of minor component lie behind those of the matrix of major component. This may provide a solution of crucial problem that

the heterogeneous organic material with the island-matrix structure is unable to improve the properties in spite of change in the volume fraction of the components. Furthermore, the nanomatrix structure is useful to freeze the deformed structure in the non-equilibrium state, which may result in the anisotropic structure[6]. The properties of the organic material with the anisotropic structure may be expected to be different from those with the isotropic structure.

1.3 Formation of nanomatrix structure

The nanomatrix structure may be formed by covering particles with a nano-layer followed by coagulation of the resulting nano-layer-covered particles[17]. In this case, the particles are required to chemically link to the nano-layer, in order to stabilize the nanomatrix structure in equilibrium state. Especially, for the polymeric materials, the chemical linkages may be formed by graft-copolymerization of a monomer onto polymer-particles in latex stage[18], since the particles in the latex are dispersed in water. In this regard, natural rubber has attracted much attention, since natural rubber is isolated from *Hevea Brasiliensis* as the latex. However, natural rubber contains proteins on the surface of the rubber particle. It is, thus, important to remove the proteins from natural rubber latex, since the proteins trap radicals to inhibit the graft-copolymerization of vinyl monomer [19].

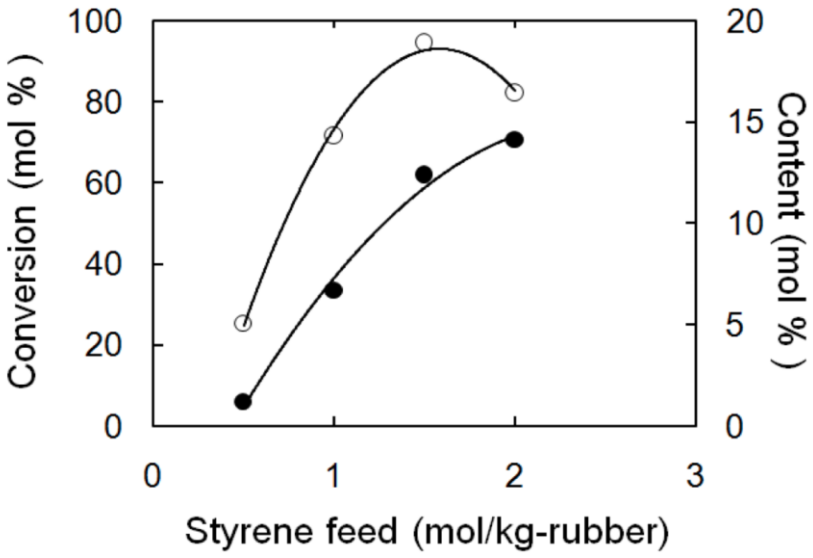

Figure 1-3 Conversion and content of styrene for DPNR-*graft*-PS.

In the previous works, the nanomatrix structure was formed by graft-copolymerization of styrene onto deproteinized natural rubber[17]. Figure 1-3 shows the conversion of styrene and content of styrene units. Both of the content and conversion were dependent upon the feed of styrene[18]; for instance, the higher the feed of styrene, the higher the content of styrene units. In contrast, a locus of convex curve was drawn for the conversion of styrene, in which a maximum appeared at 1.5 mol/kg-rubber styrene-feed.

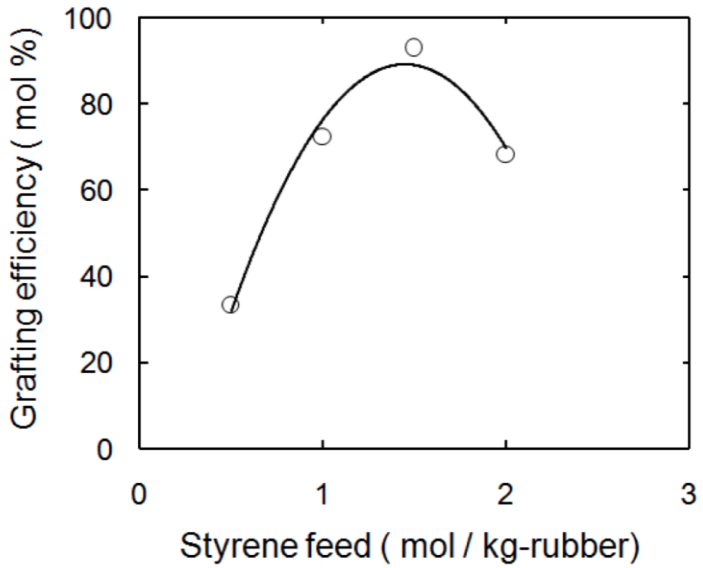

Figure 1-4 Grafting efficiency for DPNR-*graft*-PS.

Figure 1-4 shows grafting efficiency of styrene for DPNR-*graft*-PS. The grafting efficiency was significantly dependent upon the feed of styrene and it showed a maximum at 1.5 mol/kg-rubber feed of styrene, as in the case of the conversion of styrene. This may be explained to be due to deactivation and chain transfer of the radicals. At 1.5 mol/kg-rubber feed of styrene, almost all polystyrene, thus produced, was proved to link up to natural rubber as a grafting polymer.

1.4 Preliminary results on mechanical properties of natural rubber with nanomatrix structure

Figure 1-5 shows a plot of storage modulus in plateau region (plateau-modulus) *versus* frequency for natural rubber, the rubber with the nanomatrix structure (DPNR-*graft*-PS) and the rubber with the island-matrix structure[6]. The value of the plateau-modulus of natural rubber was about

10^5 Pa, as in the case of that reported in the literature. When the nanomatrix structure was formed in natural rubber, the plateau-modulus of the rubber increased about 10 times as high as that of natural rubber. In contrast, the plateau-modulus increased a little[20], about 1.3 times, when the island-matrix structure was formed in natural rubber. The large increase in the plateau-modulus is an advantage of the nanomatrix structure, compared to the island-matrix structure. Further increase in the plateau-modulus of the rubber with nanomatrix structure was found after annealing it at 403 K, above glass transition temperature of polystyrene.

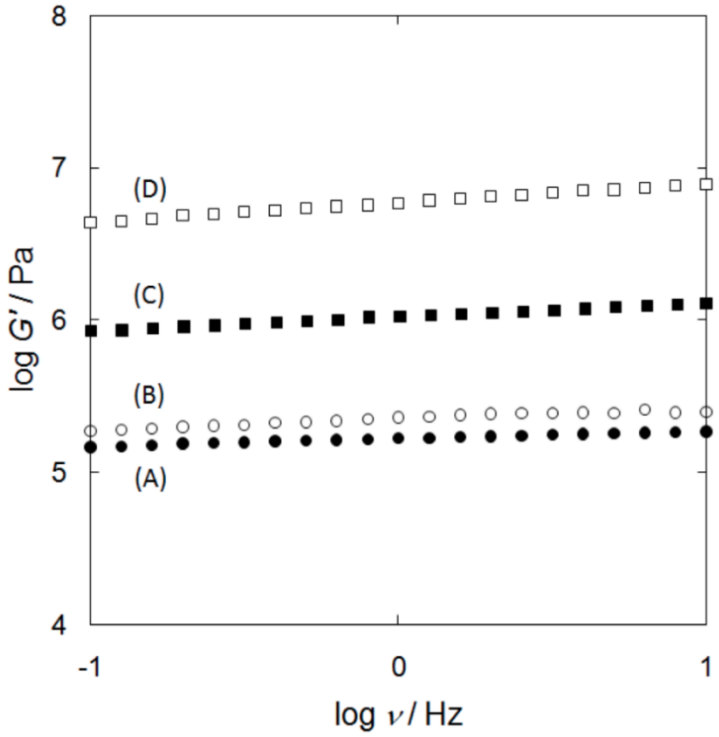

Figure 1-5 Storage modulus at plateau region *versus* frequency for (A) natural rubber,
(B) DPNR-*graft*-PS (PS: ca 10%) with island-matrix structure,
(C) DPNR-*graft*-PS (PS: ca 10%) with the nanomatrix structure annealed at 303 K and
(D) DPNR-*graft*-PS (PS: ca 10%) with the nanomatrix structure annealed at 403 K.

Figure 1-6 shows a plot of loss tangent, tanδ, *versus* frequency at plateau regain[6]. The value of tanδ of natural rubber was in a range of 0.1 to 0.15. When the nanomatrix structure was formed, the value of the product increased dramatically in high frequency region but a little in low frequency region. After annealing the product at 403 K, the tanδ increased significantly over whole frequency range at plateau region. This may be explained to be due to the well-connected nanomatrix. Thus, the

product was proved to accomplish not only high storage modulus but also outstanding loss modulus, which were attributed to a change in the morphology.

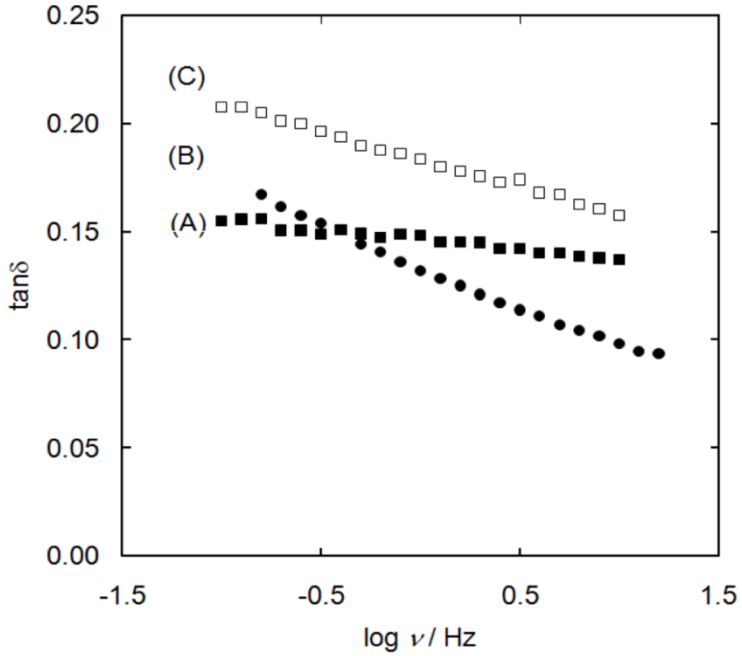

Figure 1-6 Loss tangent at plateau region *versus* frequency for (A) natural rubber,
(B) DPNR-*graft*-PS (PS: ca 10%) with the nanomatrix structure annealed at 303 K and
(C) DPNR-*graft*-PS (PS: ca 10%) with the nanomatrix structure annealed at 403 K.

1.5 Theoretical estimation of modulus of natural rubber with nanomatrix structure

The morphology is closely related to the mechanical properties. For instance, the value of complex modulus for polymeric multicomponent materials, in which phase 2 are dispersed in the matrix of phase 1, can be estimated using Takayanagi model[21,22],

$$E^* = \left\{ \frac{\phi}{\lambda E_2^* + (1-\lambda) E_1^*} + \frac{1-\phi}{E_1^*} \right\}^{-1} \qquad (1\text{-}1)$$

where E^*i is a complex modulus of i component and λ and ϕ are parameters relating to the volume fraction and mixing state of materials, as shown in Figure 1-7.

When dispersoid is sphere, λ and ϕ are related to volume fraction of phase 2, V_2, as follows:

$$\lambda = (2 + 3V_2)/5 \qquad (1\text{-}2)$$

$$\phi = 5V_2/(2 + 3V_2) \qquad (1\text{-}3)$$

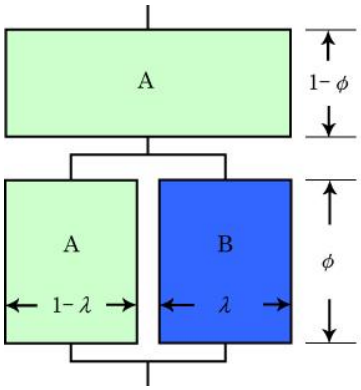

Figure 1-7 Schematic illustration of combination of series and parallel models.

The advantage of the nanomatrix structure may be explained with a simple model shown in Figure 1-8. Based on the schematic illustration, storage moduli for the island-matrix structure and the nano-matrix structure were estimated, respectively, where the values of storage moduli used were literature values[23], that is, $E_{NR}=10^5$ Pa and $E_{PS}=10^9$ Pa. In an ordinary circumstance, island-matrix structure is formed for a polymer blend; hence, a combination of parallel model and series model is shown in Figure 1-8 (A) for the island-matrix structure, according to Takayanagi model.

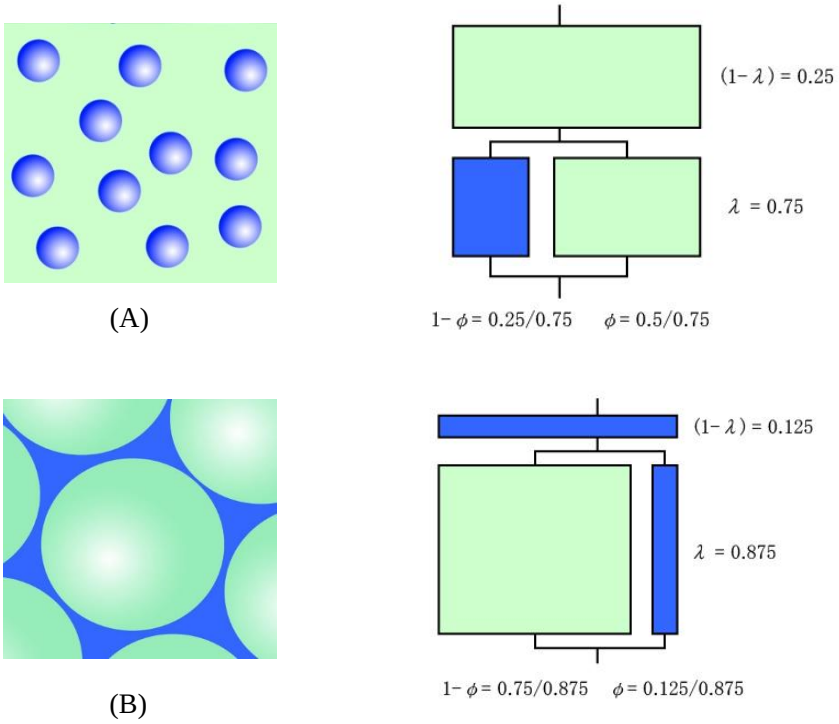

Figure 1-8 Takayanagi model: (A), island-matrix structure; (B), nanomatrix structure.

The storage modulus may increase a little bit, that is, about 1.25 times, when the island-matrix structure is formed for natural rubber/polystyrene (90/10) blend. In contrast, for nanomatrix structure, a unique combination of parallel model and series model is formed due to phase inversion, despite the same ratio of natural rubber to polystyrene. The estimated value of the storage modulus for the nanomatrix structure is 5.53×10^7 Pa. This is absolutely different from the value for the island-matrix structure ; the value for nanomatrix structure is about 500 times as high as that for island-matrix structure. However, the complex modulus, reported in the previous works, was significantly low for natural rubber with the nanomatrix structure, as mentioned in section 1.4. It is necessary to observe the nanomatrix structure through FIB-SEM and electron tomography technique.

1.6 ^{1}H-conductivity and nanomatrix channel

The nanomatrix structure may be useful to transport molecular and ionic species as a 3D nano-network. It is necessary to connect the nanomatrix, completely, for the transportation. Figure 1-9 shows TEM images for (a) DPNR-*graft*-PS-1.5, (b) DPNR-*graft*-PS-4.5 and (c) DPNR-*graft*-PS-5.5[24], in which the bright domains represent polystyrene and the dark domains represent natural rubber.

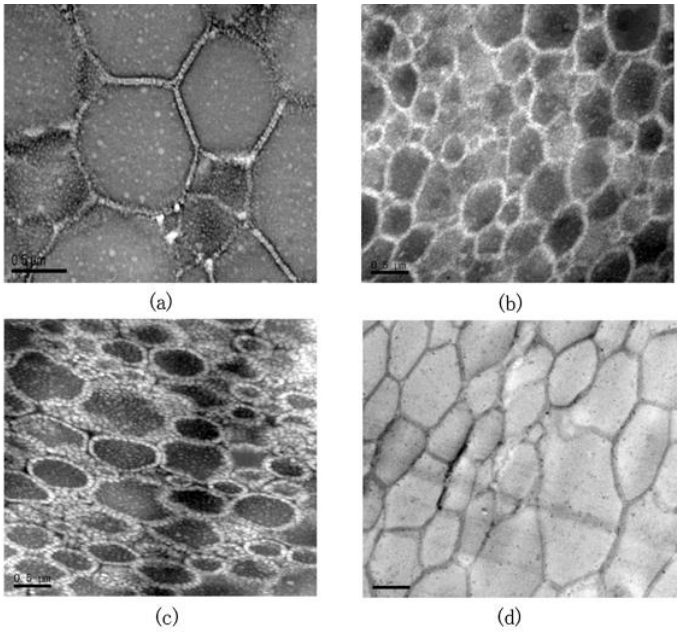

Figure 1-9 TEM images for (a) DPNR-*graft*-PS-1.5, (b) DPNR-*graft*-PS-4.5
(c) DPNR-*graft*-PS-5.5 and (d) sulfonated DPNR-*graft*-PS-5.5

As for the DPNR-*graft*-PS-1.5, the natural rubber particles of about 1 μm in average diameter, ranging from 50 nm to 3 μm in volume mean particle diameter, were well dispersed in PS nanomatrix of about 15 nm in thickness. In contrast, for the DPNR-*graft*-PS-4.5 and the DPNR-*graft*-PS-5.5, the natural rubber particles of about 1 μm in average diameter were dispersed into discontinuous nanomatrix of condensed PS particles of about 60 nm in diameter that are densely close to each other in the matrix. On the other hand, Figure 1-9 (d) shows TEM images for the sulfonated DPNR-*graft*-PS-5.5, which was prepared by sulfonation of the DPNR-*graft*-PS-5.5. The bright domains represent natural rubber and the dark domains represent polystyrene. The sulfonation of DPNR-*graft*-PS-5.5 made connecting the PS particles to form completely continuous nanomatrix, since the PS particles were dissolved into chloroform before sulfonation with chlorosulfonic acid, but the DPNR particles were not due to three-dimensional network structure. Thickness of the connected nanomatrix is about 80 nm, reflecting that several PS particles of about 60 nm in diameter fuse to each other after sulfonation.

Table 1-1 T_g, sulfur content, and electrochemical properties of sulfonated DPNR-*graft*-PS, sulfonated PS and Nafion®117

	Sulfur content wt%	IEC meq/g	Conductivity S/cm	Water uptake wt%
Sulfonated DPNR-*graft*-PS	75	2.43	9.5×10^{-2}	24.3
Sulfonated PS	-	1.50	3.2×10^{-2}	340.0
Nafion®117	-	1.02	8.0×10^{-2}	18.6

Electro-chemical properties of the sulfonated DPNR-*graft*-PS are compared with those of the proton-conductive perfluorosulfonic acid membrane, Nafion®117, as a reference. The nanomatrix of the sulfonated DPNR-*graft*-PS5.5 is activated with sulfuric acid solution to the nanomatrix-channel. Ion exchange capacity (IEC) and water swelling content of the sulfonated DPNR-*graft*-PS5.5 are dependent upon the sulfonic acid group content, as shown in Table 1-1. The value of the IEC of the sulfonated DPNR-*graft*-PS5.5 was larger than the value of the IEC of sulfonated PS and Nafion®117.

The proton-conductivity of the sulfonated DPNR-*graft*-PS5.5 is correlated to the IEC[18,25]. The proton-conductivity of the sulfonated DPNR-*graft*-PS5.5 increases as the sulfonic acid content increases. The value of the proton-conductivity of the sulfonated DPNR-*graft*-PS is larger than that of Nafion®117, as in the case of IEC. The advantage of the sulfonated DPNR-*graft*-PS5.5 is quite low water swelling content, in spite of the excellent proton-conductivity and high IEC, which corresponds to those of Nafion®117. It is 1/15 times as low as the water swelling content of sulfonated PS. In spite of the high proton-conductivity and low water uptake, however, mechanism of the proton-conductivity of the nanomatrix channel remains unclear.

1.7 Chapters

This dissertation was divided into 7 chapters in order to elucidate the relationship between the nanomatrix structure and the properties. Brief synopsis was described below.

In Chapter 1 "General Introduction", background and current status is described on deproteinization of natural rubber, nanomatrix structure, 3D observation, heterogeneous structure in equilibrium and non-equilibrium states, relationship between morphology and properties, ^{1}H-conductivity and nanomatrix channel.

In Chapter 2 "Morphology Change due to Removal of Proteins from Natural Rubber", removals of proteins from glove and latex of natural rubber were performed by leaching and deproteinization. The extractable protein content and nitrogen content of the glove and latex film were measured by modified Lowry method and Kjeldahl method and morphology was observed by TEM and FIB-SEM. The extractable protein content and the nitrogen of the glove and the latex film decreased after leaching and deproteinization in which the nanomatrix of non-rubber components disappeared.

In Chapter 3 "Nanomatrix Structure Formed by Graft Copolymerization of Styrene onto Natural Rubber", fresh natural rubber was used to prepare natural rubber with the nanomatrix structure. The nanomatrix structure was formed by graft-copolymerization of styrene onto deproteinized fresh

natural rubber (fresh DPNR) in latex stage. Under a suitable condition of the graft-copolymerization, conversion and grafting efficiency of styrene was 98 mol% and 80 mol%, respectively. The rubber particles of about 1 μm in average diameter were found to be dispersed in polystyrene matrix of 10-30 nm in thickness, as observed by TEM. Tensile properties of fresh DPNR were dramatically improved by forming the nanomatrix structure, as compared with DPNR.

In Chapter 4 "FIB Processing for Natural Rubber with Nanomatrix Structure", focused ion beam (FIB) processing was performed to prepare an ultra-thin section of DPNR-*graft*-PS, in order to obtain a 3D image of the nanomatrix structure through electron tomography technique. The DPNR-*graft*-PS was immersed into OsO_4 solution for more than 7 days. The ultra-thin section prepared by FIB processing was compared with that prepared with a cryo-microtome in the electron tomography observation. A distinctly clear electron tomography image of the nanomatrix structure was obtained with the ultra-thin section prepared by FIB processing, but not with that prepared with the cryo-microtome. The FIB processing was proved to be indispensable for the electron tomography observation of the nano-structure of the soft-materials.

In Chapter 5 "Observation of Anisotropically Deformed Nanomatrix Structure in Frozen Non-equilibrium State through 3D FIB-SEM and electron tomography", effect of frozen non-equilibrium structure for anisotropically deformed natural rubber with the nanomatrix structure on mechanical properties was investigated with respect to 3D morphology analysis by electron tomography technique and FIB-SEM. The nanomatrix structure in isotropic state was precisely analyzed by electron tomography technique and synchrotron scattering technique. The nanomatrix structure was found to consist of natural rubber particles and polystyrene nano-particles. The frequency independent loss tangent at plateau region was attributed to the discontinuous nanomatrix structure. After annealing at 403 K and 7 MPa, the nanomatrix became continuous, which resulted in the increases in stress at strain of 1 and storage modulus as well as increase in loss tangent.

In Chapter 6 "Preparation of Polymer Electrolyte Membrane with Nanomatrix Channel Structure", mechanism of proton-transport of a polymer electrolyte membrane (PEM) with nanomatrix

channel was investigated with respect to the activation energy of proton-conductivity. The PEM with nanomatrix channel was prepared by graft-copolymerization of styrene onto DPNR followed by sulfonation with chlorosulfonic acid. The resulting sulfonated graft-copolymer (SDPNR-*graft*-PS) was characterized by FT-IR spectroscopy, solid state ^{13}C CP/MAS NMR spectroscopy, elemental analysis, TEM and impedance analysis. The sulfonated graft-copolymer (SDPNR-*graft*-PS) was found to form completely continuous nanomatrix. The value of the activation energy of proton-conductivity estimated from the slope of Arrhenius plot was 12 kJ/mol for SDPNR-*graft*-PS, suggesting that the proton-transport occurred in a manner of Grotthuss mechanism.

In Chapter 7 "General Conclusion", the conclusion was described on the effect of the nanomatrix structure. The increase in the tensile strength, unique behavior of dynamic viscoelastic properties and increase in the ^{1}H-conductivity were explained to be due to the formation of the nanomatrix structure.

1.7 References

1. Kato, M.; Ito, T.; Aoyama, Y.; Sawa, K.; Kaneko, T.; Kawase, N.; Jinnai, H. *J. Polym. Sci. Part B: Polym. Phys.* **2007**, 45, 677-683.
2. Kaneko, T.; Nishioka, H.; Nishi, T.; Jinnai, H. *J. Electron Micros.* **2005**, 54, 437-444.
3. Kawase, N.; Kato, M.; Nishioka, H.; Jinnai, H. *Ultramicroscopy* **2007**, 107, 8-15.
4. Brostow, W.; Gorman, B. P.; Olea-Mejia O. *Mater. Lett.* **2007**, 61, 1333-1336.
5. Beach, E.; Keefe, M.; Heeschen, W.; Rothe, D. *Polymer* **2005**, 46, 11195-11197.
6. Kawahara S.; Yamamoto Y.; Fujii S., Isono Y., Niihara K., Jinnai H., Nishioka H. and Takaoka A. *Macromolecules* **2008**, 41, 4510-4513.
7. Akabori, K; Yamamoto, Y.; Kawahara, S.; Jinnai, H.; Nishioka H. *J. Phys. Conf. Ser.*, **2009**, 184, 012027.
8. Kaneko, T.; Nishioka, H.; Nishi, T.; Jinnai, H. *J. Electron Micros.* **2005**, 54, 437-44.
9. Kawase, N.; Kato, M.; Nishioka, H.; Jinnai, H. (2007). *Ultramicroscopy* **2007**, 107(1), 8-15.

10. Brostow, W.; Gorman, B. P.; Olea-Mejia, O. *Materials Letters* **2007**, 61, 1333-1336.

11. Beach, E.; Keefe, M.; Heeschen, W.; Rothe, D. *Polymer* **2005**, 46, 11195-11197.

12. Kawahara, S.; Isono, Y.; Washino, K.; Morita, T.; Tanaka, Y. *Rubber Chem. Technol.* **2001**, 74, 295-302.

13. Yamamoto, Y.; Kawahara, S. "Properties and Nano-Observation of Natural Rubber with Nanomatrix Structure", in *"Advances in Materials Science, Vol.2, Natural Polymers, Biopolymers, Biomaterials, and Their Composites, Blends, and IPNs"*,Eds. S. Thomas, N. Ninan, S. Mohan, Apple Academic Press, Oakville, Canada, P327-343, **2013**.

14. Tinker, A.; Jones, K. P. "Blends of Natural Rubber: Novel Techniques for Blending with Speciality Polymers", Springer Science & Business Media, **1998**.

15. Kawahara, S.; Yamamoto, Y. *Rubber World* **2007**, 237, 26-31.

16. Shonaike, G. O.; Simon, G. P. "Polymer Blends and Alloys", CRC Press, **1999**.

17. Kawahara, S.; Kawazura, T.; Sawada, T.; Isono Y. *Polymer* **2003**, 44, 4527-4531.

18. Pukkate, N.; Kitai, T.; Yamamoto, Y.; Kawazura, T.; Sakdapipanich, J.; Kawahara, S. *Eur. Polym. J.* **2007**, 43, 3208-3214.

19. Tuampoemsab, S.; Sakdapipanich, J. *Kautsch. Gummi Kunst.* **2007**, 57, 678-684.

20. Roberts A. D. Natural Rubber Science and Technology, Oxford University Press, Oxford, USA, **1988**.

21. Takayanagi, M.; Imada, K.; Kajiyama, T. *J. Polym. Sci., Polym. Symp.* **1966**, 15, 263-80.

22. Takayanagi, M.; Harima, H.; Iwata, Y. *Zairyo* **1963**, 12, 389-394.

23. Brandrup, J.; Immerugut, E. H. "Polymer Handbook" 3rd Ed., John Wiley & Sons, **1989**.

24. Suksawad, P.; Kosugi, K.; Yamamoto, Y.; Akabori, K.; Kuroda, H.; Kawahara, S. *J. Appl. Polym. Sci.* **2011**, 122, 2403-2414.

25. Kawahara, S.; Suksawad, P.; Yamamoto, Y.; Kuroda, H. *Macromolecules* **2009**, 42, 8557-8560.

Chapter 2

Morphology Change due to Removal of Proteins from Natural Rubber

2.1 Introduction

Removal of proteins from natural rubber is one of the key-technologies to make a chemical modification of the rubber such as graft-copolymerization[1-5]. Various techniques to remove the proteins from natural rubber have been developed in the last three decades[6]: that is, deproteinization with enzyme[7-12], deproteinization with urea[13-15], deproteinization with sodium dodecyl sulfate (SDS)[16], leaching with hot water[17-21] and so forth. Two of these, i.e., the deproteinization with urea and the leaching with hot water, are the focus of the attention to prepare low protein natural rubber and protein free natural rubber, since they have a potential to meet the requirement of the Food and Drug Administration of USA, entitled "Recommendations for Labeling Medical Products to Inform Users that the Product or Product Container is not Made with Natural Rubber Latex"[22].

The removal of proteins to prepare the low-protein natural rubber[13,14-23] and the protein free natural rubber[24,25] may be efficiently performed in latex stage, since the proteins attach to the surface of the rubber particles, isolated from *Hevea brasiliensis*. The spontaneous transfer of the proteins from the rubber particles to serum phase may allow to apply a centrifugation and membrane separation to the latex, after denaturing the proteins with proteolytic enzyme or urea in the presence of SDS. The centrifugation or the membrane separation may exhaust the detached proteins away from the latex. In contrast, the leaching with hot water is useful for washing the natural rubber products to remove the proteins present in natural rubber. In particular, the proteins existing on the surface of the natural rubber products may be removed by leaching but not those inside the products. The leaching is, thus, expected to solve the latex allergy issue, as well as the deproteinization with urea.

The deproteinization with urea has been developed in the previous work[13,14-23], when the structure of natural rubber was analyzed; that is, no proteins chemically linked to natural rubber and

urea was effective to denature the proteins existing on the surface of the rubber particles. These findings resulted in a breakthrough on the deproteinization of natural rubber; so that, proteolytic enzyme was no more needed to denature the proteins of natural rubber. This may provide great advantage of the deproteinization with urea as is compared with the deproteinization with proteolytic enzyme. One may use various denaturants for the deproteinization and shorten the incubation time. For instance, the incubation time was shortened from 24 h or longer for deproteinization with proteolytic enzyme to 10 min or shorter for deproteinization with urea. Furthermore, the nitrogen content and the extractable protein content of natural rubber were reduced from ca. 0.4 w/w% and 10^3 μg/ml to very low levels; in fact, the nitrogen content and the extractable protein content were less than 0.01 w/w% and 1.0 μg/ml after urea treatment, whereas they were 0.02 w/w% and 3.2 μg/ml after deproteinization with proteolytic enzyme. The nitrogen content and the extractable protein content of natural rubber deproteinized with urea was significantly lower than those of natural rubber deproteinized with proteolytic enzyme. Now, one may have protein free natural rubber[24,25], whose nitrogen content and extractable protein content were less than 0.000 w/w% and 0.0 μg/ml after three times centrifugation. In contrast, the nitrogen content and the extractable protein content were rather high after leaching. They were more than ca. 0.1 w/w% and 50 μg/ml.

In the present study, an attempt to reduce the extractable protein content of the natural rubber product were carried out to achieve the level close to that of the protein free natural rubber through leaching. Measurements of the extractable protein content and the nitrogen content were carried out by modified Lowly method (ISO12243:2003) and Kjeldahl method after leaching the product at various pHs and temperatures. Morphology was observed by focused ion beam / scanning electron microscopy, FIB-SEM.

2.2 Experimental

2.2.1 Samples and Reagents

Natural rubber samples used in this study were commercial high ammonia latex (HANR) purchased from Golden hope company (Malaysia) and commercial natural rubber gloves, i.e., Glove A and Glove B. Total solid content and the dry rubber content of the HANR latex were 62.1 and 60.7 w/w%, respectively. Sodium dodecyl sulfate (SDS) was purchased from Kishida Co.Ltd., Japan. Sulfuric acid (H_2SO_4), sodium hydroxide, potassium anhydrate, copper sulfate, selenium and 25 w/v% glutaraldehyde solution were purchased from Nacalai Tesque Inc., Japan. Osmium tetraoxide (OsO_4) aqueous solution (4 w/w%) was purchased from Heraeus Chemicals Sa (Pty) Ltd., South Africa. Other reagents used were analytical grade.

2.2.2 Purification of Natural Rubber

Deproteinization of HANR latex and fresh NR latex was carried out by incubation with 0.1 w/w% urea in the presence of SDS and acetone at room temperature. The cream fraction was re-dispersed in the surfactant and the solvent used to make 30 w/w% DRC latex and was washed twice or three times by centrifugation. The rubber was recovered by centrifugation followed by coagulation with methanol and dried under reduced pressure at ambient temperature until constant weight. A schematic representation of the experimental procedure is shown schematic mechanism in Figure 2-1.

Leaching of Glove A (1 g) was performed with water (50mL) under various conditions for 6 h. The pH and temperature, applied in this study, were 1 - 10 at 313 K and 293 - 373 K at pH of 5.5. The Glove A was dried at 323 K for a week under reduced pressure.

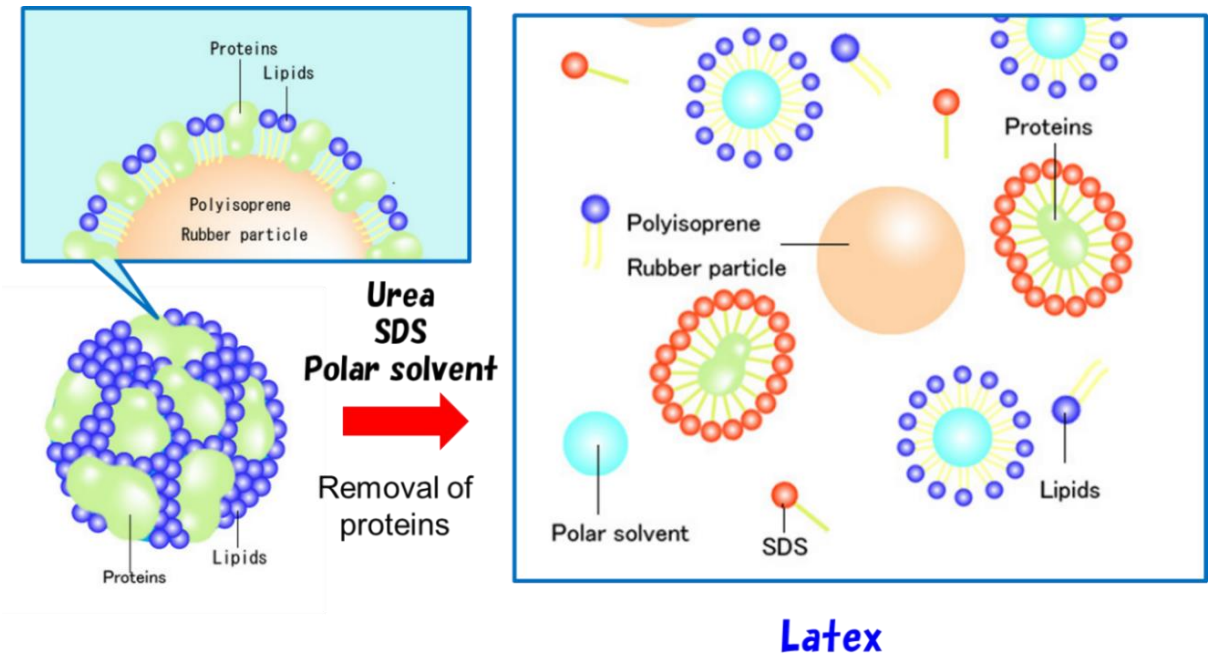

Figure 2-1 Schematic illustration of removal of the proteins from natural rubber with urea and polar solvent in the presence of SDS.

2.2.3 Measurements

Measurement of nitrogen content of the rubbers was made by Kjeldahl method as described in the Rubber Research Institute of Malaysia (RRIM) Test Method B7.[26] Rubber sample, mixed with catalyst mixture, i.e. potassium sulphate: copper sulphate: selenium in the weight ratio of 15:2:1, was digested with concentrated H_2SO_4. The resulting solution was distilled, and distillates were titrated with 0.005 M H_2SO_4 using methyl red as an indicator.

The amount of extractable proteins in the rubber samples was measured by DC protein assay[27]. The rubbers with dimension of 2×2 cm^2 were extracted with phosphate buffer (1/15 M, pH 7). A ratio of the rubbers to the phosphate buffer was 1 g rubber/5 ml phosphate buffer. The protein extraction was performed with continuous stirring at 313 K for 6 h. Then the samples were filtered and protein contents in supernatants were determined by the Bio-Rad DC protein assay, using bovine gamma globulin (BGG) as a standard.

Morphology of the rubber samples were observed with a transmission electron microscope (TEM), JEOL JEM-2100 at accelerating voltage of 200 kV. The ultrathin sections of the rubber samples used for the TEM observation were prepared by a microtome (Ultracut N, Reichert - Nissei FC S) at a temperature lower than glass transition temperature of the samples (about 193 K). The thin sections with the thickness of about 100 nm were stained with phosphotungstic acid (PTA) at room temperature for 10 min.

The block specimen of the rubber was immersed in 25 w/w% glutaraldehyde aqueous solution at room temperatures for 12 h, and then it was rinsed with distilled water for 1h. Finally, the specimen was stained with 4 w/w% OsO_4 aqueous solution at various temperatures for 48 h. FIB-SEM observation was carried out with a SII Nano Technology SMI-3050SE. To prevent curving the surface during the process, a thin carbon layer was deposited at the surface of the specimen. Gallium ion beam at accelerating voltage of 30 kV was used for etching the surface with about 30 nm intervals to make a cross section. SEM observation for the cross section was carried out with electron beam at accelerating voltage of 2 kV. Since the cross section was directed diagonally to the SEM optics, length of obtained SEM images was corrected.

2.3 Results and Discussion

Table 2-1 shows nitrogen content, extractable protein content of natural rubber (HANR) and deproteinized natural rubber, where A represents acetone and 0.025 represents content of acetone (0.025 w/w%), which was fed into the latex. The nitrogen content and extractable protein content of natural rubber were reduced from 0.279 w/w% and 115.2 μg/ml to 0.021 w/w% and 3.2 μg/ml, after incubation of the latex with urea and SDS for 1 hour followed by centrifugation, twice. The values of nitrogen content and extractable protein content of deproteinized natural rubber (DPNR) were quite similar to those of enzymatically deproteinized natural rubber, which is prepared by incubation of the latex with proteolytic enzyme and SDS for 24 hours or more followed by centrifugation, twice.

Table 2-1 Nitrogen content and extractable protein content of natural rubber (HANR), deproteinized natural rubber (DPNR) and protein free natural rubber (PFNR).

Sample	Centrifugation	Nitrogen content (w/w%)	Extractable protein content (μg/ml)
HANR	-	0.279 ± 0.003	115.2
DPNR	1 times	0.116 ± 0.010	
DPNR_A0.025[a)]		0.053 ± 0.005	
DPNR	2 times	0.021 ± 0.004	3.2
DPNR_A0.025[a] (PFNR)		0.000 ± 0.000	0.0

[a)] "A "represents acetone and "0.025" represents amount of acetone, i.e., 0.025 w/w%

The dramatically shortened time of incubation may be explained to be due to the use of urea as a denaturant instead of proteolytic enzyme; for instance, denaturation of the proteins with urea is attributed to deformation of higher order structure due to scission of hydrogen bonds, whereas that with proteolytic enzyme is attributed to acylation due to hydrolysis.

The values of the nitrogen content and extractable protein content was further reduced to 0.000 w/w% and 0.0 μg/ml, after incubation of the latex with urea, acetone and SDS for 1 hour followed by centrifugation, twice. In other words, the proteins were completely removed from natural rubber with urea, acetone and SDS. This may be explained to be due to the effect of acetone[25], which is a good solvent of lipids and fatty acids (Figure 2-1).

The lipids and fatty acids may detach from the rubber particles to form their micelles in aqueous phase, which may result in free space on the rubber particles. The free space may make possible more to release the proteins from natural rubber after denaturing them with urea and SDS, since the volume contraction of the proteins occurs due to cleavage of the hydrogen bonds. The released proteins may be stabilized with urea and SDS in aqueous phase, since the hydrophobic parts of the proteins are covered with urea and SDS. Consequently, spontaneous removal of the proteins may occur from natural rubber due to loose packing on the rubber particles after removal of the lipids and fatty acids.

The resulting purified natural rubber is said to be protein free natural rubber, since it does not contain the proteins. In the present work, it is found that the two times centrifugation is required for the complete removal of the proteins from natural rubber.

Table 2-2 Nitrogen content and extractable protein content of natural rubber glove A (Glove A) and natural rubber glove B (Glove B).

Specimen	Nitrogen content (w/w%)	Extractable protein content (μg/g-rubber)
Glove A	0.251	692
Glove B	0.189	322

In Table 2-2 are shown the nitrogen content and extractable protein content of natural rubber Glove A (Glove A) and natural rubber glove B (Glove B), which were commercially available products. Values of the nitrogen content for the Glove A and Glove B were similar to each other. In contrast, a value of the extractable protein content for the Glove A was about twice as large as that for the Glove B. The value of the extractable protein content was significantly larger than that of the labeling claim (50 μg/g-rubber or less), recommended by the Food and Drug Administration of USA in 1992 and modified in 2013. Thus, the Glove A and Glove B are contrary to the regulation; hence, they are not able to be imported into USA. In the present work, the Glove A as a sample for leaching test was used, since the values of the nitrogen content and extractable protein content were lager than 0.2 w/w% and 600 μg/g-rubber, respectively.

Figure 2-2 shows TEM images for natural rubber (HANR), protein-free natural rubber and Glove A. Gloomy domains represent the proteins and bright domains represent natural rubber, since the proteins were stained with phosphotungstic acid, PTA. As is clearly seen in Figure 2-2 (A), the HANR possessed the nanomatrix structure, which consisted of the natural rubber particles of about 1 μm in average diameter as a major component and the matrix of the proteins of about 15 nm in average thickness. The nanomatrix structure disappeared after removal of proteins from HANR, as

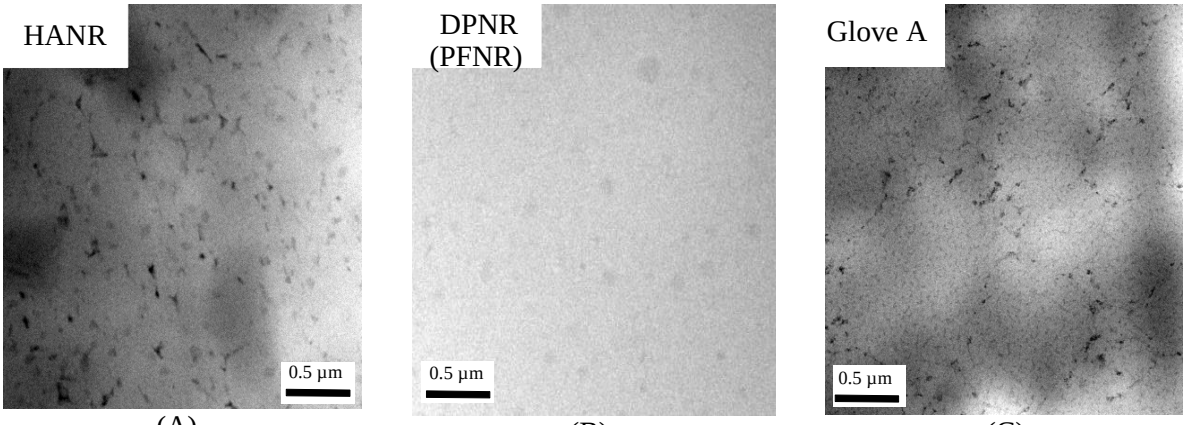

(A) (B) (C)

Figure 2-2 TEM images of (A) natural rubber (HANR), (B) protein free natural rubber (PFNR) and (C) natural rubber glove A (Glove A).

show in TEM image for the protein free natural rubber (PFNR) (Figure 2-2 (B)). This implies that the nanomatrix structure appears as natural rubber containings the proteins. The thickness of the nanomatrix may be dependent upon the protein content, as reported in the previous literature[25].

The nanomatrix structure is also shown for the Glove A, as shown in Figure 2-2 (C). The nanomatrix structure of the Glove A was almost similar to that of HANR; for instance, the thickness of the nanomatrix was about 15 nm. This may be explained to be due to the high nitrogen content (0.251 w/w%) and high extractable protein content (692 µg/g-rubber) of the Glove A, which corresponds to those of the HANR. It is, therefore, proved that the Glove A contains relatively huge amount of the proteins as a commercial product, which is sufficiently enough to form the nanomatrix structure.

Figure 2-3 shows a plot of extractable protein content *versus* pH of leaching test for the Glove A, in which the leaching was performed at 313 K for 6 hours. The extractable protein content was significantly dependent upon the pH of the leaching test. The extractable protein content was reduced to 86 µg/g-rubber from 692 µg/g-rubber at pH of 1.9 after leaching and it was less than 200 µg/g-rubber at pH between 6.8 or more. The less extractable protein content demonstrates that much more proteins are removed by leaching the Glove A. In contrast, the extractable protein content of the leached Glove A was 633 µg/g-rubber and 611 µg/g-rubber at pH of 4 and 5.5, respectively, which

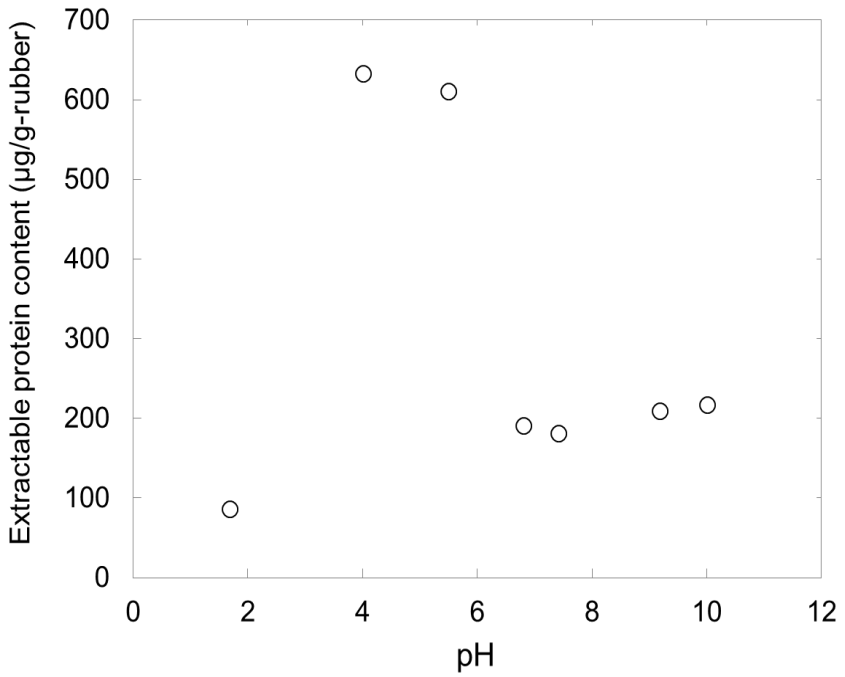

Figure 2-3 Plot of extractable protein content of natural rubber glove A (Glove A) *versus* pH. The value of extractable protein content was significantly dependent upon pH.

was close to the extractable protein content of the untreated Glove A, i.e. 692 μg/g-rubber. The change in the extractable protein content of the Glove A *versus* pH of the leaching test may be associated with the stability of the proteins present in natural rubber, i.e. *Hevein*; for instance, the *Hevein* is unstable at pH between 4 and 6 at 313 K (moderate condition), since the isoelectric point of the *Hevein* is pKa of about 4. The unstable proteins in aqueous phase may go back to the surface of the natural rubberparticles, which may result in the increase in the extractable protein content. The similar situation may take place for natural rubber glove in use. The proteins may not be extracted from the glove under moderate condition, since the pH and temperature of skin of human beings is 4.5 - 6 and about 313 K. However, the amount of the proteins extracted from the glove may increase with sweat, since the pH of the sweat is 7 - 8. This may result in the latex allergy; for instance, persons in good health may contract the latex allergy in a ratio of 30 %, according to the previous work[6], when they contact with the Glove A such as high protein natural rubber glove. Furthermore, it is found that the temperature of 313 K is insufficient to remove the proteins from natural rubber and it is unable to accomplish the labeling claim of FDA, i.e.50 μg/g-rubber.

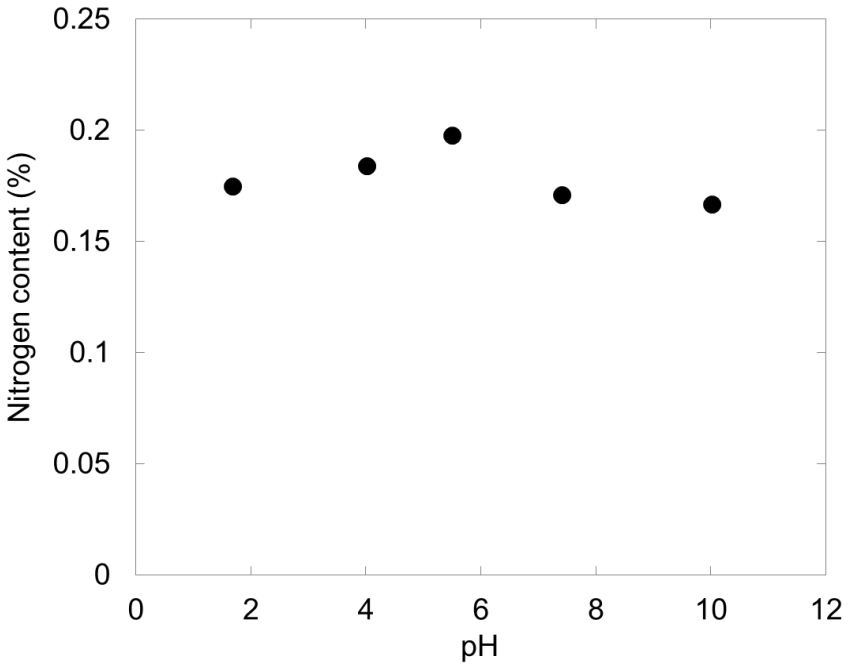

Figure 2-4 Plot of nitrogen content of natural rubber glove A (Glove A) versus pH. The value of nitrogen content was almost independent of pH.

The effect of pH on the nitrogen content for the Glove A is shown in Figure 2-4. The nitrogen content was almost independent of pH of leaching, which was performed at 313 K for 6 hours. This implies that the amount of the proteins present on the surface of the natural rubber particles are a little as compared with total amount of the proteins. Strictly speaking, however, the nitrogen content of the leached Glove A was a little bit higher at pH4 and pH5.5. The higher nitrogen content may be related to the higher extractable protein content, suggesting that the significant amount of proteins remained after leaching. The exact value of the nitrogen content after leaching was 0.2 w/w% or less, which was smaller than that of the Glove A, i.e., 0.251 w/w%. Thus, the amount of the removed proteins was approximately 20 % of the total amount of the proteins present in natural rubber. The leaching is, consequently, confirmed to be effective to remove only the proteins present on the surface of the rubber particles.

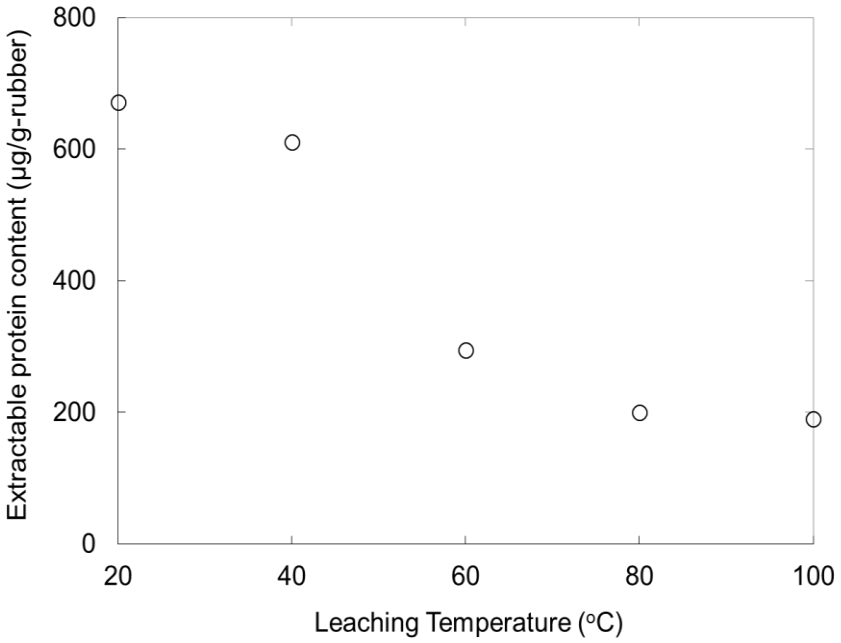

Figure 2-5 Dependency of extractable protein content of natural rubber glove A (Glove A) on temperature.

Figure 2-5 shows the extractable protein content of the Glove A, after leaching at various temperatures for 6 hours at pH5.5. The extractable protein content was higher after leaching at 293 K and 303 K for 6 hours, reflecting less removal of the proteins during leaching. In contrast, the extractable protein content was less than 200 μg/g-rubber, which was about 1/3 level of the untreated Glove A, when the leaching was performed at 333, 353 and 373 K. From the results of Figures 5 and 3, it is found that a suitable condition for the leaching is temperature of higher than 333 K and pH of higher than 7.

Figure 2-6 shows the nitrogen content of the Glove A, after leaching at various temperatures for 6 hours at pH5.5. The nitrogen content of the Glove A didn't change after leaching at 293 K, whereas it was reduced to 0.2 w/w% or less at 313 K and higher. It is, thus, found that the leaching temperature is one of the important factors to remove the proteins from natural rubber and the temperature of 333 K is a critical temperature, at which 20 - 30 % of the proteins are removed away.

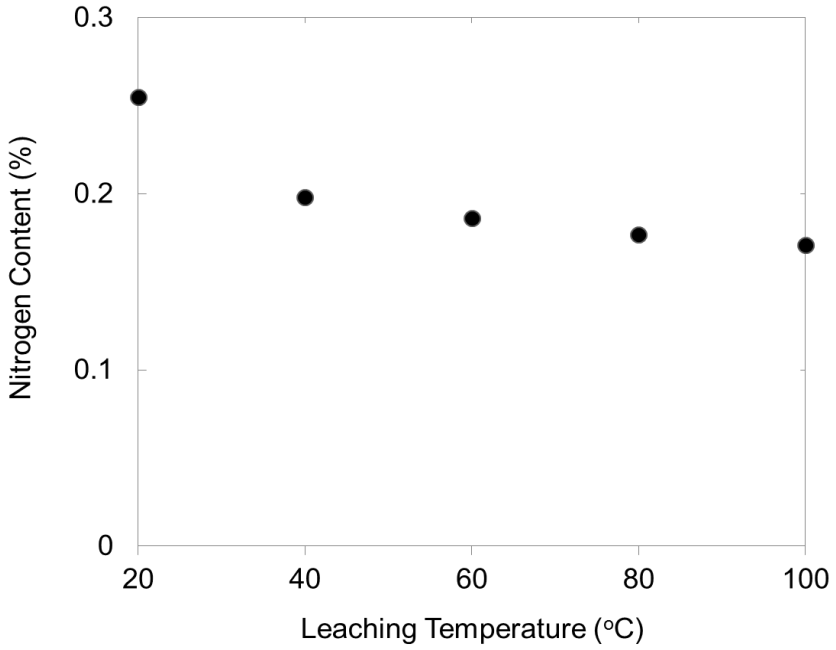

Figure 2-6 Dependency of nitrogen content of natural rubber glove A (Glove A) on temperature. The value of nitrogen content decreased as temperature rose.

FIB-SEM images for the Glove A and the leached Glove A are shown in Figure 2-7, in which the leaching was performed at various temperatures for 6 hours at pH 5.5. The gloomy domains represent natural rubber and the bright domains represent the non-rubber components such as the proteins and phospholipids. As for the Glove A as a control, the nanomatrix structure was observed in the FIB-SEM image after etching it with Ga ion from the surface to 20 μm in depth. The natural rubber particle of about 1 μm in average diameter was well dispersed in the nanomatrix of the non-rubber components such as the proteins and phospholipids. The nanomatrix structure observed by FIB-SEM (Figure 2-7) was the same as that observed by TEM (Figure 2-2), suggesting that the nanomatrix structure was uniformly formed from surface to inside. The nanomatrix structure remained unchanged after leaching the Glove A at 293 K, since the nitrogen content and the extractable protein content did not change. However, the nanomatrix structure disappeared after leaching the Glove A at 333 and 353 K and no heterogeneous structure was observed in the FIB-SEM image. Assuming that the thickness of the Glove A was about 0.4 mm and the 20 % proteins were removed selectively from the surface of Glove A by leaching, the removal of the proteins were

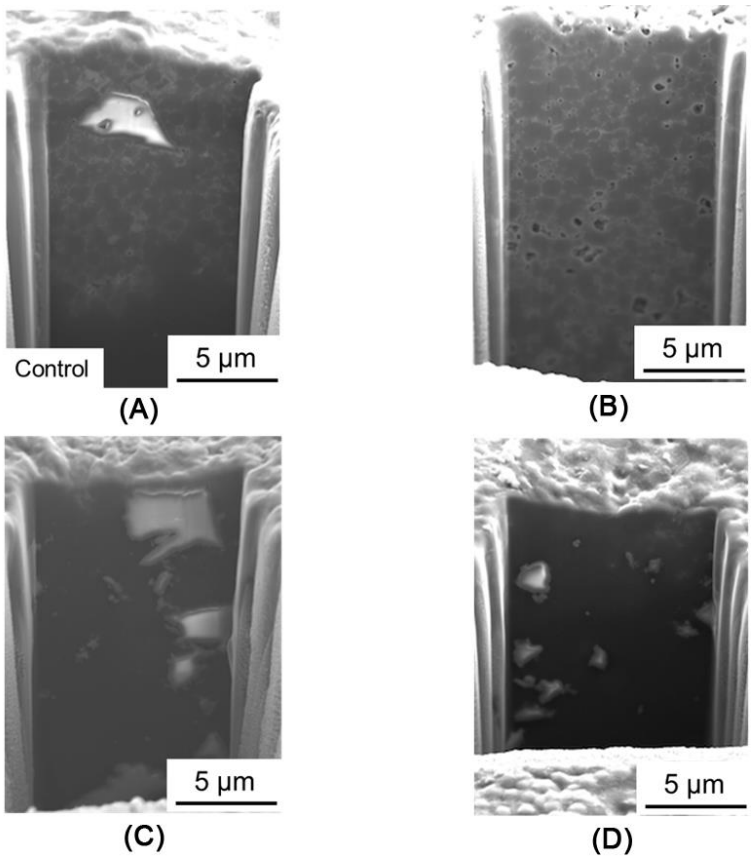

Figure 2-7 FIB-SEM images for Glove A, after leaching at various temperatures: (A) Control, (B) 293 K, (C) 333 K and (D) 353 K.

estimated to occur on the surface of 100 μm in depth. The estimated thickness of surface layer of the protein-removal is consistent with the result shown in Figure 2-7, which represented that no heterogeneous structure was observed from the surface to 20 μm in depth after leaching. The leaching was proved to be effective to remove the proteins from the surface of the rubber glove under specific condition: that is, temperature of higher than 333 K and pH of higher than 7.

2.3 Conclusion

The protein free natural rubber and the leached natural rubber gloves were prepared under various conditions, and their morphologies were observed by TEM and FIB-SEM. The nitrogen content and extractable protein content were 0.000 w/w% and 0.0 μg/g-rubber for the protein free natural rubber and they were 0.175 w/w% and 86 μg/g-rubber for the leached natural rubber glove. It

was found that two times centrifugation was needed for the preparation of the protein free natural rubber. The nanomatrix of the non-rubber components disappeared after removal of the proteins: no heterogeneous nano-structure was observed for the whole portion of the protein free natural rubber and the surface (20 μm depth from the surface) of the leached natural rubber glove, although the structure appeared before removing the proteins.

2.4 Reference

1. Roberts, A.D. Natural Rubber Science and Technology; Oxford University Press: Oxford, **1988**.
2. Fukushima, Y.; Kawahara, S.; Tanaka, Y. *J. Rubb. Res*. **1998**, 1, 154.
3. Kawahara, S.; Kawazura, T.; Sawada, T.; Isono, Y. *Polymer* **2003**, 44, 4527.
4. Pukkate, N.; Yamamoto, Y.; Kawahara, S. *Colloid Polym. Sci*. **2008**, 286, 411.
5. Tanaka, Y. *Rubber Chem. Technol.* **2001**, 74, 355.
6. Nakade, S. *Nippon Gomu Kyokaish* **2009**, 82, 430.
7. Wallerstein, L. US Pat. **1935**, 2,116,089.
8. Wentworth, V. H. Br. Pat. **1941**,551,666.
9. Jennings, W. K. Br. Pat. **1940**, No. 586,830.
10. Khoo, T. C.; Abdul, R. R.; Kamarul, B. B. "Deproteinised Natural Rubber (DPNR)", Malaysian Rubber Board.
11. Eng, A. H. ; Tanaka, Y. ; Gan, S. N. *J. nat. Rubber Res*. **1992**,7, 152.
12. Eng, A. H.; Kawahara, S. Tanaka, Y. *J. nat. Rubber Res*. **1993**, 8, 109.
13. Kawahara, S.; Klinklai, W.; Kuroda, H.; Isono, Y. *Polym. Adv. Technol*. **2004**, 15, 181.
14. Klinklai, W.; Saito, T.; Kawahara, S.; Tashiro, K; Suzuki, Y.; Sakdapipanich, J. T.; Isono,Y. *J. Appl. Polym. Sci*. **2004**, 93, 555.
15. Manroshan, S.; Asurul M.; Mok K. L.; Kawahara S.; Amir-Hashim M. Y.; Booten K. *J. Rubber Res.* **2009**, 12, 1.

16. Tangboriboonrat, P.; Tiyapiboonchaiya, C.; Lertititrakul, C. *Polymer bulletin* **1998**, 41, 601.

17. Blackley, D. C. "Polymer Latices", Springer Science & Business Media, **1997**.

18. Frank W. P.; Anthony A. G. *Methods* **2002**, 27, 77.

19. Maznah K. S.; Baharin A.; Hanafi I.; Azhar M. E.; Mas Rosemal Hakim M. H. *Polymer Testing* **2008**, 27, 1013.

20. Lundberg M.; Wrangsjo K.; Eriksson-Widblom K.; Johansson S. G. O. *Allergy* **1997**, 52, 1057.

21. Field, E. A. *J. Dentistry* **1997**, 25, 209.

22. Food and Drug Administration, U. S. Department of Health and Human Services, "Draft Guidance for Industry and Food and Drug Administration Staff – Recommendations for Labeling Medical Products to Inform Users that the Product or Product Container is not Made with Natural Rubber", Contains Nonbinding Recommendations, 11th March, **2013**.

23. Yamamoto, Y.; Nghia, P. T.; Klinklai, W.; Saito, T.; Kawahara, S. *J. Appl. Polym. Sci*. **2008**, 107, 2329.

24. Chaikumpollert, O.; Yamamoto, Y.; Suchiva, K.; Kawahara, S. *Colloid. Polym*. Sci. **2012**, 290, 331-338.

25. Chaikumpollert, O.; Yamamoto, Y.; Suchiva, K.; Nghia, P. T.; Kawahara, S. *Polym. Adv. Tech.* **2012**, 23, 825-828.

26. Rubber Research Institute of Malaysia. *SMR Bulletin* **1973**, No. 17.

27. ISO12243: **2003**

Chapter 3

Nanomatrix Structure Formed by Graft Copolymerization of Styrene onto Fresh Natural Rubber

3.1 Introduction

Nanomatrix structure is a nano-phase separated structure for a polymeric multi component system, which may provide excellent mechanical, optical and electrical properties. The structure is defined to consist of rubber particles as dispersoid of a major component and polymer nano-layer as matrix of a minor component [1,2]. The size of dispersoid is micrometer in diameter and the size of matrix is nanometer in thickness, as shown in Figure 3-1. It is required to form chemical linkages between the dispersoid and the matrix in order to concrete the nanomatrix structure, because the structure is distinguished from a thermodynamically stable island-matrix structure. The nanomatrix structure is, thus, expected to be applicable to engine mount as a antivibrator, seismic insulator as a high performance damper and proton conductive polymer as a polymer electrolyte membrane, [3-5] which may solve a problem of grain-boundary inherently formed for ordinary cylinder, gyroid and lamellar for block- and graft-copolymers. [6-8] Furthermore, the nanomatrix structure may possess both outstanding properties of the rubber particles and functional properties of the polymer matrix, according to an empirical rule, where the properties of the polymeric multi component system are governed by major component and matrix polymer.

The nanomatrix structure may be formed by graft-copolymerization of any vinyl monomer onto the natural rubber particles in latex stage with radical initiator. The rubber particles may be covered with grafted polymers in latex stage, and the resulting latex may be coagulated to form the nanomatrix

structure. The chemical linkages between the rubber particles and the grafted polymer are required to stabilize the structure in equilibrium state. To form the chemical linkages between the rubber particles and the polymer matrix, high conversion and high grafting efficiency are necessarily requirement for the graft-copolymerization.

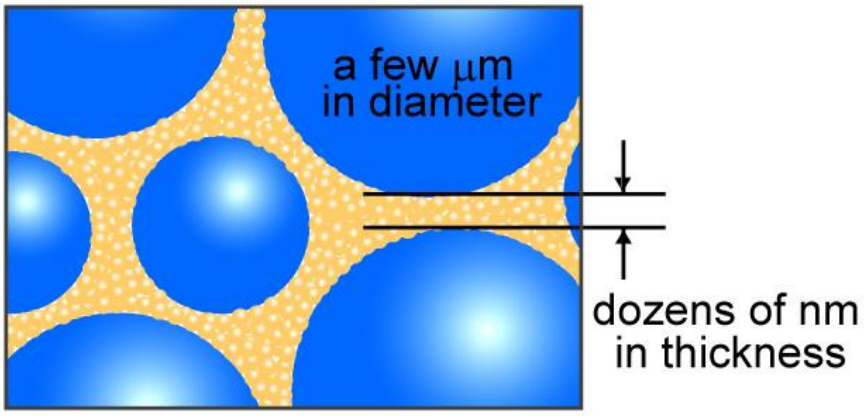

Figure 3-1 Nanomatrix structure

In the previous works[9-11], conversion and grafting efficiency of vinyl monomers for the graft-copolymerization were reported to be quite low, due to side reactions of non-rubber components, i.e., proteins, phospholipids and so forth present in natural rubber. In order to form the nanomatrix structure, therefore, it is necessary to remove the proteins from natural rubber in latex stage before graft-copolymerization.[12, 13] Recently, a novel purification procedure of natural rubber was developed. The nitrogen content (N%) of natural rubber, which was proportional to the protein content, was reduced from about 0.4 to 0.02 w/w% by deproteinization of the latex with urea and surfactant.[14] From the resulting deproteinized natural rubber (DPNR) latex, a graft-copolymer of DPNR with polystyrene (DPNR-*graft*-PS), which possessed the nanomatrix structure was prepared.[1, 2, 12, 13] Mechanical properties of natural rubber were improved by forming the nanomatrix structure; for example, a value of stress at break of the DPNR-*graft*-PS with the nanomatrix structure was about 16.5 MPa, which was

about 9 times as large as that of DPNR. Further improvement is expected for the DPNR-*graft*-PS with the nanomatrix structure, when the proteins were completely removed from natural rubber. Lately, the nitrogen content (N%) of natural rubber was reduced to 0.004 wt% or lower, using fresh natural rubber latex as a source [15], which was isolated from *Hevea brasiliensis* just after tapping. The decrease in nitrogen content enables to enhance the conversion and grafting efficiency for the graft-copolymerization of the monomer onto natural rubber to prepare the DPNR-*graft*-PS without the side reaction.

In the present study, an attempt to achieve outstanding properties of natural rubber with the nanomatrix structure was performed by graft-copolymerization of styrene onto fresh DPNR with *tert*-butyl hydroperoxide/tetraethylenepentamine (TBHPO/TEPA) as an initiator in latex stage. Structure and morphology of the graft-copolymer of fresh DPNR with PS were analyzed by NMR spectroscopy and transmission electron microscopy (TEM). Mechanical properties of the fresh DPNR-*graft*-PS were investigated in relation to the structure and morphology.

3.2 Experimental

3.2.1 Materials

Latex used in this study was the fresh natural rubber latex provided by Thai Rubber Latex Corporation (Thailand), which contained ammonia as a preservative. High ammonia natural rubber (HANR) latex was purchased from Golden Hope, Malaysia, which contained ammonia, tetramethylthiuram disulfide (TMTD) and ZnO. Sodium dodecyl sulfate (SDS), TBHPO and TEPA were purchased from Kishida Chemical Co., Ltd. Styrene (99%) as a monomer was purchased from Tokyo Chemical Industry Co., Ltd.

3.2.2 Deproteinization of natural rubber

Preparation of fresh DPNR latex was made by incubation of the fresh natural rubber latex with 0.1 w/w% urea in the presence of 1 w/w% SDS at 303 K for 1 h followed by centrifugation at 10^4 *g*. The cream fraction was redispersed in 0.5 w/w% SDS solution to make 30 w/w% dry rubber content (DRC) latex and it was washed twice by centrifugation. The DRC and SDS content of the fresh DPNR latex was adjusted to 30 w/w% and 0.1 w/w%, respectively.

3.2.3 Graft-copolymerization

Graft-copolymerization of styrene onto the fresh DPNR latex was carried out with TBHPO/TEPA as an initiator. The fresh DPNR latex was charged with N_2 gas for 1 h at 303 K. The initiator and monomer were added to the latex, respectively. The reaction was carried out by stirring the latex at about 400 rpm for 2 h at 303 K. The unreacted monomer was removed with a rotary evaporator under reduced pressure. As-cast film of the resulting graft-copolymer (gross polymer) was prepared by casting the latex onto Petri dish and it was dried under reduced pressure at an ambient temperature for more than a week. Free polystyrene in the film was removed by extraction with acetone/2-butanone 3:1 mixture with a Soxhlet apparatus for 24 h under nitrogen atmosphere in the dark and it was dried under reduced pressure for a week.

3.2.4 Characterization

Proton Nuclear Magnetic Resonance (^{1}H-NMR) measurements were carried out at 323 K with a JEOL AL-400 NMR spectrometer at pulse repetition time of 7 s. Morphology observation for the

graft-copolymer was made with a transmission electron microscope (TEM), JEOL JEM-2100, at accelerating voltage of 200 kV. The ultra-thin sections of the graft-copolymer were prepared by a Reichert-Nissei FC S Ultra-microtome at a temperature lower than T_g of NR. The thin sections were stained with OsO_4. The tensile properties of fresh DPNR-*graft*-PS were measured with an Instron universal tester 3365 at room temperature. Film specimen was prepared by casting the latex into Petri dish followed by drying under reduced pressure at 323 K. The test was made by gripping ends of a dumbbell type specimen with 12 mm of gauge length and 1 mm of thickness, according to JIS K6251 No.7. The crosshead speed was 200 mm/min.

3.3 Results and Discussion

3.3.1 Characterization of graft-copolymer

Figure 3-2 shows a typical ^{1}H-NMR spectra for fresh DPNR and the fresh DPNR-*graft*-PS at the styrene feed of 1.5 mol/kg-rubber. In the spectrum of fresh DPNR, three major signals appeared at 1.76, 2.10 and 5.13 ppm, which were assigned to methyl, methylene and unsaturated methyne protons of isoprene units, respectively. After graft-copolymerization of styrene, broad signals which was characteristic for phenyl proton of styrene units appeared at 6-7 ppm, whose intensity was dependent upon the feed of styrene monomer; that is, the higher the monomer concentration, the higher the intensity of the resonance peak at 6-7 ppm. These evidences indicated that polystyrene was successfully polymerized in the graft-copolymerization.

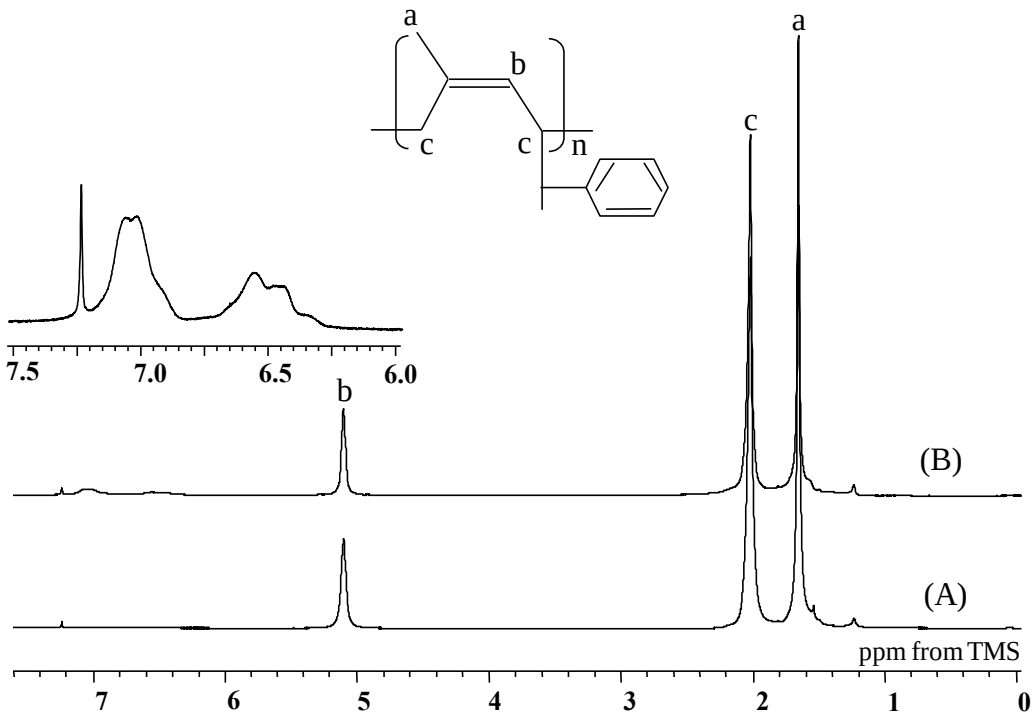

Figure 3-2 ^{1}H-NMR spectra for (A)-DPNR and (B)-Fresh DPNR

In order to investigate the initiator and monomer concentration on the graft copolymerization, styrene content in fresh DPNR-*graft*-PS and conversion of styrene were estimated according to the expression as follows:

$$\text{Styrene content (\%)} = \frac{\text{Weight of polystyrene in gross polymer}}{\text{Weight of gross polymer}} \times 100 \qquad (3\text{-}1)$$

$$\text{Styrene conversion (\%)} = \frac{\text{Weight of polystyrene in gross polymer}}{\text{Weight of styrene feed}} \times 100 \qquad (3\text{-}2)$$

where weight of polystyrene in gross polymer, weight of styrene feed and the weight of polystyrene in gross polymer were estimated by gravimetric method, since the styrene content estimated from a ratio of signal intensity for phenyl proton of styrene units to methyl proton of *cis*-1,4-isoprene units was quite similar to that estimated from gravimetric method, as reported in the previous study.[1]

To determine how much the polystyrene was grafted onto NR particles, grafting efficiency was estimated for the fresh DPNR-*graft*-PS. To estimate grafting efficiency, free polystyrene was removed from the mixture with the graft-copolymer by using Soxhlet extraction with acetone/2-butanone 3:1 mixture, whose molecular weight was about 10,000 as reported in the previous study. [12] The grafting efficiency was estimated from weight of polystyrene linking to natural rubber and weight of polystyrene produced during graft-copolymerization, as shown in the following expression:

$$\text{Grafting efficiency}\,(\%) = \frac{\text{Weight of polystyrene linking to natural rubber}}{\text{Weight of polystyrene produced during graft - copolymerization}} \times 100 \qquad (3\text{-}3)$$

To determine the suitable condition for the graft-copolymerization, plots of conversion and grafting efficiency of styrene *versus* initiator concentration were made as shown in Figure 3-2. The conversion and grafting efficiency of styrene was dependent upon initiator concentration, and their values were the highest, i.e. 98 and 80 mol%, respectively, at 3.3×10^{-2} mol/kg-rubber of initiator. A suitable initiator concentration was, thus, determined to be 3.3×10^{-2} mol/kg-rubber.

In the previous work, values of conversion and grafting efficiency of styrene were reported to be 90 and 96 mol%, respectively, for the graft-copolymerization of styrene onto DPNR prepared from HANR in latex stage.[1] The difference in the conversion between fresh DPNR and DPNR, which are prepared from fresh natural rubber and HANR, respectively, may be attributed to the residual amount of proteins present in the rubbers. For instance, the conversion of fresh DPNR (N%=0.004 w/w% or lower) was higher than that of DPNR (N%=0.02 w/w%) due to the side reaction with the residual proteins. In contrast, the grafting efficiency decreased with decreasing the nitrogen content; that is, the

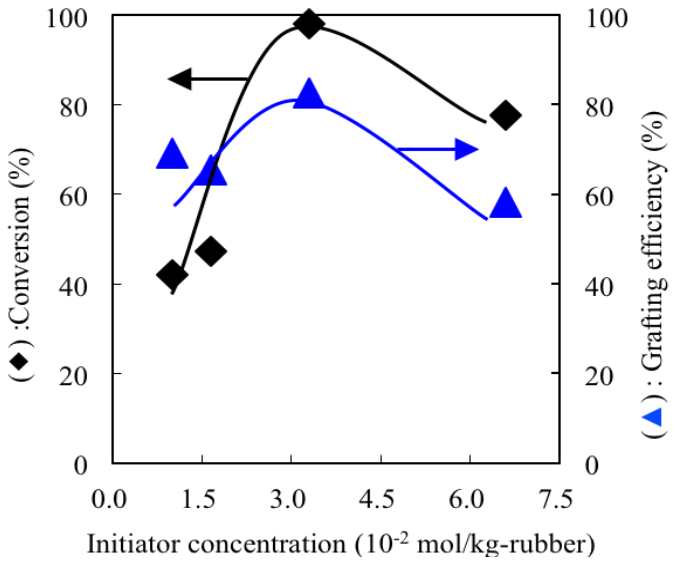

Figure 3-3 Initiator concentration dependence of
(◆): conversion, (▲): grafting efficiency of styrene

higher the purity, the lower the grafting efficiency. The decrease in the grafting efficiency is inconsistent with the increase in the conversion with purity. This may be explained to be due to the homo-polymerization of styrene occurring in aqueous phase, since the radical concentration increased in not only surface of the rubber particles but also aqueous phase, which are dependent upon the residual amount of the proteins.

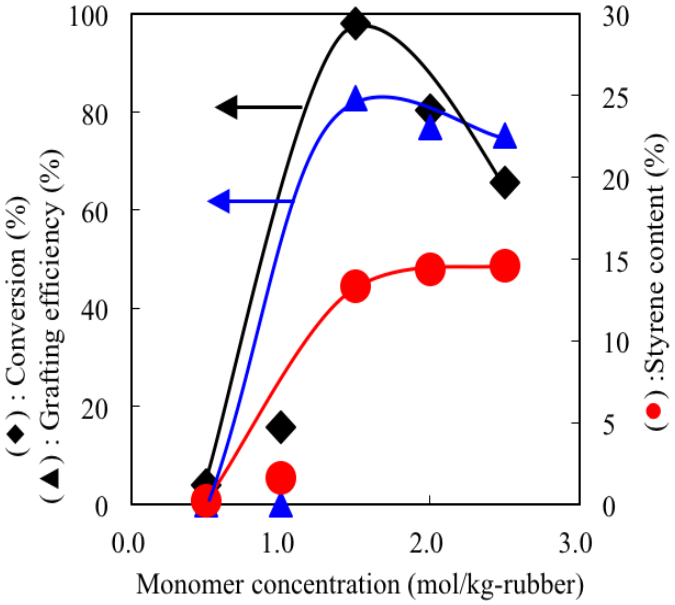

Figure 3-4 Monomer concentration dependence of (◆): conversion,
(▲): grafting efficiency and (●): styrene content

Figure 3-4 shows the dependence of the conversion, the grafting efficiency and styrene content upon styrene concentration. The maximum value of conversion and grafting efficiency was achieved at 1.5 mol/kg-rubber of monomer. This may be attributed to deactivation and chain transfer of radicals due to less and large amounts of styrene, respectively. In contrast, the styrene content at 1.5 mol/kg-rubber of monomer increased as the concentration of styrene increased. This demonstrates that a suitable monomer concentration is 1.5 mol/kg-rubber for the high conversion and grafting-efficiency.

3.3.2 Morphology

The styrene unit content of the rubber was an important factor to form the nanomatrix structure. In the previous study, the morphology of the DPNR-*graft*-PS was found to be dependent upon styrene unit content, which was prepared from HANR; that is, the nanomatrix structure was formed at the styrene unit contents of 12.3 mol%, whereas PS nano-particles were individually dispersed near the interface between the rubber particles at the styrene unit contents of 1.2 and 6.7 mol%. The dependency of the morphology on the styrene unit content may be almost similar for fresh DPNR; hence, the nanomatrix structure is formed for fresh DPNR with more than 10 mol% styrene.[1] In the present study, thus, fresh DPNR-*graft*-PS containing 13.0 mol% styrene unit content was prepared. Figure 3-4 shows TEM photographs for fresh DPNR-*graft*-PS, prepared under the suitable condition, in which a gloomy domain represents natural rubber and a bright domain represents polystyrene. The natural rubber particles of about 1 μm in average diameter were dispersed in polystyrene matrix of 10-30 nm in thickness. This demonstrates that the nanomatrix structure was formed by graft-copolymerization of styrene onto the fresh DPNR under the suitable condition.

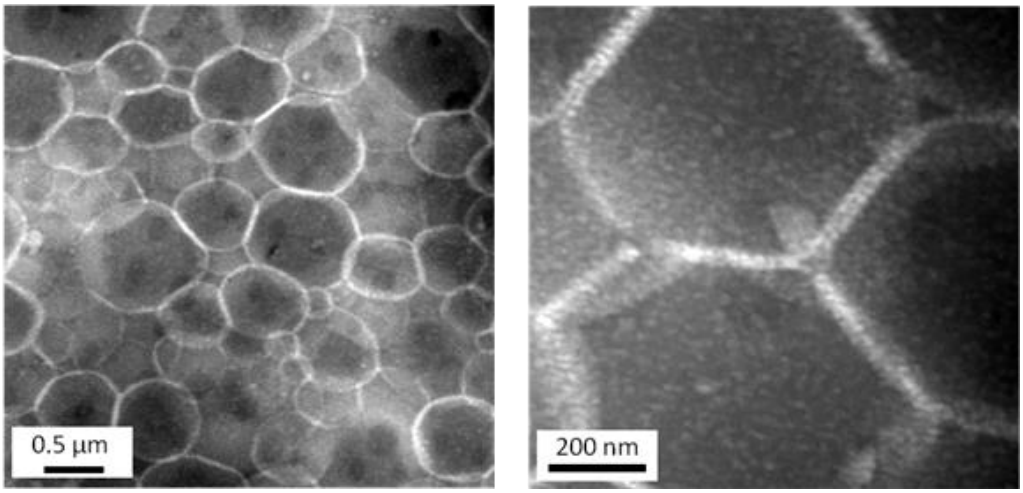

(a) (b)

Figure 3-5 TEM photographs for nanomatrix structure formed with fresh DPNR under suitable condition: (a) ×5000, (b) ×20000.

3.3.3 Mechanical Properties

Figure 3-6 shows stress–strain curves for fresh NR, HANR, fresh DPNR-*graft*-PS and DPNR-*graft*-PS, which were unvulcanized rubbers. Styrene content of both fresh DPNR-*graft*-PS and DPNR-*graft*-PS was about 13 mol%, whose value is known to result in the outstanding tensile properties. [1] Values of stress at break of fresh NR and HANR were about 3 MPa, whereas those of fresh DPNR-*graft*-PS and DPNR-*graft*-PS were 21 MPa and 17 MPa, respectively. This remarkable increase in the stress at break may be explained to be due to the formation of the nanomatrix structure, which was shown in TEM photographs. Furthermore, the value of stress at break of fresh DPNR-*graft*-PS was found to be larger than that of DPNR-*graft*-PS. The conversions for graft-copolymerization of styrene onto fresh DPNR and DPNR were 98 mol% and 90 mol%, respectively, since the nitrogen content of fresh DPNR was lower than that of DPNR. Moreover, the values of the grafting efficiency for graft-copolymerization of styrene onto fresh DPNR and DPNR were 80 mol% and 96 mol%, respectively. The difference in the stress-strain curve and the tensile properties may be related to the grafting efficiency. For instance, the initial stress, i.e., stress at strain of 1, is dependent upon the

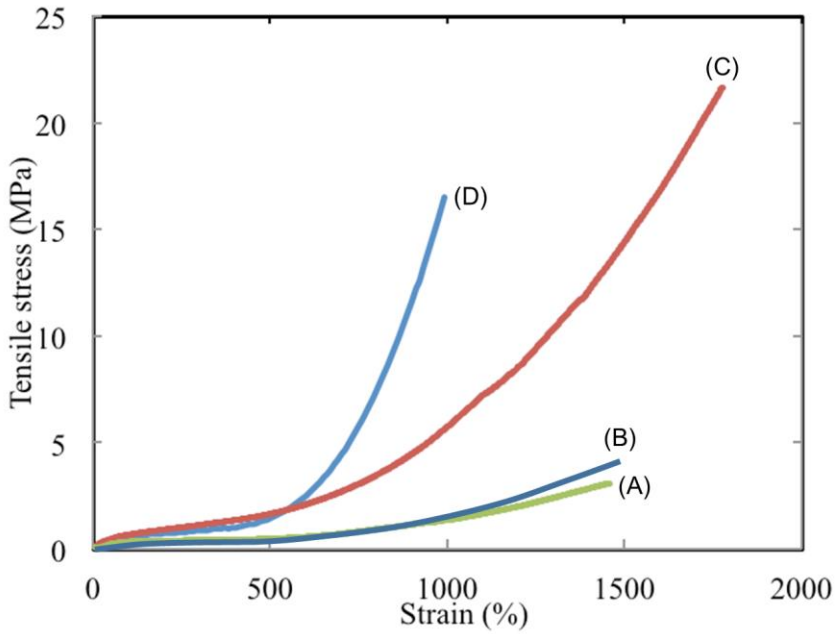

Figure 3-6 Stress-strain curves for (A) fresh NR, (B) HANR, (C) fresh DPNR-*graft*-PS and (D) DPNR-*graft*-PS.

amount of PS, whereas the tensile properties are dependent upon the effective amount of PS that is proportional to grafting efficiency, i.e., number of physical crosslinking junctions. As is clearly seen in Figure 3-5, the value of the initial stress of fresh DPNR-*graft*-PS was similar to that of DPNR-*graft*-PS, whereas the values of stress at break and elongation at break of the fresh DPNR-graft-PS were larger than those of DPNR-*graft*-PS. The same values of the initial stress may be attributed to the same styrene unit content of the grafted natural rubbers, i.e., about 13 mol%. In contrast, the larger values of stress at break and elongation at break may be explained to be due to the difference in the effective amount of PS. The effective amount of PS for fresh DPNR-*graft*-PS is smaller than that for DPNR-*graft*-PS; that is, the effective physical crosslink density of fresh DPNR-*graft*-PS is lower than that of DPNR-*graft*-PS. The lower physical crosslink density may result in the increases in the stress at break and elongation at break, as in the case of the vulcanized natural rubber. The slight deference in the grafting efficiency may make a big difference in tensile properties of the products. The very high tensile properties without chemical crosslinking junctions are a

strong evidence that the nanomatrix structure plays an important role in the outstanding mechanical properties for natural rubber.

3.4 Conclusion

Graft-copolymerization of styrene onto fresh DPNR was carried out with *tert*-butyl hydroperoxide/tetraethylenepentamine as an initiator in latex stage. The highest styrene conversion of 98 mol% and the grafting efficiency of 80 mol% were achieved at 1.5 mol/kg-rubber of styrene and 3.3×10^{-2} mol/kg-rubber of initiator. The nanomatrix structure was observed in TEM photographs of the fresh DPNR-*graft*-PS. The value of the stress at break of the fresh DPNR-*graft*-PS was 21 MPa, in spite of no crosslinking.

3.5 References

1. Kawahara, S.; Kawazura, T.; T. Sawada, Isono, Y. *Polymer* **2003**, 44, 4527.
2. Kawahara, S.; Yamamoto, Y.; Fujii, S.; Isono, Y.; Niihara, K.; Jinnai, H.; Nishioka, H.; Takaoka, A. *Macromolecules* **2008**, 41, 4510.
3. Kado, N.; Suksawad, P.; Akabori, K.; Yamamoto, Y.; Kawahara, S. *Kautschuk Gummi Kunststoffe* **2012**, 65, 26.
4. Suksawad, P.; Kosugi, K;. Yamamoto, Y.; Akabori, K.; Kuroda, H.; Kawahara, S. *J. Appl. Polym. Sci.* **2011**, 122, 2403.
5. Kawahara, S.; Suksawad, P.; Yamamoto, Y.; Kuroda, H. *Macromolecules* **2009**, 42, 8557.
6. Jinnai, H.; Sawa, K.; Nishi, T. *Macromolecule* **2006**, 39, 5815.

7. Jinnai, H.; Yasuda, K.; Nishi, T. *Macromol. Symp.* **2006**, 245, 170.

8. Kato, M.; Ito, T.; Aoyama, Y.; Sawa, K.; Kaneko, T.; Kawase, N.; Jinnai, H. *J. Polym. Sci. Part B: Polym. Phy.* **2007**, 45, 677.

9. Nakason, C.; Kaesaman, A.; Yimwan, N. *J. Appl. Polym. Sci.* **2003**, 87, 68.

10. Arayapranee, W.; Rempel, G. L. *J. Appl. Polym. Sci.* **2008**, 110, 2475.

11. Bloomfield, G. F.; Merrett, F. M. *Rubber World* **1954**, 131, 358.

12. Pukkate, N.; Kitai, T.; Yamamoto, Y.; T. Kawazura, J. Sakdapipanich, S. Kawahara, *Eur. Polym. J.* **2007**, 43, 3208.

13. Pukkate, N.; Yamamoto, Y.; Kawahara, S. *Colloid Polym. Sci.* **2008**, 286, 411.

14. Kawahara, S.; Klinklai, W.; Kuroda, H.; Isono, Y. *Polym. Adv. Technol.* **2004**, 15, 181.

15. Klinklai, W.; Saito, T.; Kawahara, S.; Tashiro, K.; Suzuki, Y.; Sakdapipanich, J. T. *J. Appl. Polym. Sci.* **2004**, 93, 555.

Chapter 4

FIB Processing for Natural Rubber with Nanomatrix Structure

4.1 Introduction

Hard, soft rubber, which results in increase in both dynamic storage modulus and dynamic loss modulus with increasing frequency in rubbery plateau region, attracts much attention as a novel viscoelastic material. This may be distinguished from ordinary rubbers as a soft material and ordinary plastics as a hard material. Recently, the hard, soft rubber with inordinate dynamic viscoelastic properties were prepared by means of a modulation of nano-phase separated structure; that is, both dynamic storage modulus and dynamic loss modulus of natural rubber with the nanomatrix structure increased in the rubbery plateau region as displacement frequency rose. It is, thus, hypothesized that the inordinate dynamic viscoelastic properties are attributed to the nanomatrix structure. In order to elucidate the relationship between the nanomatrix structure and the dynamic viscoelastic properties, It is necessary to develop a new technique to observe the morphology of natural rubber with the nanomatrix structure on the basis of a novel concept.

Focused ion beam (FIB) processing is a powerful technique to form a smooth cross sectional area of materials having nano-structure, because it is performed by irradiating Ga ion laser beam into the materials[1]. The FIB processing is, thus, distinguished from the conventional ultra-fine processing with a microtome[2-5], which causes shear deformation of the nano-structure of the materials due to a force loaded on them to prepare an ultra-thin section with glass or diamond knives. Thus, a physical contact of the materials with the knives may be prevented, in order to maintain a spatial position of the nano-structure of the materials, as long as the FIB processing is adapted[6]. The FIB processing is, thus, expected to be indispensable for the observation of the morphology through electron tomography method[7,8], which provides 3-dimensional (3D) image of the nano-structure.

The requirement for the FIB processing is *in-situ* observation of the cross sectional area of the materials in order to obtain the fine ultra-thin section. A combination of field emission scanning electron microscope (FE-SEM) and FIB microscope[9,10] may meet our need; for instance, the surface obtained during the FIB processing is observed with FE-SEM. Furthermore, the FIB-SEM has been used for obtaining 3D SEM images after reconstructing 2-dimensional (2D) images obtained by observing the surfaces of the materials[11-14], which are etched with the FIB at each interval of less than 100 nm.

In the last decade, the FIB processing has been extensively carried out for inorganic materials such as ceramics, metals and so forth[15,16]. The ultra-thin sections of the inorganic materials were well prepared by the FIB processing and they were subjected to transmission electron microscope (TEM) observation, in order to obtain sophisticated images of crystalline structures[17]. In contrast, for the organic materials, few works were reported on the FIB processing to prepare the ultra-thin sections. Morphology of the solar cells[18], polymer light emitting diodes[19] and block copolymer thin films[20] was observed by TEM, in which the ultra-thin sections were prepared by the FIB processing. However, recently, damages of the materials during the FIB processing have been found to be a serious issue for the preparation of the ultra-thin sections through the FIB processing[21]. For instance, in the case of the inorganic materials, two types of processing damages were reported: that is, the formation of amorphous layers that contain implanted Ga atoms and the precipitation of particles due to deterioration, i.e. melting, of surface with heat during the FIB processing. These damages were cured by micro-sampling method and cool ion milling method. On the other hand, more serious damages were reported for the organic materials. Sometimes, the etched surfaces were scorched during the FIB processing due to over-heating with the FIB at local portion of the area. The FIB processing has been performed after staining the organic materials with osmium tetroxide (OsO_4) at lower temperature, in order to prevent charge-up with the FIB [4,21].

In the previous work, a graft-copolymer of deproteinized natural rubber and polystyrene

(DPNR-*graft*-PS) with the nanomatrix structure were prepared, which consists of deproteinized natural rubber particles of about 1 μm in average diameter and polystyrene nanomatrix of about 15 nm in thickness[22]. 3D images of DPNR-*graft*-PS was obtained with the nanomatrix structure through FIB-SEM and electron tomography observations[23]. It was found that the polystyrene nanomatrix was not continuous; hence, the value of the Young's modulus of the DPNR-*graft*-PS was smaller than expected one. In addition, the images obtained by the electron tomography method were unclear, because the ultra-thin sections were prepared by using cryo-microtome with the glass knife. The relationship between the structure and properties of DPNR-*graft*-PS with the nanomatrix structure still remains ambiguous.

In the present work, an attempt to prepare the ultra-thin sections of DPNR-*graft*-PS was made by the FIB processing with the FIB-SEM in order to elucidate the relationship the nanomatrix structure and the dynamic viscoelastic properties. First, natural rubber with the nanomatrix structure was prepared to confirm the finding that both dynamic storage modulus and dynamic loss modulus of natural rubber with the nanomatrix structure increased in the rubbery plateau region as displacement frequency rose. Second, the 3D image was obtained by reconstructing 2D images of the FIB-SEM. Conditions to prepare the ultra-thin sections were investigated for the FIB processing. The observations of the nanomatrix structure were performed by TEM and electron tomography method for DPNR-*graft*-PS, where the nanomatrix structure is defined to consist of natural rubber micro-particles and polystyrene nanomatrix.

4.2 Experimental procedure

4.2.1 Sample preparation

Natural rubber latex used in the present study was commercial high-ammonia natural rubber latex. The incubation of the latex was made with 0.1 w/w% urea in the presence of 1 w/w% sodium dodecyl sulfate (SDS) at 303 K followed by centrifugation at 10,000 rpm. Cream fraction was

re-dispersed in 1 w/w% SDS to make 30 w/w% dry rubber content (DRC) latex and it was washed twice by centrifugation to prepare deproteinized natural rubber (DPNR) latex[24]. The DPNR latex was diluted with distilled water to adjust 10 w/w% DRC and concentration of SDS was adjusted to 0.1 w/w%.

Graft-copolymerization of styrene onto DPNR was carried out in latex stage with *tert*-butyl hydroperoxide / tetraethylene pentamine as an initiator. The DPNR latex was charged with N_2 gas for 1 hour at 303 K. The initiator of 3.3×10^{-2} mol/kg-rubber and styrene of 1.5 mol/kg-rubber were added to the latex, respectively. The reaction was performed by stirring the latex at about 400 rpm for 2 hours at 303 K. The unreacted styrene was removed by using a rotary evaporator under reduced pressure. A film specimen of the grafted natural rubber was prepared by dipping the glass tube into the reacted latex and it was dried under reduced pressure at ambient temperature for more than a week.

4.2.2 Observation

Observation of morphology of the grafted natural rubber was made with a TEM, JEOL JEM-2100 at accelerating voltage of 200 kV and FIB-SEM, SII SMI-3050SE at accelerating voltage of 3 kV. The FIB-SEM was also used to make a ultra-thin section of grafted natural rubber according to the literature[4]. The ultra-thin section of the graft-copolymer was prepared by a Sorvall Instruments MT6000 Ultra Microtome at 193 K. The thin sections were stained with OsO_4, after annealing the section at 353 K for 30 min.

3D images were obtained by reconstructing more than 100 2D images, i.e. TEM images. The sections with *ca.* 100 nm thick were prepared and stained with Ruthenium tetroxide (RuO_4) and OsO_4 in the similar way as described above. A special specimen holder that enables us to rotate the section up to -70° - +70° was used to take a high resolution 3D image. Tilt angular range in the particular experiment was -59° to +63° with an increment of 1°, which was aligned and reconstructed according to the protocol described in ref.[25]

4.3 Results and Discussion

Figure 4-1 shows a plot of storage modulus *versus* displacement frequency in the rubbery plateau region for natural rubber and natural rubber with the nanomatrix structure (DPNR-*graft*-PS). The value of the storage modulus of natural rubber and DPNR-*graft*-PS increased as the frequency increased. The increase in the value of the storage modulus may be explained to be due to the viscoelastic properties of the rubbers in the rubbery plateau region; the higher the frequency, the higher the storage modulus. The rubbers are more elastic in the high frequency region.

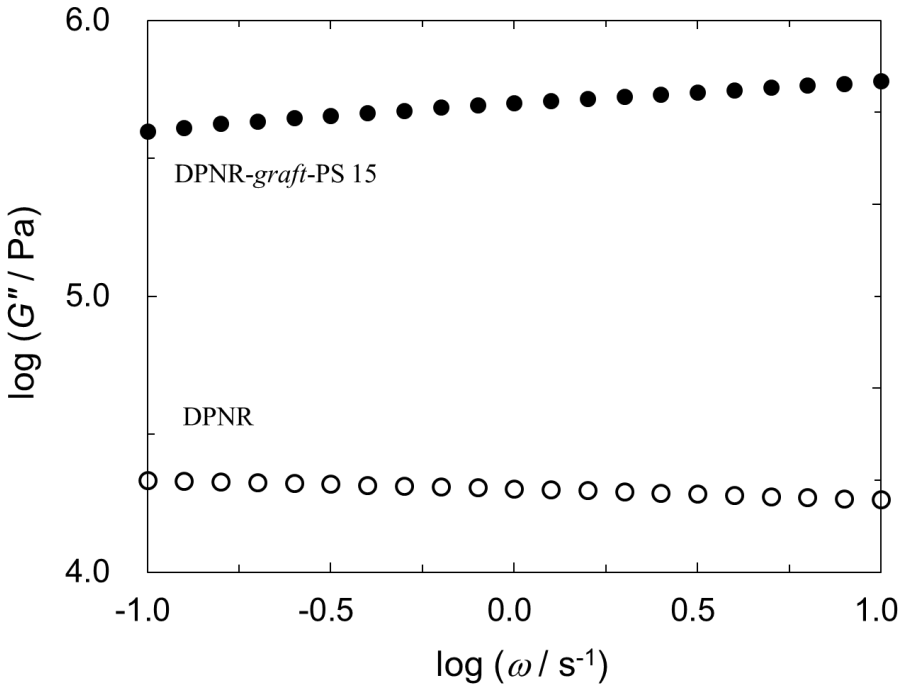

Figure 4-1 Logarithmic plot of storage modulus *versus* displacement frequency in the rubbery plateau region for natural rubber and natural rubber with the nanomatrix structure (DPNR-*graft*-PS). Open circles represent natural rubber and closed circles represent DPNR-*graft*-PS.

Figure 4-2 shows a plot of loss modulus *versus* displacement frequency in the rubbery plateau region for natural rubber and DPNR-*graft*-PS. The value of the loss modulus of natural rubber decreased as the frequency increased. In contrast, the value of the loss modulus of DPNR-*graft*-PS increased, as the frequency increased. The decrease in the value of the loss modulus in the high

frequency region may correspond to increase in the value of the storage modulus, since the elasticity is inconsistent with the viscosity. However, it is quite difficult to explain the fact that the values of both loss modulus and storage modulus of DPNR-*graft*-PS increase as the frequency increases. It is necessary to explain the reason why the elasticity and viscosity increase with increasing the frequency in the view point of the morphology. Thus, an attempt to develop a new technique to observe the nanomatrix structure in nano-meteric scale was made in the present study.

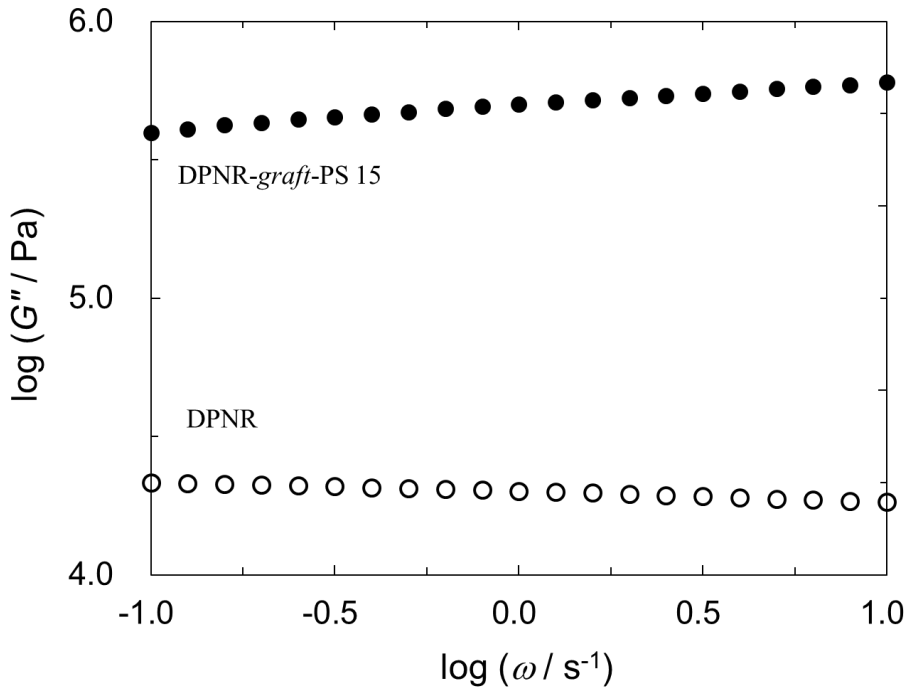

Figure 4-2 Logarithmic plot of loss modulus *versus* displacement frequency in the rubbery plateau region for natural rubber and natural rubber with the nanomatrix structure (DPNR-*graft*-PS). Open circles represent natural rubber and closed circles represent DPNR-*graft*-PS.

Figure 4-3 shows FE-SEM image of the etched surface of the DPNR-*graft*-PS, in which carbon coating was performed to prevent damage of an edge of the surface etched with the Ga ion beam. The rough surface of the coated carbon may be explained to be due to non-uniform deposition of the carbon on the DPNR-*graft*-PS. The image was taken in an oblique direction by FE-SEM, because the film specimen of the DPNR-*graft*-PS, placed on a flat plate in a chamber, was perpendicularly etched with the FIB and it was observed in the oblique direction. The bright domains

represent polystyrene (PS) and dark domains represent deproteinized natural rubber (DPNR) [24], since it was stained with OsO_4. The contrast of the domains was sufficient to take the FE-SEM image, since the DPNR-*graft*-PS was stained with OsO_4 for more than 7 days, which prevented the damage of the DPNR-*graft*-PS during FIB processing. In general, it is known that insufficient staining (short time) may result in a significant damage of the DPNR-*graft*-PS due to local heating by charging up a specimen during FIB processing, whereas over-staining (long time) may lead to less contrast because OsO_4 goes into not only DPNR phase but also PS phase (over-staining). Thus, a suitable time was determined to be 7 days to stain the DPNR-*graft*-PS with OsO_4. In the image, the sample surface was rather bright and rough, which was assigned to polystyrene. This assignment was proved by the image of etched surface; for instance, the bright domains existed on the sample surface and the matrix, because the film specimen was prepared by coagulation of DPNR-*graft*-PS latex, in which natural rubber particles of about 1 μm in average diameter, covered with PS layer, were dispersed in water.

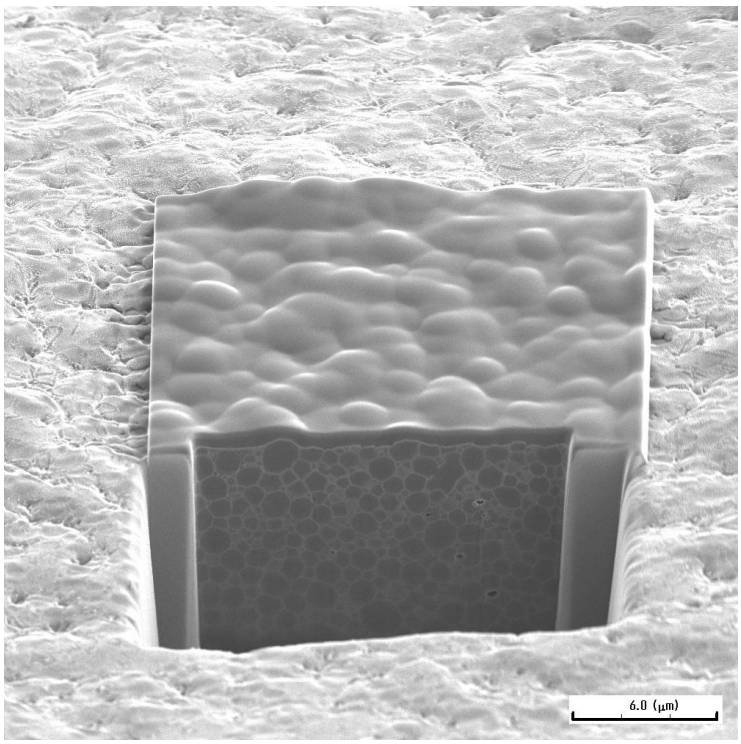

Figure 4-3 FE-SEM image of the etched surface of the DPNR-*graft*-PS.

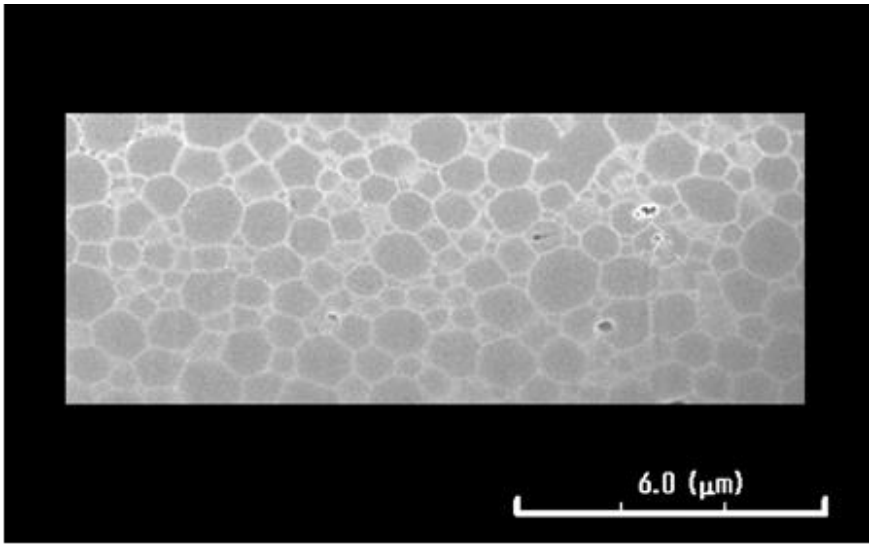

Figure 4-4 Expanded 2D FE-SEM image of the etched surface.

Expanded image of the etched surface is shown in Figure 4-4. The edge of the etched surface shown at top in Figure 4-4 was situated rather front compared with a bottom bed; hence, the magnification of the top edge is a little bit higher than that of the bottom bed. This may be explained to be due to the oblique angle between an electron-gun and sample surface. The image was, thus, modified by correction of voxel dimensions for oblique-angle imaging (55^{o}) and overlay correction for x-y drift. The absolute dimensions in the x-direction are obtained from a calibrated FIB magnification scale. Because of oblique FE-SEM imaging at an angle of 55^{o}, distances in the y-direction have to be corrected in terms of projection effects using $y' = y \sin(55^{o})$.

The corrected 2D FE-SEM image of the DPNR-*graft*-PS is shown in Figure 4-5, in which a contrast of the image is extensively enhanced to distinguish the bright PS domains from the gloomy DPNR domains. The bright PS nanomatrix was quite distinct near the top of the image, whereas this turned into ambiguous near the bottom. This is attributed to a difference between distances of secondary electron detector from top and bottom of the etched surface, due to the oblique angle; the lower the height from the top of the etched surface along to the Y-axis, the worse was the focus. Thus, the scanning region was limited in Y-direction, which resulted in the rectangular image in Figure 4-5.

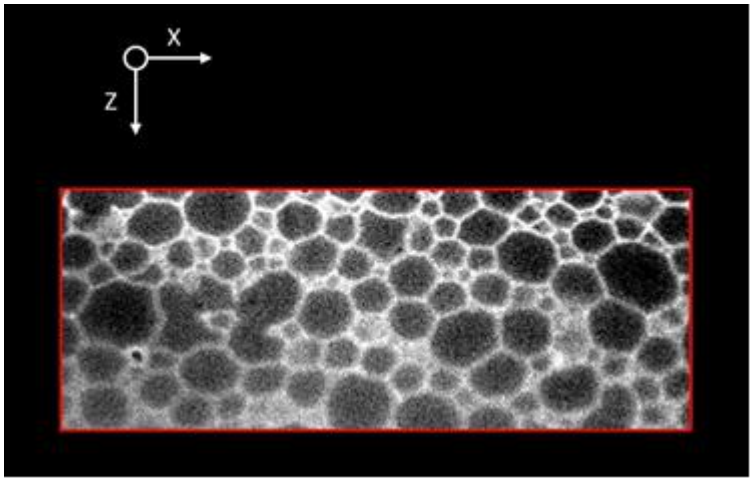

Figure 4-5 Corrected 2D FE-SEM image of the DPNR-graft-PS. The absolute dimensions in the x-direction are obtained from a calibrated FIB magnification scale.

The image was almost similar to that obtained by TEM observation (shown below in Figure 4-6), suggesting that the structure of the DPNR-*graft*-PS was not damaged by FIB processing.

Figure 4-6 shows TEM image for the ultra-thin section of the DPNR-*graft*-PS prepared by FIB processing, in which the dark domains represent PS and the bright domains represent DPNR, because the ultra-thin section was stained with RuO_4. The image of the ultra-thin section was taken after putting it on the grid substrate. The dimension of the ultra-thin section, thus obtained, was about 6 μm×9 μm×54 nm. The thickness of 54 nm may be a remarkable virtue of the FIB processing, because the thickness of the ultra-thin section prepared with the cryo-microtome is more than 100 nm in an ordinary circumstance.

Furthermore, in Figure 4-6, several damages of the ultra-thin section were found in the image: for instance, curled edge of the ultra-thin section and white spot as a void due to over-heating with the FIB at local portion of the area during the FIB processing. This may be explained to be due to charge-up caused by less staining with RuO_4; hence, the nanomatrix structure was not seen near the curled edge and white spot.

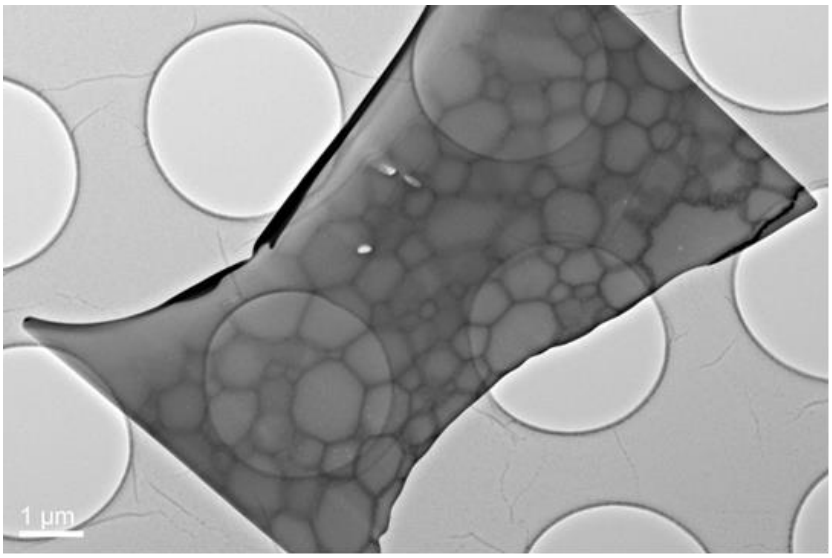

Figure 4-6 TEM image for the ultra-thin section of the DPNR-graft-PS prepared by FIB processing.

TEM image for the ultra-thin section of the DPNR-*graft*-PS prepared with the cryo-microtome equipped with the glass knife is shown in Figure 4-7. The bright domains represent PS and the dark domains represent DPNR, because the ultra-thin section was stained with OsO_4. The dimension of the ultra-thin section obtained with the cryo-microtome was significantly larger, when it was compared with that obtained by FIB processing. The thickness and width of the ultra-thin section were about 130 nm and at least 20 μm, respectively. In the TEM image, some voids were found in the ultra-thin section as a brilliant domain due to charge-up; more exactly, they existed on the right hand side of the ultra-thin section. The voids were considered to be formed by cutting with the knife, because they existed with several non-periodic waves in the ultra-thin section. Perhaps, the film specimen may be deformed, when the force was applied to prepare the ultra-thin section. The cavitation may occur in the nanomatrix to form the voids due to weak attractive force between the PS nano-particles and natural rubber. The formation of the voids may be one of the disadvantages of the cryo-microtome.

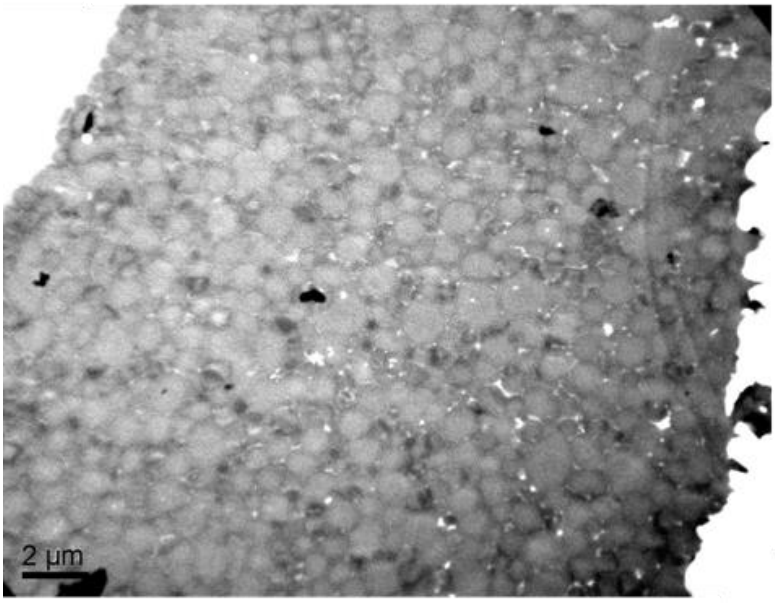

Figure 4-7 TEM image for the ultra-thin section of the DPNR-*graft*-PS prepared with the cryo-microtome equipped with the glass knife.

Disadvantage was also recognized for the FIB processing. Figure 4-8 shows TEM image for the ultra-thin section of the DPNR-*graft*-PS prepared by the FIB processing, which is an expanded image of a part of the ultra-thin section shown in Figure 4-6. In the TEM image was found a sharp crack (marked as white arrow), whose width and length were about 10 nm and 6.6 μm, respectively.

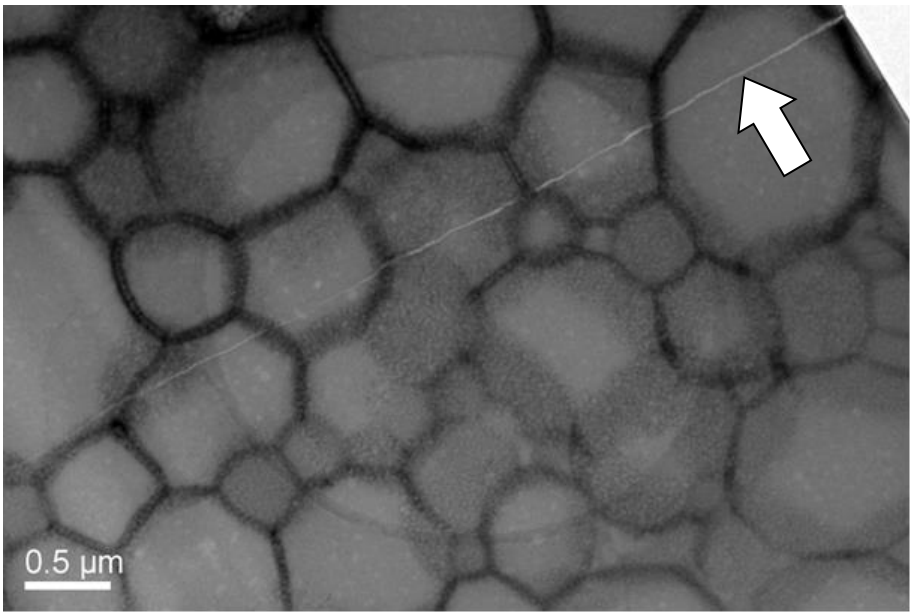

Figure 4-8 TEM image for the ultra-thin section of the DPNR-graft-PS prepared by the FIB processing, which is an expanded image of Figure 4-6. The white arrow represents a crack propagating in the ultra-thin section.

The crack may be formed by rapid volume contraction due to quick cooling, after heating the ultra-thin section during the FIB processing. The crack propagation may occur to release local strain energy of the ultra-thin section due to quick cooling and it remains appeared due to the staining with OsO_4 as a chemical pinning agent. This implies a conflict between the advantage and disadvantage of the FIB processing; that is, the advantage to prepare thin film becomes the disadvantage to form sharp crack due to quick thermal transport. This fracture behavior is completely distinguished from the mechanical fracture behavior that forms a large crack. Consequently, it is found that the slow cooling is a necessarily requirement for the preparation of the ultra-thin section with the FIB.

Figure 4-9 shows expanded TEM images of the DPNR-*graft*-PS, in which (A) represents the TEM image for the ultra-thin section prepared by FIB processing and (B) represents the TEM image for the ultra-thin section prepared with the cryo-microtome. Two staining agents were used to distinguish the images from each other: that is, RuO_4 for (A) and OsO_4 for (B), which were known to stain PS phase and natural rubber phase, respectively. In Figure 4-9 (A) and (B), various sizes of the natural rubber particles were distributed in the PS nanomatrix, reflecting the wide distribution of particle size of natural rubber latex. In contrast, the thickness of the nanomatrix could not be

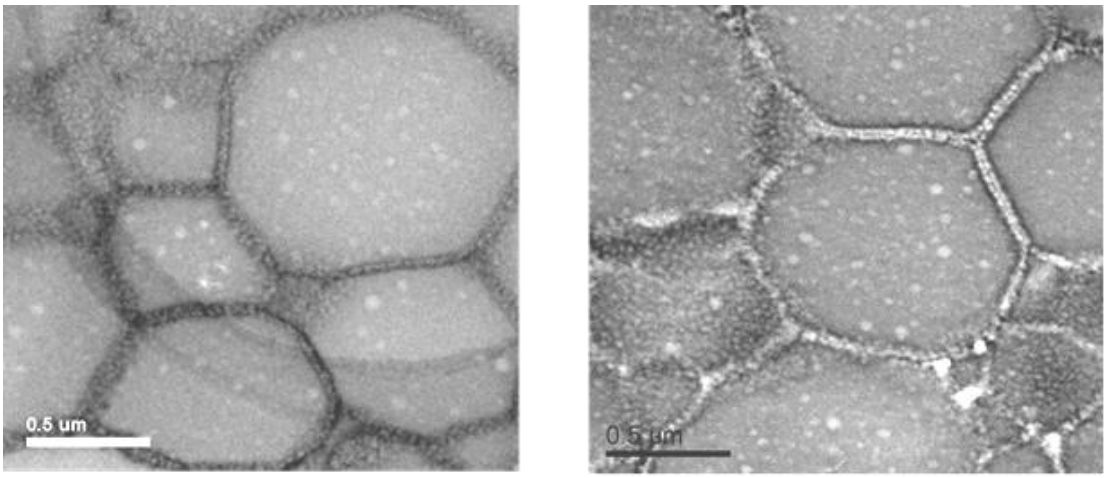

(A) (B)

Figure 4-9 Expanded TEM images for the DPNR-graft-PS, in which (A) represents the TEM image for the ultra-thin section prepared by FIB processing and (B) represents the TEM image for the ultra-thin section prepared with the cryo-microtome.

determined, because the 2D-image was made with transmitted electron, which may be different from a real image. For instance, the thickness of the nanomatrix shown in 2D-image may become apparently larger than that in the real image, when the nanomatrix possesses curvature (Figure 4-10).

Thus, it is necessary to perform 3D-observation of the ultra-thin section, in order to obtain quantitative results.

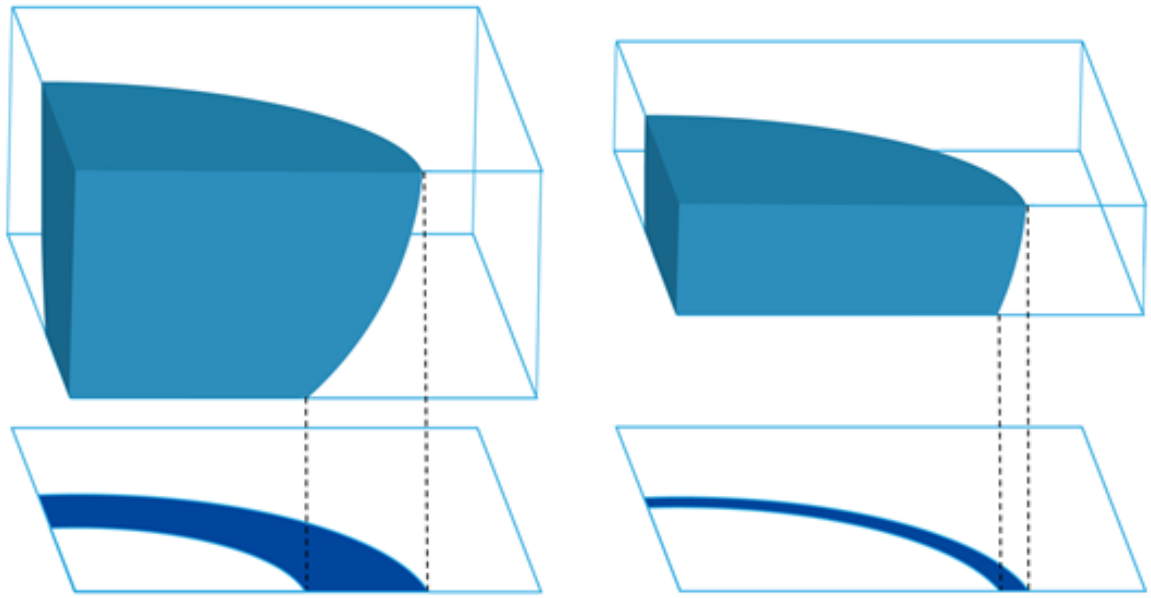

Figure 4-10 Schematic illustration of nanomatrix structure in the ultra-thin section. The relationship between 2D-image and 3D image are well represented in the schematic illustration. The interface in the 2D image is thicker than that in the 3D image.

3D electron tomography image for the ultra-thin section prepared by the FIB processing is shown in Figure 4-11, in conjunction with that prepared with the cryo-microtome, where the magnification is similar to that of Figure 4-9. Bright domains in the images represent PS and dark domains represent natural rubber. The natural rubber particles of about 1 μm in average diameter were shown to be well dispersed in the PS nanomatrix. Curvatures of the natural rubber particles were slightly shown in the image, because average size of the natural rubber particles was absolutely larger than the thickness of the ultra-thin section.

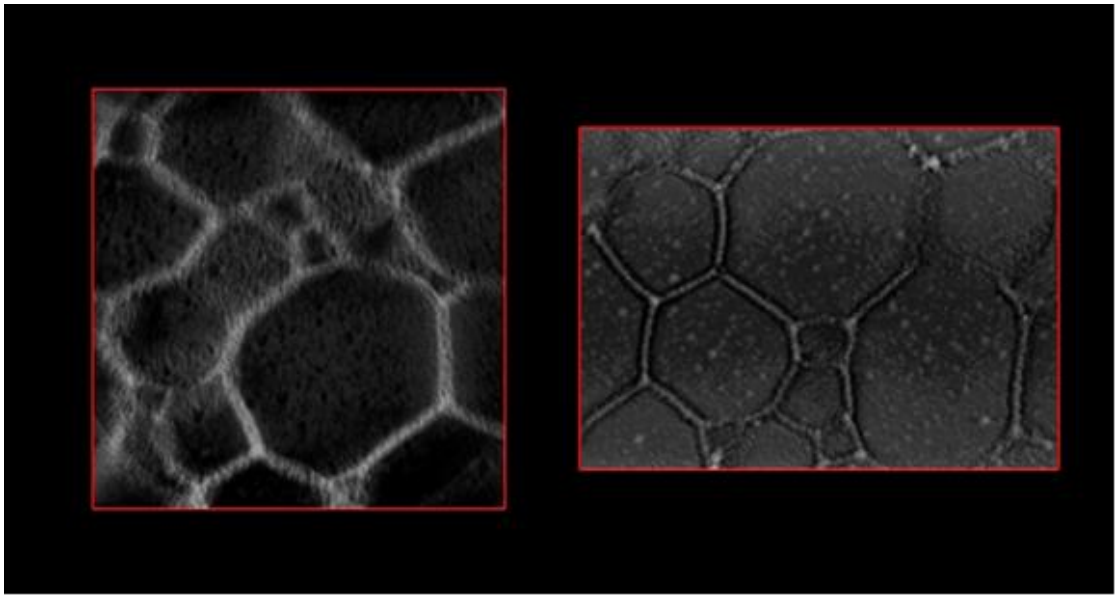

(A) (B)

Figure 4-11 3D electron tomography images for (A) the ultra-thin section prepared by the FIB processing and (B) the ultra-thin section prepared with the cryo-microtome.

The 3D image for the ultra-thin section prepared by the FIB processing appeared to be the same as that prepared with the cryo-microtome. Furthermore, the 3D images were quite similar to the 2D images shown in Figure 4-9, since the size of rubber particles was quite large as compared with the thickness of the ultra-thin section. The 3D observation was, thus, not effective for the nanomatrix structure at this low magnification, i.e. micro-metric scale. This demonstrates that the 3D image is more effective to observe nano-structure at high magnification, i.e. nano-metric scale.

Figure 4-12 shows 3D electron tomography image for the ultra-thin section prepared by the FIB processing in conjunction with that prepared with the cryo-microtome at extremely high magnification, i.e. nano-metric scale. In the images, the nanomatrix of about 15 nm in thickness was observed in detail. The nanomatrix was discontinuous. Especially, in the 3D electron tomography image for the ultra-thin section prepared by FIB processing (Figure 4-12 (A)), the PS nano-particles of about 5 nm in diameter were found to be closely dispersed in the nanomatrix. In contrast, partially disconnected nanomatrix was shown in the 3D electron tomography image for the ultra-thin section prepared with the cryo-microtome (Figure 4-12 (B)). The difference in the image between Figure 4-12

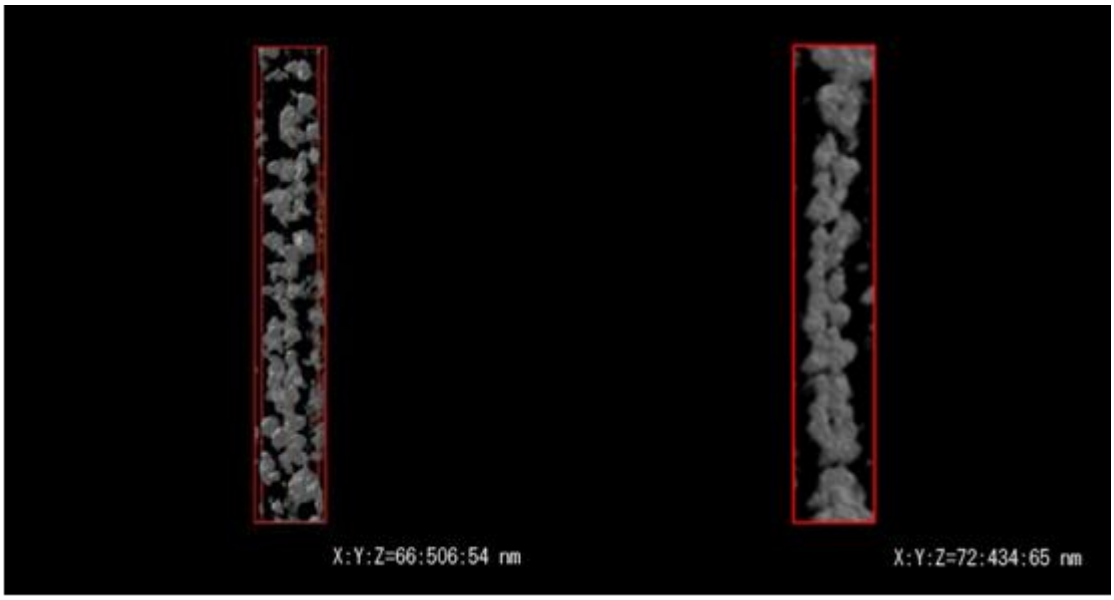

(A) (B)

Figure 4-12 3D electron tomography images for (A) the ultra-thin section prepared by the FIB processing and (B) the ultra-thin section prepared by cryo-microtome processing at extremely high magnification.

(A) and (B) may be explained to be due to the preparation method of the ultra-thin section. In an ordinary circumstance, the spatial position of the nano-phase separated structure is maintained by the FIB processing due to no physical contact, whereas it is distorted with the cryo-microtome due to the physical contact with the glass knife. Based upon this empirical rule, the spatial position of the PS nano-particles may be maintained in the nanomatrix in the case of the FIB processing. However, the position may be distorted in the case of the cryo-microtome processing. This demonstrates that the FIB processing is indispensable for the observation of the nanomatrix structure.

Furthermore, by adapting the FIB processing for the preparation of the ultra-thin section, the distance between the PS nano-particles was found to be about 5 nm. Perhaps, in the nanomatrix, natural rubber may be placed in between the PS nano-particles; so that, the nanomatrix may consist of the PS nano-particles and natural rubber. Consequently, it was proved by electron tomography observation of the ultra-thin section prepared by the FIB processing that the nanomatrix structure was complexly hieratical structure comprising of the natural rubber micro-particles and the nanomatrix of

the PS nano-particles / natural rubber. The complexly hieratical structure may provide various strain fields into natural rubber. Thus, the observed morphology may be closely related to the inordinate viscoelastic properties of natural rubber with the nanomatrix structure (DPNR-*graft*-PS); that is, the elasticity and viscosity increased with increasing the frequency.

4.4 Conclusion

TEM and electron tomography observations of the ultra-thin sections prepared by FIB processing were made for the DPNR-*graft*-PS with the nanomatrix structure. The dimension of the ultra-thin section prepared by FIB processing was about 6 μm × 9 μm × 54 nm, which was extremely smaller than that prepared with the cryo-microtome. The ultra-thin section was completely stained with OsO_4 for more than 7 days to enhance the contrast of the electron tomography image during the FIB processing. It was demonstrated by TEM and electron tomography observations that the FIB processing was superior in non-destructive nature to prepare the ultra-thin section; that is, the spatial position of the nanomatrix structure was maintained by the FIB-processing due to no physical contact, whereas it was distorted with the cryo-microtome due to the physical contact with the glass knife. The nanomatrix structure was found to be the complexly hieratical structure comprising of the natural rubber micro-particles and the nanomatrix of PS nano-particles / natural rubber. In the nanomatrix, the PS nano-particles of about 5 nm in diameter were closely dispersed, whose distance was about 5 nm. The FIB processing was proved to be indispensable for the electron tomography observation of the nano-strucutre, i.e. the nanomatrix structure of DPNR-*graft*-PS.

4.5 References

1. Ishitani, T.; Tsuboi, H. *Scanning* **1997**, 22. 489-497.
2. Jacobs, EG.; Foster, L.A.; Wu Y.; Wilson, AR.; Pinizzotto, R.F. *J Mater Res* **1993**, 8, 87-94.
3. Osumi, M.J. *Electron Microsc* **2012**, 61, 343-6-365.
4. Niihara, K.; Kaneko, T.; Suzuki, T.; Sato, Y;. Nishioka, H.; Nishikawa, Y.; Nishi, T.; Jinnai, H. *Macromolecules* **2005**, 38, 3048-3050.
5. Ohta, K.; Sadayam,a S.; Togo, A.; Higashi R.; Tanoue, R.; Nakamura, K. *Micron* **2012**, 43, 612-620.
6. Gierak, J.; Mailly, D.; Faini, G.; Pelouard, J.L.; Denk, P.; Pardo, F.; Marzin, J.Y.; Septier, A.; Schmid, G.; Ferre, J.; Hydman, R.; Chapper, C.; Flicstein, J.; Gayral, B.; Gerard, JM. *Microelectronic Engineering* **2001**, 57-58, 865-875.
7. Jinnai, H.; Tsuchiya, T.; Motoki, S.; Kaneko, T.; Higuchi, T.; Takahara, A. *Microscopy* **2013**, 62, 243-258.
8. Jinnai, H.; Spontak, R.J.; Nishi, T. *Macromolecules* **2010**, 43, 1675-1688.
9. Saxey, D.W.; Cairney, J.M. McGrouther, D.; Honma, T.; Ringer, S.P. *Ultramicroscopy* **2007**, 107, 756-60.
10. Stokes, D.J.; Wilhelmi, O.; Reyntjens, S.; Jiao, C.; Roussel, L.*J. Nanosci Nanotechnol* **2009**, 9, 1268-1271.
11. Kato, M.; Ito, T.; Aoyama, Y.; Sawa, K.; Kaneko, T.; Kawase, N.; Jinnai, H. *J. Polym. Sci. Polym. Phys.* **2007**, 45, 677-683.
12. Ink;son, B.; Mulvihill, M.; Mobus, G. *Scr Mater* **2001**, 45, 753-758.
13. Wu, H.Z.; Roberts, S.G.; Mobus, G.; Inkson, B.J. *Acta Mater* **2003**, 51, 149-163.
14. Zuschlag, A.; Schwab, M.; Merhof, D.; Hahn, G.*Solid State Phenomena* **2013**, 205-206, 136-141.

15. Adams, D.P.; Vasile, M.J.; Benavides, G.; Campbell, A.N.*Precision Engineering* **2001**, 25, 107-113.

16. Cairney, J.M.; Munroe, P.R. *Materials Characterization* **2011**, 46, 297-304.

17. Petersen, C.; Lasagni, A.; Holzapfel, C.; Daniel, C.; Mucklich, F.; Veith, M. *Appl Surf Sci* **2007**, 253, 8022-8027.

18. White, H.; Pu, Y.; Rafailovich, M.; Sokolov, J.; King, A.H.; Giannuzzi, L.A.; Urbanik-Shannon, C.;Kempshall, B,W.; Eisenberg, A.; Schwarz, S.A.; Strzhemechny, Y.M. *Polymer* **2001**, 42, 1613-1619.

19. Loos, J.; van Duren, J.K.J.; Morrissey, F.; Janssen, R.A.J. *Polymer* **2002**, 43, 7493-7496.

20. Son, DI.; Kim, H.H.; Cho, S.; Hwang, D.K.; Seo, J.W.; Choi, W.K. *Organics Electronics* **2014**, 15, 886-892.

21. Kim, S.; Park, M.J.; Balsara, N.P.; Liu, G.; Minor, A.M. *Ultramicroscopy* **2011**, 111, 191-199.

22. Kawahara, S.; Kawazura, T.; Sawada, T.; Isono, Y. *Polymer* **2003**, 44, 4527-4531.

23. Kawahara, S.; Yamamoto, Y.; Fujii, S.; Isono, Y.; Niihara, K.; Jinnai, H.; Nishioka, H; Takaoka ,A. *Macromolecules* **2008**, 41, 4510-4513.

24. Klinklai, W.; Saito, T.; Kawahara, S.; Tashiro, K.; Suzuki, Y.; Sakdapipanich, J.T.; Isono, Y. *J Appl Polym Sci* **2004**, 93, 555-559.

25. Spontak, R.J.; Fung, J.C.; Braunfeld, M.B.; Sedat, J.W.; Agard, D.A.; Kane, L.; Smith, S.D.; Satkowski, M.M.; Ashraf, A.; Hadjuk, D.A.; Gruner, S.M. *Macromolecules* **1996**, 29, 4494-4507.

Chapter 5

Observation of Anisotropically Deformed Nanomatrix Structure in Frozen Non-equilibrium State through 3D FIB-SEM and Electron Tomography

5.1 Introduction

Anisotropically deformed material is attracted to be a novel soft material due to its unique properties. It is of importance to analyze the anisotropic structure through three-dimensional (3D) imaging techniques in order to elucidate a relationship between the anisotropic structure and properties after freezing the non-equilibrium structure. The relationship may play an important role in designing and forming the unique properties in the rational basis. The analytical technique may be required to evolve in observation of morphology through not only tomography technique of electron and X-ray but also compatible technique in order to enhance precision and accuracy. In fact, in the last decade, grain boundary and structural defects of the nano-structure were investigated by 3D imaging techniques.[1, 2] However, it is difficult to relate the properties to distortion of the nano-structure with load force. In order to investigate the relationship between the properties and external stress field as well as internal stress field, a compilation of database is needed for the relationship between the anisotropic structure and properties.

The method to form anisotropic structure is roughly classified into two categories: that is, freeze of the non-equilibrium structure and deformation of the structure with load force. The freeze of the non-equilibrium structure is performed by vitrification and crystallization of the soft materials.[3, 4] In addition, formation of the chemical linkages is also useful for freezing the non-equilibrium structure.[5] In contrast, the deformation of the structure with load force is carried out under constant strain and stress. Relaxation and permanent set may occur under constant strain, whereas creep may take place under constant stress. The anisotropic structure, thus prepared, may be observed by focused ion beam-scanning electron microscopy, FIB-SEM, and electron tomography technique. The

combination of the techniques to form anisotropic structure and to observe morphology may open a new field of the structural analysis.

In the previous works, various heterogeneous structures have been observed by FIB-SEM and electron tomography: that is, island-sea, cylinder, gyroid and lamellar structures for block and graft-copolymers [1,2] as well as dispersion of primary nano-particles, structure of secondary aggregates and 3D filler-network structure for filled polymers.[6-8] Some important findings were achieved by 3D observations through FIB-SEM and electron tomography. Furthermore, the analytical techniques were devoted to visualize dispersions of particles and aggregates for the filled polymers. These heterogeneous structures were closely related to mechanical properties. Thus, the 3D observations may be indispensable to study structures and properties of the polymers.

The 3D observation has been performed for materials possessing equilibrium structure, so far; for instance, the materials were annealed for long time to achieve equilibrium state.[9] However, materials in use are practically utilized in the non-equilibrium state. Thus, the frozen non-equilibrium structure or deformed structure may be observed by a suitable technique. In the previous work, the deformed structure was observed by using deformation module equipped with TEM, although the quantitative analysis was less performed.[10] It is necessary to develop a well sophisticated method to accomplish the observation of non-equilibrium structure.

In the present study, an attempt to observe the non-equilibrium structure was made for natural rubber with the nanomatrix structure after annealing. The FIB-SEM and 3D TEM techniques were applied to observe the non-equilibrium structure through 3D imaging techniques. The observed structure was related to the mechanical properties, i.e., tensile properties and viscoelastic properties.

5.2 Experimental

5.2.1 Sample preparation

Natural rubber latex used in the present study was commercial high-ammonia natural rubber latex. The incubation of the latex was made with 0.1 w/w% urea in the presence of 1 w/w% sodium dodecyl sulfate (SDS) at 303 K followed by centrifugation at 10,000 rpm. Cream fraction was re-dispersed in 1 w/w% SDS to make 30 w/w% dry rubber content (DRC) latex and it was washed twice by centrifugation to prepare deproteinized natural rubber (DPNR) latex.[11,12] The DPNR latex was diluted with distilled water to adjust 10 w/w% DRC and concentration of SDS was adjusted to 0.1 w/w%. The resulting DPNR latex was used for the graft-copolymerization, since the proteins were well known to trap radicals during the graft-copolymerization. [13]

Graft-copolymerization of styrene onto DPNR was carried out in latex stage with *tert*-butyl hydroperoxide / tetraethylene pentamine as an initiator. The DPNR latex was charged with N_2 gas for 1 hour at 303 K. The initiator of 3.3×10^{-2} mol/kg-rubber and styrene of 1.5 mol/kg-rubber were added to the latex, respectively. The reaction was performed by stirring the latex at about 400 rpm for 2 hours at 303 K. The unreacted styrene was removed by using a rotary evaporator under reduced pressure. A film specimen of the grafted natural rubber was prepared by casting the glass tube into the reacted latex and it was dried under reduced pressure at ambient temperature for more than a week. [5, 14, 15]

5.2.2 Observation

Observation of morphology of the grafted natural rubber was made with a TEM, JEOL JEM-2100 at accelerating voltage of 200 kV and FIB-SEM, SII SMI-3050SE at accelerating voltage of 3 kV. The FIB-SEM was also used to make an ultra-thin section of grafted natural rubber according to the literature.[15] The ultra-thin section of the graft-copolymer was prepared by a Sorvall Instruments MT6000 Ultra Microtome at 193 K. The thin sections were stained with osmium tetraoxide (OsO_4) or ruthenium tetroxide (RuO_4), after annealing the section at 353 K for 30 min.

3D images were obtained by reconstructing more than 100 2D images, i.e. TEM images. The sections with ca. 100 nm thick were prepared and stained with OsO_4 in the similar way as described above. A special specimen holder that enables us to rotate the section from -70^o to +70^o was used to take a high resolution 3D image. Tilt angular range in the particular experiment was -59° to +63° with an increment of 1°, which was aligned and reconstructed according to the protocol described in 15.

Size excluded chromatography (SEC) for PS were made by GPC system of Tosoh Ltd. with a CCPD pump, a RI-8012 differential refractive index detector, a UV-8011 ultraviolet spectroscopic detector, and a series of three G4000HXL columns (beads size is 5 μm, pore size is 10^4 angstrom) with 300mm length and 7.8 mm i.d. each. THF was used as an eluent, and the flow rate was 0.5 ml/min, at room temperature. Standard polystyrenes were used for a calibration. The apparent molecular weights and molecular weight distribution was determined after ozonolysis of the grafted natural rubber was performed at 243 K in a 0.4 w/v% methylene chloride solution, in order to isolate PS without natural rubber.

Synchrotron X-ray measurement was performed with a beam line of BL40B2 at Spring-8 in Kobe, Japan. The wavelength used for measurement was 0.130 nm. Wide angle X-ray diffraction (WAXD) and small angle X-ray scattering (SAXS) patterns were recorded by CCD X-ray detector. The experiment was carried out at 298 K.

Measurement of tensile properties was carried out according to JIS K6251. The film samples with thickness of about 1 mm were cut with Dumbell-shaped Type 7. The test piece was stretched with the cross-head speed of 200 mm/min. Data of stress and strain of the sample was plotted in stress-strain curve.

Dynamic viscoelastic properties were measured with Rheometrix Ares-4. Parallel plates geometry of 12 mm diameter was used. Angular frequency range was from 0.1 to 100 rad s^{-1}. Temperature range was from 200 to 413 K. The oscillatory strain amplitudes were within the range of linear viscoelasticity in all measurements.

5.3 Results and Discussion

Figure 5-1 shows TEM image for deproteinized natural rubber (DPNR) with the nanomatrix of polystyrene (PS), in which the ultra-thin section was prepared by focused ion beam (FIB) processing. The section was stained with RuO_4; so that, dark domains represent PS, whereas bright domains represent DPNR. The nanomatrix structure, thus observed, was comprised of the natural rubber particles of about 1 μm in average diameter as a major component and PS-nanomatrix of about 15 nm in thickness as a minor component. This is distinguished from the thermodynamically stable island-sea structure that is defined to consist of island of minor component and sea of major component. The nanomatrix structure may be made by forming chemical linkages between natural rubber particles and PS-nanomatrix.[16,17] In fact, in the present study, the graft-copolymerization of styrene onto DPNR in latex stage was adopted to form the nanomatrix structure. It is worthy of note that natural rubber particles appeared to be almost circle in the ultra-thin section, implying no strain was imposed; in other words, the nanomatrix structure in Figure 5-1 is uniquely isotopic structure.

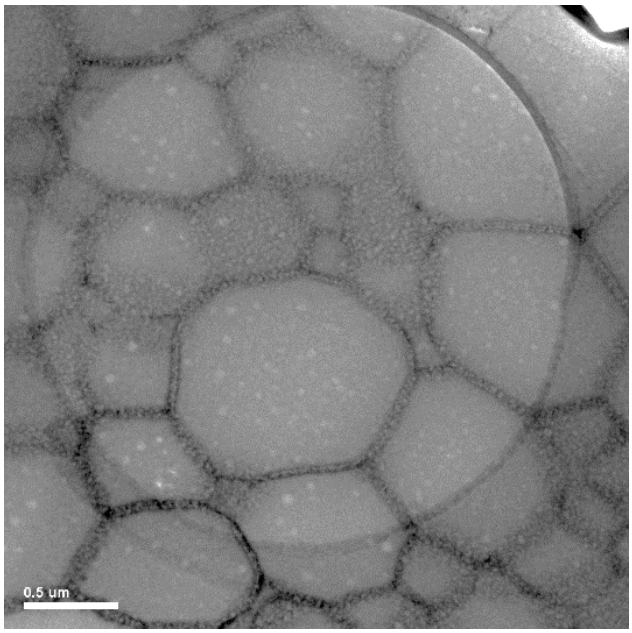

Figure 5-1 TEM image for deproteinized natural rubber (DPNR) with the nanomatrix of polystyrene (PS)

Figure 5-2 shows projection of xy-, yz- and xz-planes of the nanomatrix of DPNR-*graft*-PS in conjunction with fabricated image of xy-, yz- and xz-planes and 3D image made by reconstruction of the etched 2D images. Bright domains represent the PS nano-particles, whereas dark and gray domains represent natural rubber, in which the dark domains were artificially distinguished from the gray domains as the nanomatrix-inside was separated from its surrounding outside. In the nanomatrix, the PS-nano-particles of about 5 nm in diameter were well dispersed in the nanomatrix. The distance between the particles appears to be less than 5 nm, since xy-, yz- and xz-planes are the projection of the real image, which are made with transmitted electrons. The projection is different from the real image; for instance, the distance between the PS nano-particles may become apparently shorter than that in the real image, as shown in Figure 5-3. Therefore, the synchrotron scattering techniques were applied to the nanomatrix structure in order to obtain quantitative results.

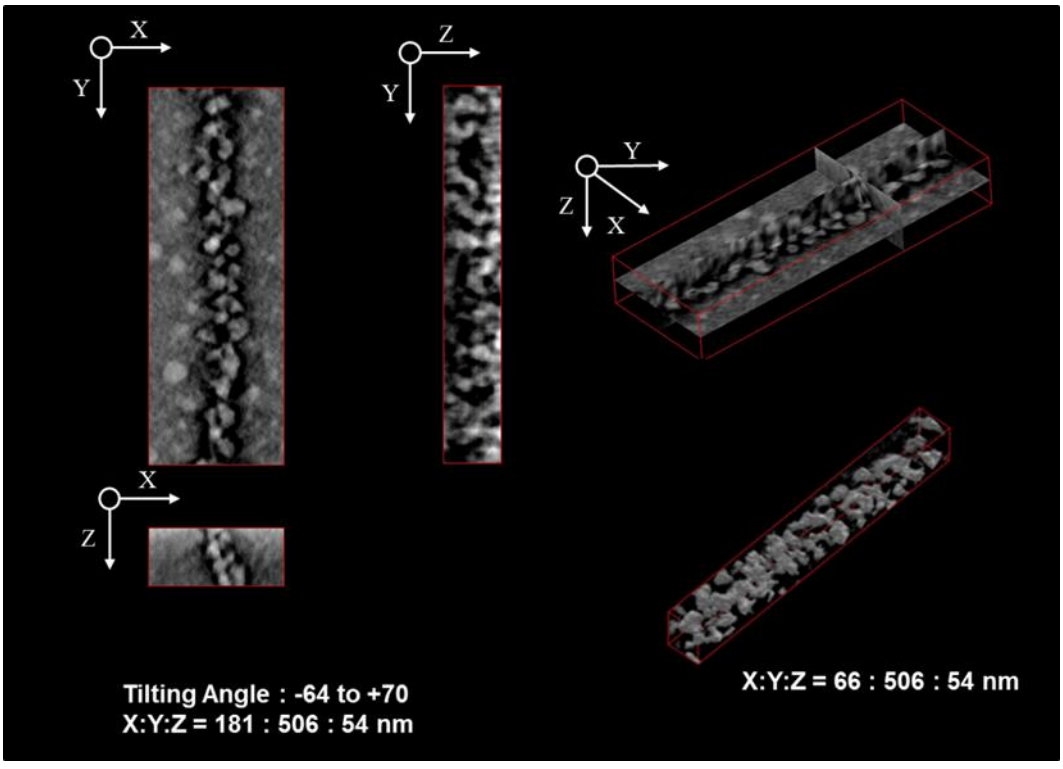

Figure 5-2 Projection of xy-, yz- and xz-planes of the nanomatrix of DPNR with the nanomatrix of PS in conjunction with fabricated image of xy-, yz- and xz-planes and 3D image made by reconstruction of the etched 2D images.

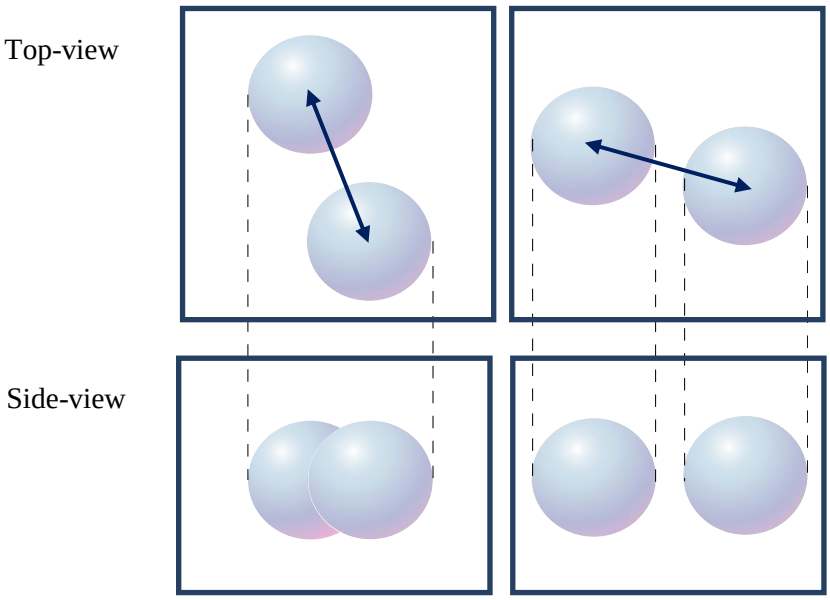

Figure 5-3 Schematic representation of alignment of PS nano-particles. The apparent distance between the PS nano-particles is dependent upon the direction of view angle. Top-view represents the same distance between two particles. But, the side view, i.e., through view, represents the apparently different distances between two particles.

Alignment of the PS- nano-particles in the nanomatrix structure was investigated by small angle X-ray scattering measurement with a beam line of BL40B2 at Spring-8. Figure 5-4 shows a plot of logarithmic intensity *versus* q square, that is, Guinier plot, where the q represents the scattering vector, $q = 4\pi/\lambda \sin\theta/2$. An apparent radius of gyration of the PS nano-particles in the nanomatrix was estimated, as a linear regression was applied to the Guinier plot in a very small q rage, as follows:

$$qR_g < 1 \qquad (5\text{-}1)$$

$$I(q) = I(0)\exp\{-R_g^2 q^2/3\} \qquad (5\text{-}2)$$

where R_g is the radius of gyration and I is the intensity. The estimated value of the apparent radius of yration of PS nano-particles was about 6 nm.

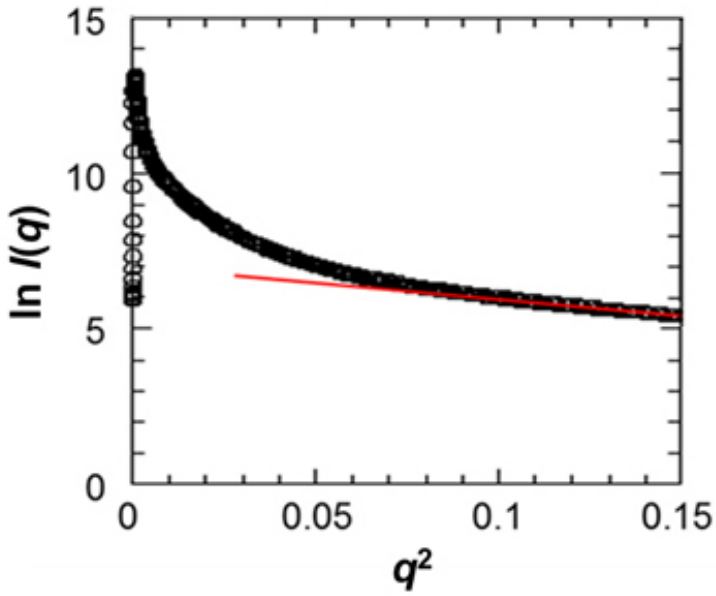

Figure 5-4 Plot of logarithmic intensity *versus q* square, that is, Guinier plot, for DPNR with the nanomatrix of PS. The red line was drawn by linear regression of the curve.

The radius of gyration is proportional to molecular weight. Especially, in the case of PS, the molecular weight may be determined by size exclusion chromatography, SEC. Thus, the SEC measurement was performed to determine the molecular weight of PS, after ozonolysis of DPNR-graft-PS. In our previous works, it was ensured that signals, assigned to carbon-carbon double bonds, disappeared in the NMR spectrum after ozonolysis of DPNR-graft-PS.[15, 19, 20] This was explained to be due to the cleavage of all carbon-carbon double bonds of natural rubber with ozone. The resulting polymer after ozonolysis may, thus, contain no isoprene unit; in other words, it is PS, itself, linking to natural rubber. The estimated value of number average molecular weight after ozonolysis was 1.5×10^4 g/mol. From the number average molecular weight, we estimated the root mean square end-to-end distance, $\langle R^2 \rangle^{1/2}$ of PS as in the following equation:

$$\langle R^2 \rangle^{1/2} = aN^{1/2} \qquad (5\text{-}3)$$

The estimated value of the $<R^2>^{1/2}$ was 7.4 nm, which was similar to the value estimated by Guinier plot. The value estimated from number average molecular weight corresponded to that of the apparent radius of gyration determined by synchrotron scattering technique. This implies that the PS nano-particle existed in the nanomatrix includes only one PS molecule. In other words, the nanomatrix is a condensed phase of nano-particles of PS one molecule.

In order to investigate a distance between PS nano-particles, scattering profile was looked in a large q range. Figure 5-5 shows scattering profile at large q range. Before annealing DPNR-*graft*-PS at 403 K, several peaks appeared in the scattering profile. The peaks are considered to come from diffraction of a lattice of PS nano-particles. Therefore, Bragg's expression was applied to the estimation of the distance between PS nano-particles, as follows:

$$< d > = 2\pi/q_{max} \qquad (5\text{-}4)$$

where $< d >$ is the distance between PS nano-particles and q_{max} is the q at the peak top. The estimated distance between PS nano-particles was about 5 nm. This suggests that, before annealing, PS nano-particles of about 6 nm in diameter are dispersed in nanomatrix at an interval of each 5 nm.

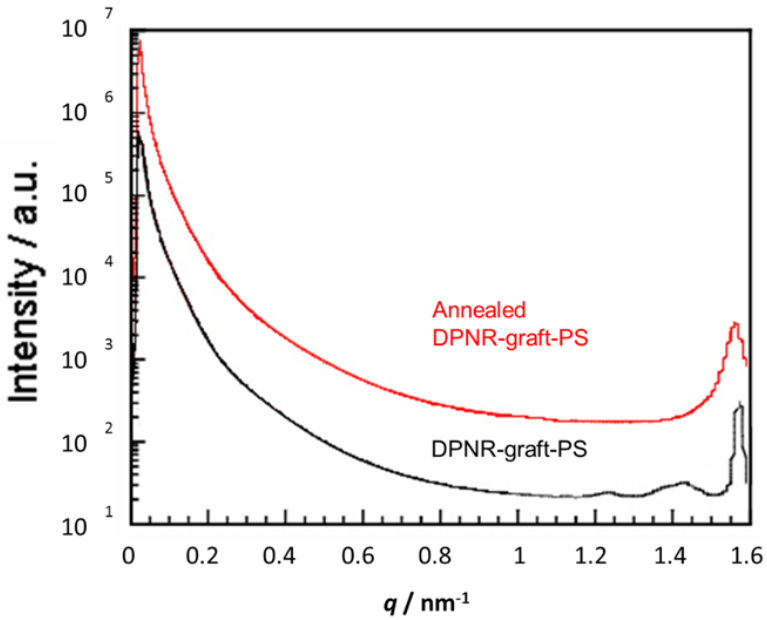

Figure 5-5 Scattering profile at large q range. Before annealing DPNR with the nanomatrix of PS at 403 K, several peaks appeared in the scattering profile.

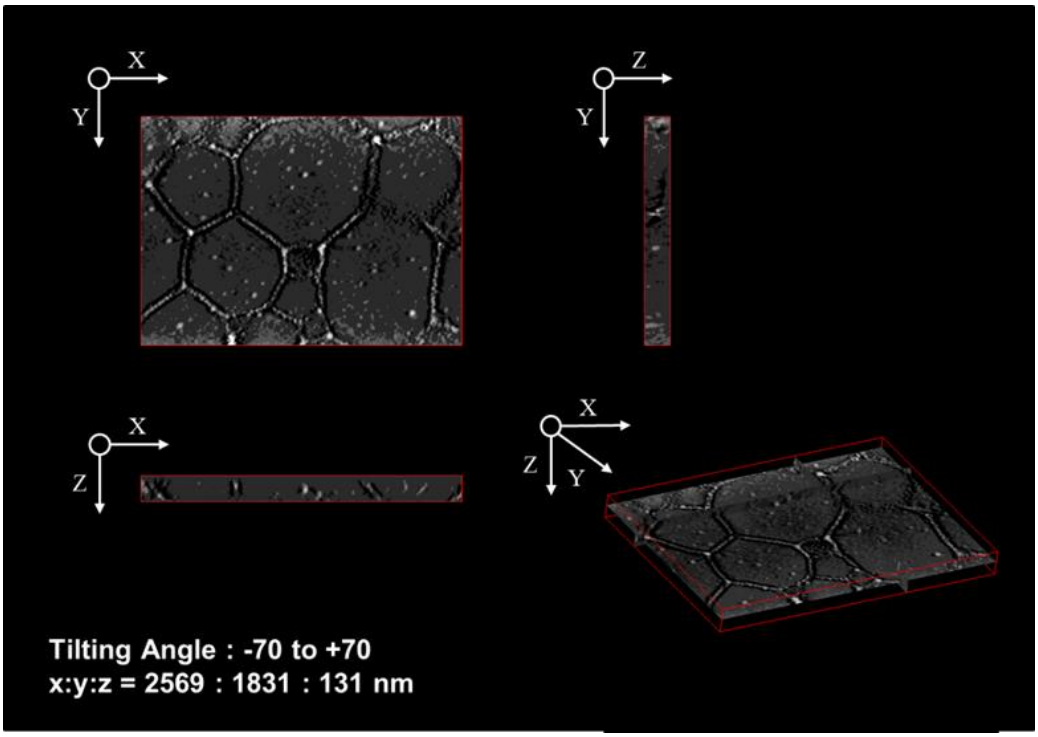

Figure 5-6 Electron tomography images for DPNR with the nanomatrix of PS, which is a projection of xy-, yz- and xz-planes in conjunction with 3D image. The bright domains represent PS, whereas dark domains represent DPNR.

Figure 5-6 shows transmission electron micro tomography images for DPNR with the nanomatrix of PS, which is a projection of xy-, yz- and xz-planes in conjunction with 3D image. The bright domains represent PS, whereas dark domains represent DPNR. The overview of the nanomatrix structure is well shown in the xy-plane. However, the yz- and xz-plans shows a part of image, i.e., a line shape of the PS-phase of the nanomatrix. For instance, in the case of isotropic structure, the curvature of the line is dependent upon the direction of normal line due to a spherical shape of the natural rubber particles. This may be explained to be due to the restriction of the dimension of the ultra-thin section for the 3D TEM observation, since the transmitted electron passing through the ultra-thin section is detected by imaging plate. The thickness of the section must be extremely thin, which is about several tens of times as small as a diameter of the natural rubber particles. Therefore, the anisotropic structure of natural rubber with the nanomatrix structure was unable to investigate in use. It is, thus, necessary to perform the 3D observation of deep depth for the nanomatrix structure;

for instance, the 3D observation may be performed by FIB-SEM and X-ray computed tomography method.

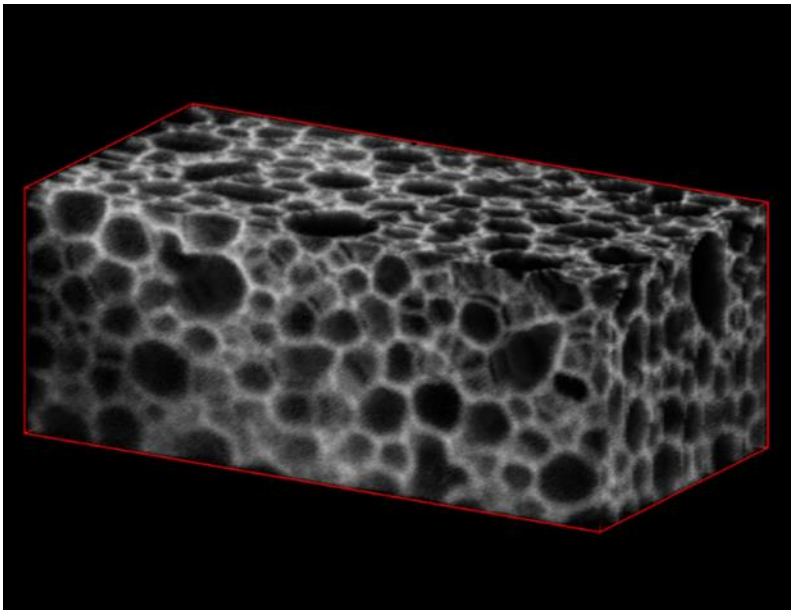

Figure 5-7 The 3D-image of DPNR with the nanomatrix of PS, obtained by FIB-SEM.

The 3D-image of the natural rubber with the nanomatrix of PS, obtained by FIB-SEM, is shown in Figure 5-7. The FIB-SEM realized the 3D observation of deep depth for the nanomatrix structure. The 3D-image of FIB-SEM demonstrates that the natural rubber particles of about 1 μm in average diameter was dispersed in the PS-nanomatrix of about 15 nm in thickness.

Figure 5-8 shows projection of the sliced images of xy-, yz- and xz-planes of the nanomatrix structure. The morphology on the surface of 3D image was just the same as that inside. The natural rubber particles were spherical, suggesting that the structure is isomeric without residual strain and thermal history. This implies that natural rubber with the nanomatrix structure, thus observed, maintained the virgin state, which is distinguished from that in use. The morphology of natural rubber with the nanomatrix structure must be observed after use, in order to elucidate the relationship between structure and properties in use.

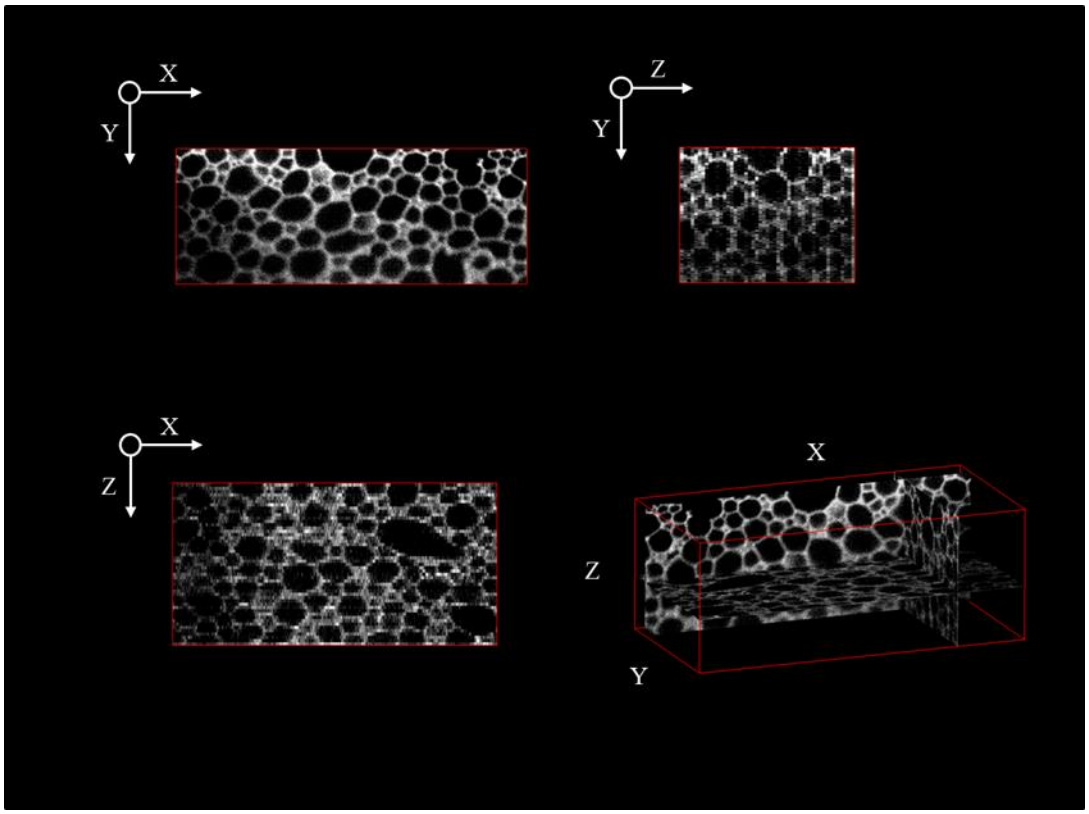

Figure 5-8 Projection of the sliced images of xy-, yz- and xz-planes of the nanomatrix structure.

Figure 5-9 shows stress-strain curves for DPNR, DPNR-*graft*-PS and DPNR-*graft*-PS annealed at 403 K and 7 MPa. The value of the stress at strain of 1 increased after graft-copolymerization. It increased further after annealing at 403 K and 7 MPa. In contrast, the value of the stress at break of DPNR-*graft*-PS was the highest among the samples; that is, the value was about 18 MPa, which is about 20 times as high as that of DPNR and it is similar to the value of peroxide cured natural rubber. The value of 18 MPa is one of the characteristic outcomes of the nanomatrix structure, since DPNR-*graft*-PS is un-crosslinked rubber. The nanomatrix structure is formed by casting DPNR-*graft*-PS latex onto Petri dish. Therefore, no chemical linkage is expected between natural rubber particles in DPNR-*graft*-PS. Nevertheless, the value of stress at break for DPNR-*graft*-PS was quite large. This may be explained to be due to the effect of the nanomatrix structure on the tensile properties.

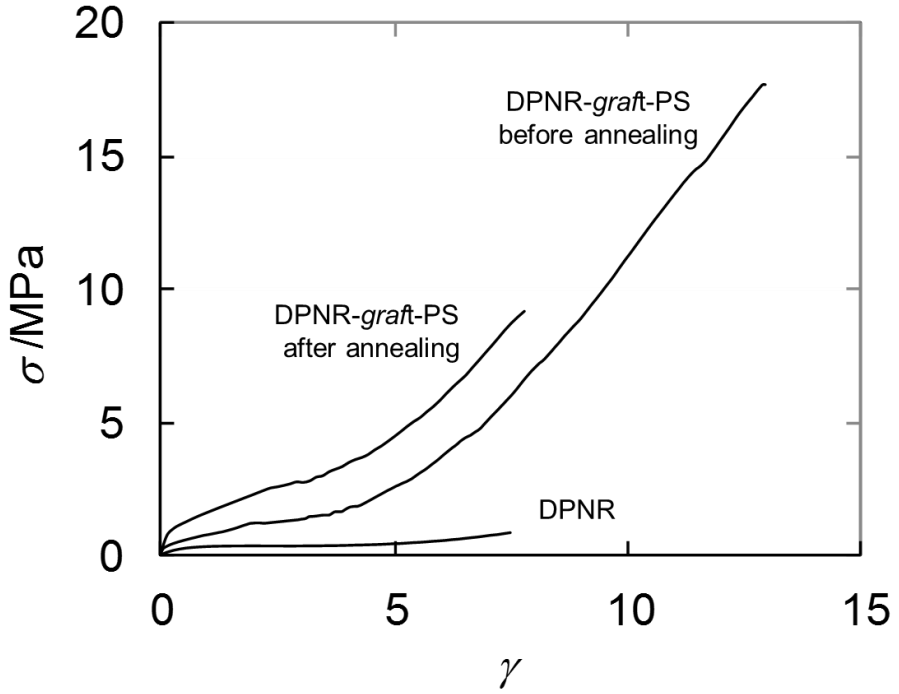

Figure 5-9 Stress-strain curves for DPNR, DPNR-*graft*-PS and DPNR-*graft*-PS annealed at 403 K

The nanomatrix structure was also known to play an important role in the viscoelastic properties. In the previous work, the relationship between the viscoelastic properties and frequency was reported for DPNR, DPNR-*graft*-PS with the nanomatrix structure, and DPNR-*graft*-PS with the nanomatrix structure annealed at 403 K and 7 MPa.[16] The plateau modulus for DPNR was about 10^5 Pa. When the nanomatrix structure was formed in DPNR, the plateau-modulus increased about 10 times as large as that of DPNR. The plateau-modulus of the grafted natural rubber with the nanomatrix structure increased further after annealing at 403 K and 7 MPa, being above glass transition temperature of PS. The 35 times increase in the plateau-modulus is a remarkable virtue characteristic of the nanomatrix structure. In contrast, tanδ in plateau region was analyzed for DPNR, DPNR-*graft*-PS with the nanomatrix structure, DPNR-*graft*-PS with the nanomatrix structure annealed at 403 K and 7 MPa. The value of tanδ of DPNR was in a range between 0.1 and 0.15. The higher the frequency, the lower the value of tanδ. When the nanomatrix structure was formed, the value of tanδ was independent of the frequency. The frequency independent tanδ may be characteristic

of the nanomatrix structure. After annealing at 403 K and 7 MPa, the tanδ increased significantly and it was dependent upon the frequency. In this case, we may expect the effects of the energetic elasticity due to the filler-filler and the filler-rubber interactions in addition to the entropic elasticity of the rubber, since the PS nanoparticles are densely dispersed in the nanomatrix. Based upon the previous study for the nanomatrix of silica, the frequency independent tanδ was concerned with not only entropic elasticity but also the energetic elasticity. [21, 22] In order to elucidate the origin of the unique tensile properties and viscoelastic properties, it is necessary to observe the morphology of DPNR-*graft*-PS with the nanomatrix structure after annealing at 403 K and 7 MPa.

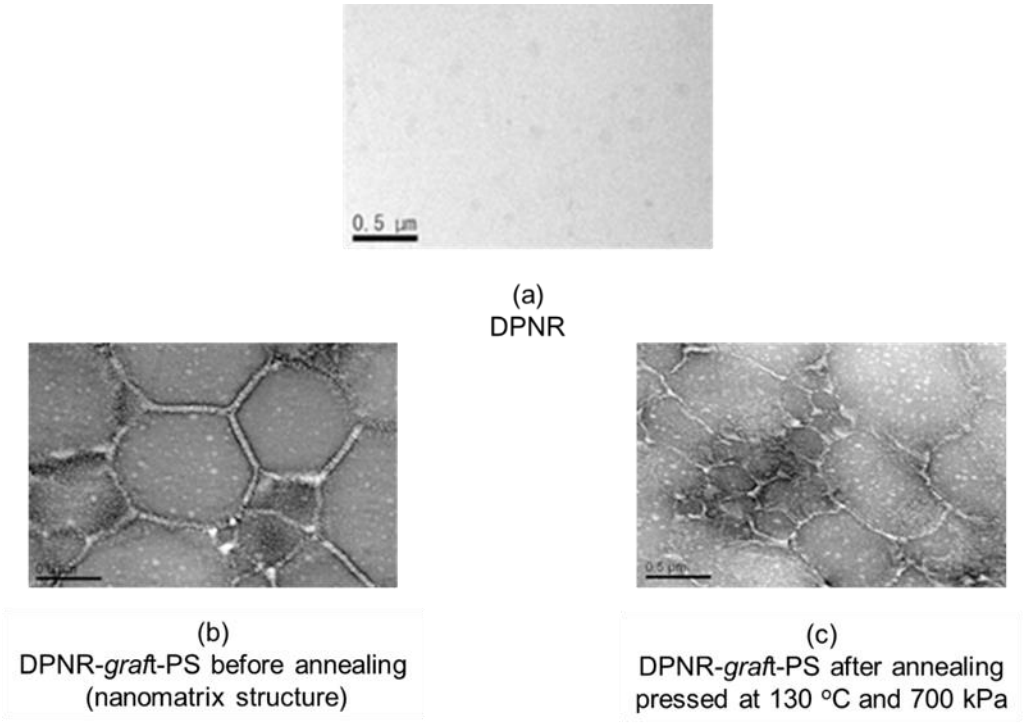

Figure 5-10 TEM images for DPNR, DPNR-*graft*-PS with the nanomatrix structure and DPNR-*graft*-PS pressed at 403 K and 7 MPa.

Figure 5-10 shows TEM images for DPNR, DPNR-*graft*-PS with the nanomatrix structure, and DPNR-*graft*-PS with the nanomatrix structure annealed at 403 K and 7 MPa. Bright domains represent PS, whereas dark domains represent natural rubber, since the film specimens were stained with OsO_4. As for DPNR, no heterogeneous structure was observed due to the removal of the proteins.

In contrast, for DPNR-*graft*-PS with the nanomatrix structure, isotropic nanomatrix structure was observed in TEM image. After annealing at 403 K and 7 MPa, the nanomatrix structure was distorted due to load force, which resulted in frozen anisotropic nanomatrix structure, which was frozen by vitrification of PS at room temperature. The morphology shown in Figure 5-10 may be related with the mechanical properties. For instance, DPNR, which possessed no heterogeneous structure, exhibited typical rubber elasticity and viscoelastic properties: that is, sigmoidal stress-strain curve with low tensile strength and frequency-dependent energy dissipation that is high at low frequency and low at high frequency. In contrast, the mechanical properties of DPNR-*graft*-PS with the nanomatrix structure was distinguished from those of DPNR, as in the previous works, which may be explained to be due to a unique morphology having PS nano-particles packed densely in the nanomatrix. In this work, DPNR-*graft*-PS with the nanomatrix structure was pressed at 403 K and 7 MPa, in order to make the nanomatrix continuous. The frozen anisotropic rubber particles were obtained in conjunction with the continuous PS-nanomatrix. This may be related to the increase in the stress at strain of 1 and 35 times increase in the storage modulus (G') as well as frequency dependent loss tangent (tanδ). Furthermore, attention was paid in the increase in the loss tangent by the factor of 1.5 (150%).

Figure 5-11 shows a projection of xy-, yz- and xz-planes in conjunction with 3D image for anisotropically deformed DPNR-*graft*-PS with the nanomatrix structure pressed at 403 K and 7 MPa. Continuous PS-nanomatrix was observed in the projection of the xy-, yz- and xz-planes, since the PS nano-particles were fused to each other. The rubber particles were found to be distorted, anisotropic in the xy-plane, i.e. non-spherical. The yz- and xz-plans show that the nanomatrix stands in oblique direction due to an anisotropic structure. This anisotropic structure may be associated with the increase in the loss tangent. The energy dissipation may occur on the interface between the natural rubber particles and the continuous PS-nanomatrix. The anisotropic structure may further increase the energy dissipation.

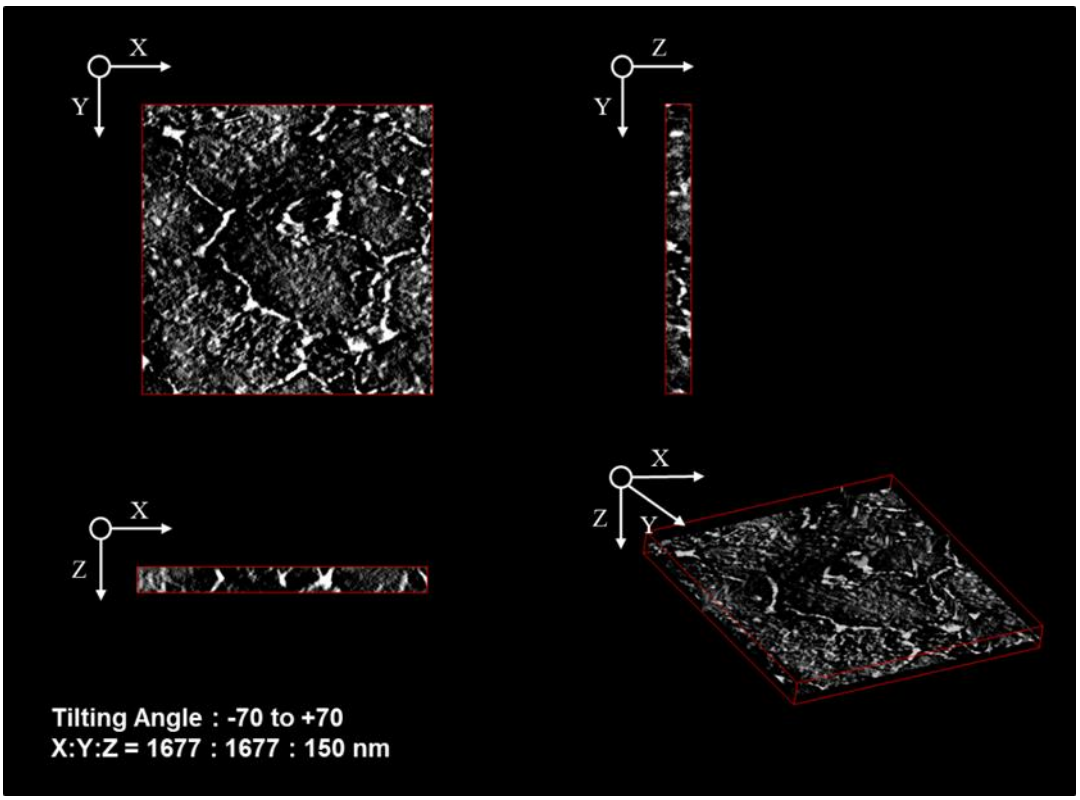

Figure 5-11 Projection of xy-, yz- and xz-planes in conjunction with 3D image for anisotropically deformed DPNR-*graft*-PS with the nanomatrix structure pressed at 403 K and 7 MPa. Continuous PS-nanomatrix was observed in the projection of the xy-, yz- and xz-planes, since the PS nano-particles were fused to each other.

5.4 Conclusion

Electron tomography method, FIB-SEM and synchrotron scattering techniques were applied to DPNR-*graft*-PS with the nanomatrix structure to elucidate the relationship between morphology and mechanical properties. The nanomatrix structure was found to consist of natural rubber particles of about 1 μm in average diameter and polystyrene nano-particles of 5.6 nm in diameter, in which the PS nano-particles were densely packed in the nanomatrix. The increase in the tensile strength and frequency independent loss tangent at plateau region were attributed to the discontinuous nanomatrix structure. DPNR-*graft*-PS with the nanomatrix structure was pressed at 403 K and 7 MPa, in order to make the nanomatrix continuous. The frozen anisotropic rubber particles were obtained in conjunction with the continuous PS-nanomatrix. The increase in the stress at strain of 1 and 35 times increase in

the storage modulus (*G*') as well as frequency dependent loss tangent (tanδ) were attributed to the continuous nanomatrix structure.

5.5 References

1. Jinnai H.; Sawa K.; Nishi T. *Macromolecules* **2006**, *39*, 5818-5819.
2. Jinnai H.; Yasuda K.; Nishi T. *Macromol. Symp.* **2006**, *245-246*, 170-174.
3. Hyttel P.; Lehn-Jensen H.; Greve T. *Acta Anatomica* **1986**, *125*, 27-31.
4. Wilkins G. M. H.; Spicer P. T.; Solomon M. J. *Langmuir* **2009**, *25*, 8951-8959.
5. Kawahara S.; Kawazura T.; Sawada T.; Isono Y. *Polymer* **2003**, *44*, 4527-4531.
6. Jinnai H.; Shinbori Y.; Kitaoka T.; Akutagawa K.; Mashita N.; Nishi T. *Macromolecules* **2007**, *40*, 6758-6764.
7. Kohjiya S.; Katoh A.; Suda T.; Shimanuki J.; Ikeda Y. *Polymer* **2006**, *47*, 3298-3301.
8. Tunnicliffe L. B.; Thomas A. G.; Busfield J. J. C. *J. Microscopy* **2012**, *246*, 77-82.
9. Yamanaka J.; Nakamura Y.; Nittono O. *Mater. Sci. Eng. A, Struct. Mater., Prop. Microstruct. Process* **1994**, *179-180*, 401-407.
10. Michler G. H. *J. Macromol. Sci. B, Phys.* **2001**, *40*, 277-296.
11. Kawahara S.; Klinklai W.; Kuroda H.; Isono Y. *Polym. Adv. Technol.* **2004**, *15*, 181-184.
12. Klinklai W.; Saito T.; Kawahara S.; Tashiro K.; Suzuki Y.; Sakdapipanich J. T.; Isono Y. *J. Appl. Polym. Sci.* **2004**, *93*, 555-559.
13. Pukkate N.; Kitai T.; Yamamoto Y.; Kawazura T.; Sakdapipanich J.; Kawahara S. *Eur. Polym. J.* **2007**, *43*, 3208-3214.
14. Pukkate N.; Yamamoto Y.; Kawahara S. *Colloid Polym. Sci.* **2008**, *286*, 411-416.
15. Fukuhara L.; Kosugi K.; Yamamoto Y.; Jinnai H.; Nishioka H.; Ishii H.; Kawahara S. *Polymer* **2015**, *57*, 143-149.

16. Kawahara S.; Yamamoto Y.; Fujii S.; Isono Y.; Niihara K.; Jinnai H.; Nishioka H.; Takaoka A. *Macromolecules* **2008**, *41*, 4510-4513.

17. Kosugi K.; Sutthangkul R.; Chaikumpollert O.; Yamamoto Y.; Sakudapipanich J.; Isono Y.; Kawahara S. *Colloid Polym. Sci.* **2012**, *290*, 1457-1462.

Chapter 6

Preparation of Polymer Electrolyte Membrane with Nanomatrix Channel through Sulfonation of Natural Rubber Grafted with Polystyrene

6.1 Introduction

Mechanism of proton-transport is widely recognized to be indispensable to understand the role of polymer electrolyte membrane (PEM) in fuel cell, which is useful to design a novel PEM as a factor. For instance, the mechanism of the proton-transport for perfluorosulfonic acid is classified into two categories: that is, Grotthuss mechanism and Vehicle mechanism, in which the protons are transported by connecting ion cluster of 20 to 30 nm in diameter through a channel of several nm in thickness.[1] The difference in the proton-transport between the two mechanisms are schematically illustrated in Figure 6-1. In the Vehicle mechanism, the protons are transported by diffusing into water as hydrated proton aggregates. In the Grotthuss mechanism,

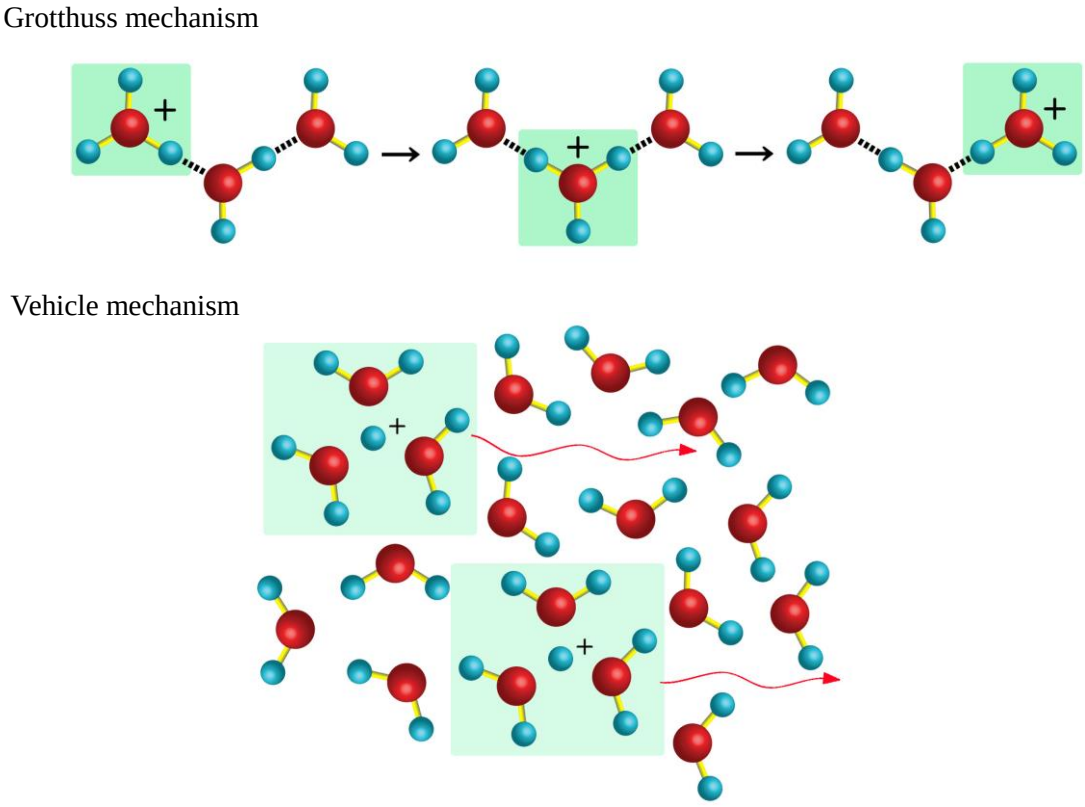

Figure 6-1 Schematic illustration of proton-transport in PEM

in contrast, the protons are transported by jumping from one sulfonic acid to the other through aqueous environment, in which an effective proton concentration may be an important factor for the proton-transport. It is, therefore, quite important to investigate the relationship between proton conductivity and temperature, since the effective proton concentration of PEM may be estimated from Arrhenius plot.

In our previous works [2-3], nanomatrix channel was proposed to be the novel nano-phase separated structure for the effective proton-transport, which consisted of particles of hydrophobic polymer of about 1 μm in diameter covered with a nano-layers of hydrophilic polymer. It possessed infinite paths of nano-channel to transport the protons, which was useful for the PEM. The nanomatrix channel was formed by graft-copolymerization of styrene onto surface of natural rubber particles in latex stage followed by sulfonation with chlorosulfonic acid, as shown in Figure 6-2. A proton conductivity of the resulting PEM (SDPNR-*graft*-PS) was higher than that of sulfonated polystyrene and perfluorosulfonic acid membranes. However, the mechanism was not investigated with respect to the proton transport of SDPNR-*graft*-PS.

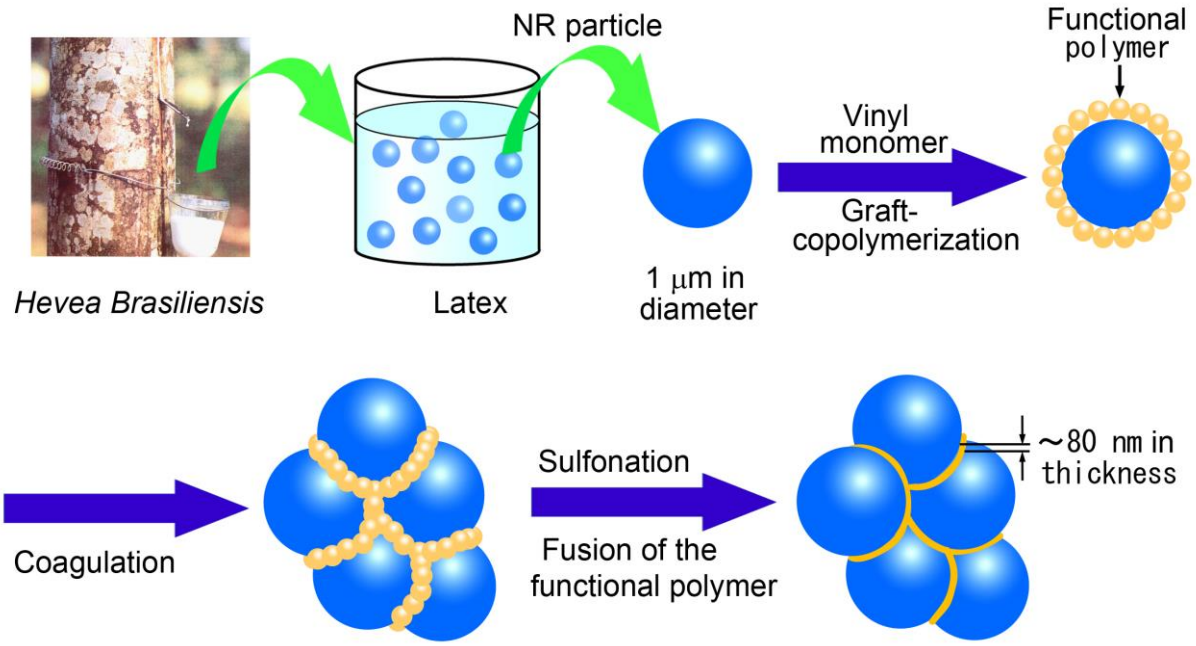

Figure 6-2 Preparation of PEM with nanomatrix channel from natural rubber

Many studies on the proton-transport of the PEM have been performed with sulfonic acid containing membranes.[4-8] Yeo and co-workers [9] reported that the proton conductivity of the PEM increased with increasing temperature and it was dependent upon water content on the basis of the ion cluster model. Moreover, Zhong and co-workers estimated an activation energy of the PEM to investigate a mechanism of the proton-transport: that is, 14-40 kJ/mol for Grotthuss mechanism and more than 40 kJ/mol for vehicle mechanism. [10] Therefore, it is possible to investigate the mechanism of the proton-transport of PEM with nanomatrix channel with respect to the activation energy of the proton conductivity.

In the present study, condition of graft-copolymerization of styrene onto deproteinized natural rubber (DPNR) in latex stage was optimized to prepare DPNR-*graft*-PS. The resulting DPNR-*graft*-PS was sulfonated with chlorosulfonic acid to prepare a PEM with nanomatrix channel. The resulting sulfonated graft-copolymer (SDPNR-*graft*-PS) was characterized by FT-IR spectroscopy, solid state ^{13}C CP/MAS NMR spectroscopy, elemental analysis, transmission electron microscopy (TEM) and impedance analyzer. The proton conductivity was analyzed as a function of temperature.

6.2 Experimental

6.2.1 Materials

Natural rubber latex used in the present study was commercial high ammonia natural rubber (HANR) latex (Golden Hope, Malaysia) of about 60% dry rubber content (DRC). Sodium dodecyl sulfate (SDS: 98%), *tert*-butyl hydroperoxide (TBHP) and tetraethylenepentamine (TEPA) were purchased from Kishida Chemical Co., Ltd. Chloroform-*d* (99.8%), chloroform (99%) and chlorosulfonic acid (97%) were purchased from Wako Pure Chemical Industry Ltd. Styrene monomer (99%) was purchased from Tokyo Chemical Industry Co., Ltd. Methanol (99.5%), toluene (99.5%), sodium hydroxide (NaOH: 97%), urea (99.5%) were purchased from Nacalai tesque Inc. Ruthenium tetroxide (RuO_4) was prepared by oxidation of ruthenium (III) chloride hydrate ($RuCl_3 \cdot H_2O$) with sodium hypochlorite solution (NaClO) purchased from Aldrich and Nacalai tesque Inc., respectively.

6.2.2 Preparation of DPNR

Deproteinization of natural rubber was performed by incubation of natural rubber latex with 0.1 wt% urea in the presence of 1 wt% SDS at room temperature for 1 h followed by centrifugation at 10^4 rpm. The cream fraction after centrifugation was re-dispersed in 0.5 wt% SDS solution to make 30 wt% DRC latex and it was washed twice by centrifugation to prepare DPNR latex. The DRC of DPNR latex was adjusted to 30 wt% with distilled water and SDS was added up to 0.1 wt %.

6.2.3 Preparation of DPNR-*graft*-PS

Graft-copolymerization of DPNR latex was carried out with styrene as a monomer, using TBHP/ TEPA as an initiator. DPNR latex was charged with N_2 gas for an hour at 303 K. 3.3×10^{-2} mol/kg-rubber of initiator and 1.5 mol/kg-rubber of monomer were added in turn to the latex, respectively. The reaction was carried out by stirring the latex at about 400 rpm for 5 h at 303 K. The un-reacted styrene was removed by using a rotary evaporator under reduced pressure. The as-cast film of the DPNR-*graft*-PS was prepared by casting the gross polymer latex into a Petri-dish and it was dried under reduced pressure at ambient temperature for more than a week. The gross polymer was extracted with acetone/2-butanone 3:1 mixture in a Soxhlet apparatus under nitrogen atmosphere in the dark and dried under reduced pressure for a week, in which the removal of almost all free-polystyrene, isolated from natural rubber, was completed by the extraction for 24 h.

6.2.4 Preparation of SDPNR-*graft*-PS

Sulfonation of DPNR-*graft*-PS was performed by the following procedure. The DPNR-*graft*-PS film was immersed in chloroform for 5 min until swollen. The sulfonation of the DPNR-*graft*-PS was carried out with a solution of 0.8 N chlorosulfonic acid in chloroform at 323 K for 5 h. After completion of the sulfonation, the resulting membrane was immersed into methanol for 30 min, followed by washed several times with ion-exchange water until water was neutral. The resulting SDPNR-*graft*-PS was dried under reduced pressure at 323 K. Prior to characterizations of the SDPNR-*graft*-PS, the

membranes were acidified with 0.5 mol/L H_2SO_4 solution at 353 K for 1 h and rinsed with water. Then, they were boiled with ion exchange water at 353 K for 1 h, twice, followed by dried under reduced pressure at 323 K for a week.

6.2.5 Characterization

NMR measurements were carried out using a JEOL ECA-400 spectrometer operating at 399.65 and 100.4 MHz for ^{1}H and ^{13}C, respectively. For a solution state ^{1}H NMR measurement, the rubber was dissolved into chloroform-*d* without tetramethylsilane (TMS). Chemical shifts were referred to chloroform in chloroform-*d*. Solid state CP/MAS NMR measurement was carried out at room temperature with spin rate of 7 kHz, scan time of 1000 scans, and contact time of 5 sec, respectively. Hexamethylbenzene was used as an external standard (17.3 ppm). The samples were crushed by JFC-300 cryogenic sample crusher before the measurement.

Sulfur content of the samples was determined by elemental analysis (YANACO MT-6 and MSU-32 microanalyzers).

Water uptake of the samples was measured by the following method. The membranes were soaked in water at room temperature for a week to reach the saturated point of the membrane. Water-droplets on the surface of swollen membranes were removed by wiping with tissue paper. The water uptake was determined from a weight of swollen membrane and dry membrane.

Ion exchange capacity (IEC) of the samples was investigated by titration method. The samples were immersed in 2 N NaCl solution for a week to replace H^+ to Na^+ ions. The H^+ ions in the solution were titrated with 0.1 N of NaOH solution in the present of phenolphthalein as an indicator. The IEC (meq/g) was calculated from the volume of NaOH solution and weight of dry membrane.

Proton conductivity was measured with a Solartron SI 1260 impedance/gain-phase analyzer and potentiostat (Solartron SI 1287 electrochemical interface) in a range of the frequency between 10 μHz and 10 MHz at AC voltage amplitude of 10 mV. The impedance was measured by placing the cell in a temperature-controlled chamber (ESPEC CORP, SU-222) under a temperature range of 323-353 K.

The membranes were hydrated by immersion in ion-exchange water for 3 h before measurement.

Observations of morphology for the samples were made with a transmission electron microscope (TEM), JEOL JEM-2100 at accelerating voltage of 200 kV. The ultra thin sections for the TEM experiments were prepared with a microtome (Ultracut N, Reichert-Nissei FC S) between 233 and 183 K. The thin sections with the thickness of about 100 nm were stained with RuO_4 at room temperature for 1 min.

6.3 Results and Discussion

Figure 6-3 shows FT-IR spectra for DPNR, polystyrene (PS) and DPNR-*graft*-PS prepared with 1.5 mol/kg-rubber of styrene and 3.3×10^{-2} mol/kg-rubber of initiator, ranging from 1500 cm^{-1} to 2000 cm^{-1}. As for DPNR (Figure 6-3(A)), two peaks appeared at 1660 and 1740 cm^{-1}, which were identified to stretching vibrations of carbon-carbon double bond of *cis*-1,4-isoprene units and carbonyl group of fatty acid contained in natural rubber as a non-rubber component, respectively. In contrast, for PS, six peaks appeared at 1580, 1600, 1740, 1800, 1870 and 1950 cm^{-1}, which was identified to phenyl group of styrene units.

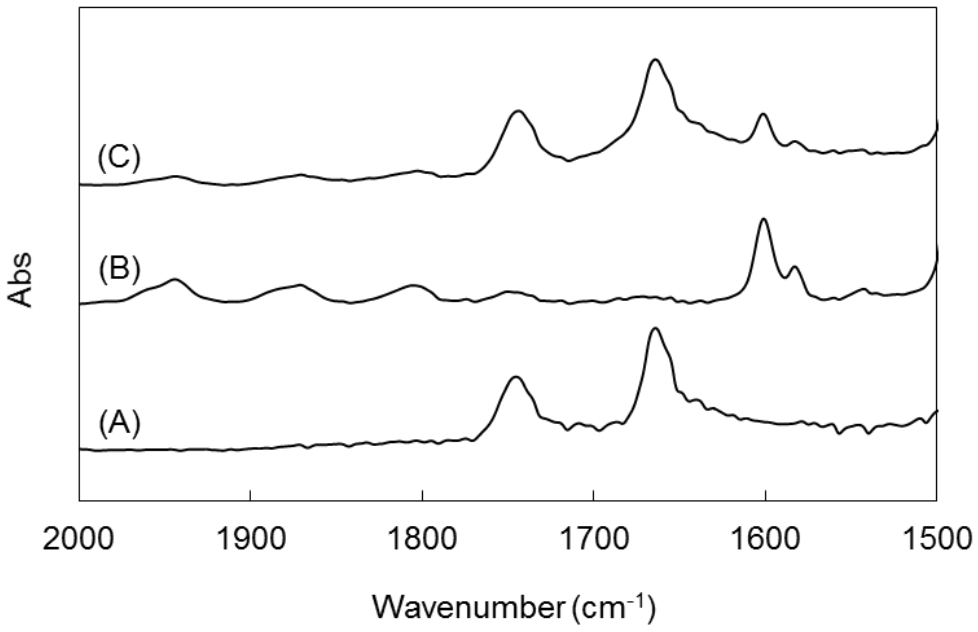

Figure 6-3 FT-IR Spectra of (A) DPNR, (B) polystyrene, and (C) DPNR-*graft*-PS

After graft-copolymerization, peaks appearing in the spectrum for DPNR-*graft*-PS were, thus, identified to *cis*-1,4-isoprene units and styrene units. The intensity of the peak at 1600 cm^{-1} was a little bit smaller than that of the peak at 1660 cm^{-1}. However, we couldn't quantitatively determine the styrene unit content of the DPNR-*graft*-PS, since it was heterogeneous multi-component system, which possessed PS domains and DPNR domains, individually. Therefore, In order to determine the styrene unit content, the DPNR-*graft*-PS was subjected to solution state ^{1}H-NMR spectroscopy.

Figure 6-4 shows solution state ^{1}H-NMR spectra for DPNR and DPNR-*graft*-PS prepared with 1.5 mol/kg-rubber of styrene and 3.3×10^{-2} mol/kg-rubber of initiator. In the spectrum for DPNR, three signals appeared at 1.8, 2.1 and 5.1 ppm, which were assigned to methyl, methylene and unsaturated methine protons of *cis*-1,4-isoprene units, respectively. After graft-copolymerization of styrene onto DPNR (Figure 6-4(B)), two broad signals appeared at 6-7 ppm, which were assigned to phenyl proton of styrene units. The signals of the aliphatic protons of polystyrene were overlapped with that of *cis*-1,4-isoprene units at 1.8-2.1 ppm. From the intensity of the signals, we estimated styrene unit contents of DPNR-*graft*-PS and, subsequently, conversion and grafting efficiency of styrene.

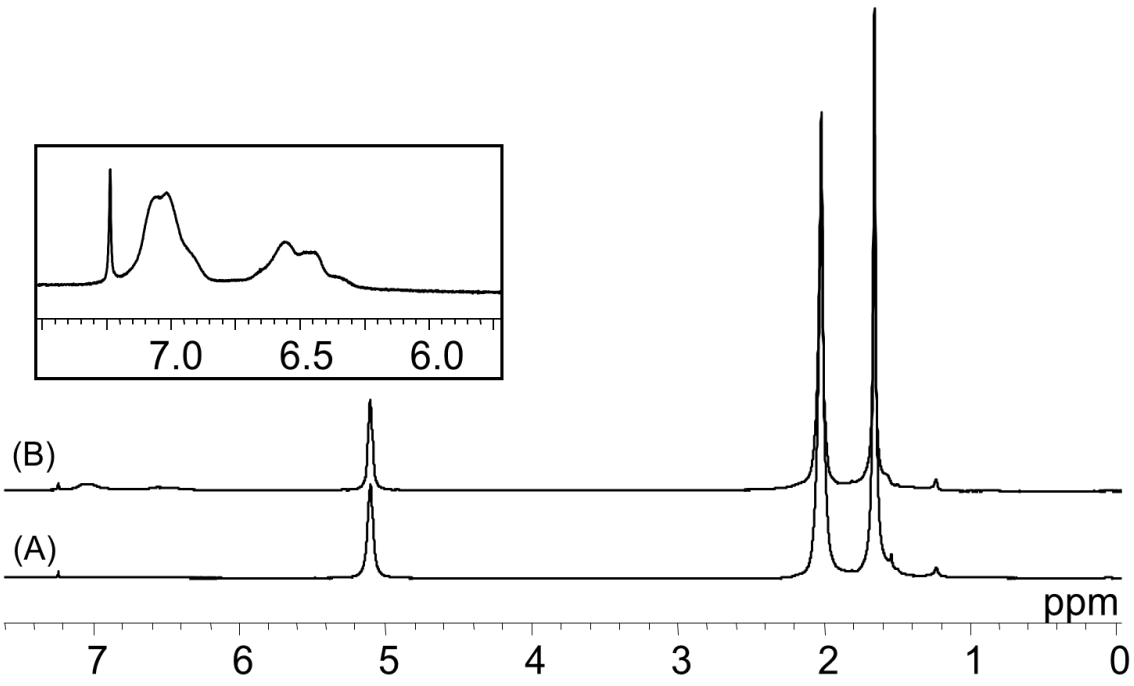

Figure 6-4 ^{1}H NMR spectra of (A) DPNR and (B) DPNR-*graft*-PS

The conversion of styrene, content of styrene units and grafting efficiency of styrene were estimated, as in the following equations:

$$\text{Conversion of styrene } (\%) = \frac{\text{Weight of polystyrene in gross polymer}}{\text{Weight of polystyrene used for the graft copolymer}} \times 100 \quad (6\text{-}1)$$

$$\text{Content of styrene } (\%) = \frac{\text{Weight of polystyrene in gross polymer}}{\text{Weight of gross polymer}} \times 100 \quad (6\text{-}2)$$

$$\text{Grafting efficiency} (\%) = \frac{\text{Mole of polystyrene linking to natural rubber}}{\text{Mole of polystyrene produced during graft copolymerization}} \times 100 \quad (6\text{-}3)$$

where mole of polystyrene in gross polymer, mole of gross polymer and mole of monomer were estimated from intensity ratios of the signals appearing in the NMR spectra and weights of specimen determined by gravimetric method. Table 6-1 shows conversion and grafting efficiency of styrene, and styrene unit content, respectively. The conversion and grafting efficiency of styrene were dependent upon the feeds of initiator and styrene; for instance, a maximum value of the conversion, i.e. 91 %, was accomplished at 1.5 mol/kg-rubber of styrene and 3.3×10^{-2} mol/kg-rubber of the initiator. In contrast, the styrene unit content of DPNR-*graft*-PS increased with increasing the feed of styrene. The styrene unit content was the highest, i.e. 12 %, at 1.5 mol/kg- rubber of styrene and 3.3×10^{-2} mol/kg-rubber of the initiator. This may be explained to be due to deactivation and chain transformation of the radicals, which may come from less and large amount of styrene, respectively. These results indicate that suitable feeds of initiator and styrene for the graft- copolymerization are 3.3×10^{-2} mol/kg-rubber and 1.5 mol/kg-rubber, respectively.

Table 6-1 Conversion, content and grafting-efficiency in the graft-copolymerization

Feed of Styrene (mol/kg-rubber)	Feed of Initiator (mol/kg-rubber)	Conversion of styrene (%)	Grafting efficiency of styrene (%)	Styrene unit content (%)
1.5	1.0×10^{-2}	42	68	6
1.5	1.7×10^{-2}	47	65	6
1.5	3.3×10^{-2}	91	91	12
1.5	6.6×10^{-2}	77	59	10
0.5	3.3×10^{-2}	4	1	1
2.0	3.3×10^{-2}	82	77	15
2.5	3.3×10^{-2}	66	75	15

Figure 6-5 shows TEM images for DPNR-*graft*-PS prepared with 1.5 mol/kg-rubber of styrene and 3.3×10^{-2} mol/kg-rubber of initiator. The bright domains represent polystyrene and the gloomy domains represent natural rubber, since DPNR-*graft*-PS was stained with OsO_4. [11] Natural rubber particles of about 1 μm in average diameter were well dispersed in the PS nanomatrix of about 30 nm in thickness, which consisted of PS nano-particles of about 5 nm in diameter to form a discontinuous nanomatrix, as reported in our previous work. [12] This implies that the matrix is less useful for proton conductivity, because of the discontinuity. Consequently, the DPNR-*graft*-PS was found to be a precursor to prepare the PEM with nanomatrix channel. It is necessary to form continuous nanomatrix and convert PS to a proton conductive medium.

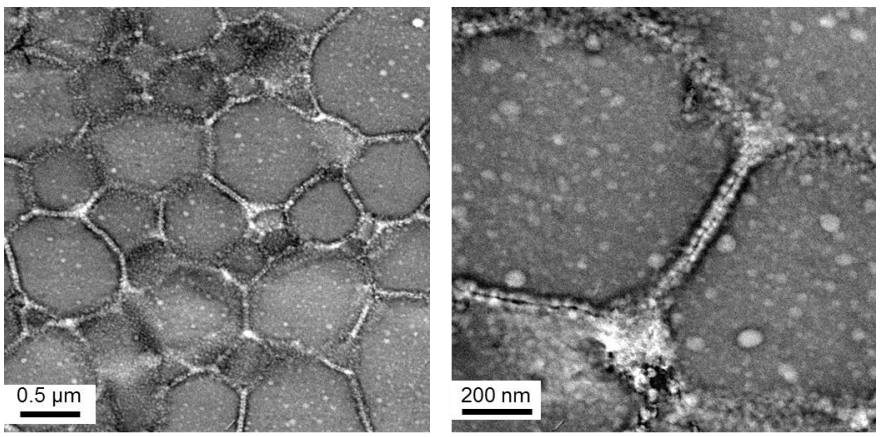

(A) (B)

Figure 6-5 TEM images of DPNR-*graft*-PS: (A) ×5000, (B) ×20000

The resulting DPNR-*graft*-PS prepared was sulfonated with chlorosulfonic acid. Figure 6-6 shows FT-IR spectra for DPNR-*graft*-PS, SDPNR-*graft*-PS and sulfonated DPNR (SDPNR). Peak height of the spectrum was normalized in comparison with a height of reference peak at 1660 cm^{-1} identified as the stretching vibration of the carbon-carbon double bond of *cis*-1,4-isoprene unit. It was found that the absorbance peaks at 3400 cm^{-1}, 1164 cm^{-1} and 1038 cm^{-1} appeared in the spectra of SDPNR-*graft*-PS (Figure 6-6(B)) and sulfonated DPNR (Figure 6-6(C)) whereas they did not appear in the spectrum of DPNR-*graft*-PS (Figure 6-6(A)). The absorbance peaks at 3400 cm^{-1}, 1164 cm^{-1} and 1038 cm^{-1} were identified to OH stretching vibration, S=O asymmetric stretching vibration and S=O symmetric stretching vibration of the sulfonic acid group, respectively. Furthermore, the peak at 1009 cm^{-1} was identified to the in-plane bending vibration of a para-substituted aromatic ring of the sulfonated polystyrene. [13] These results suggested that the sulfonic acid groups were incorporated into not only styrene units of DPNR-*graft*-PS but also natural rubber, after sulfonation of DPNR-*graft*-PS with chlorosulfonic acid.

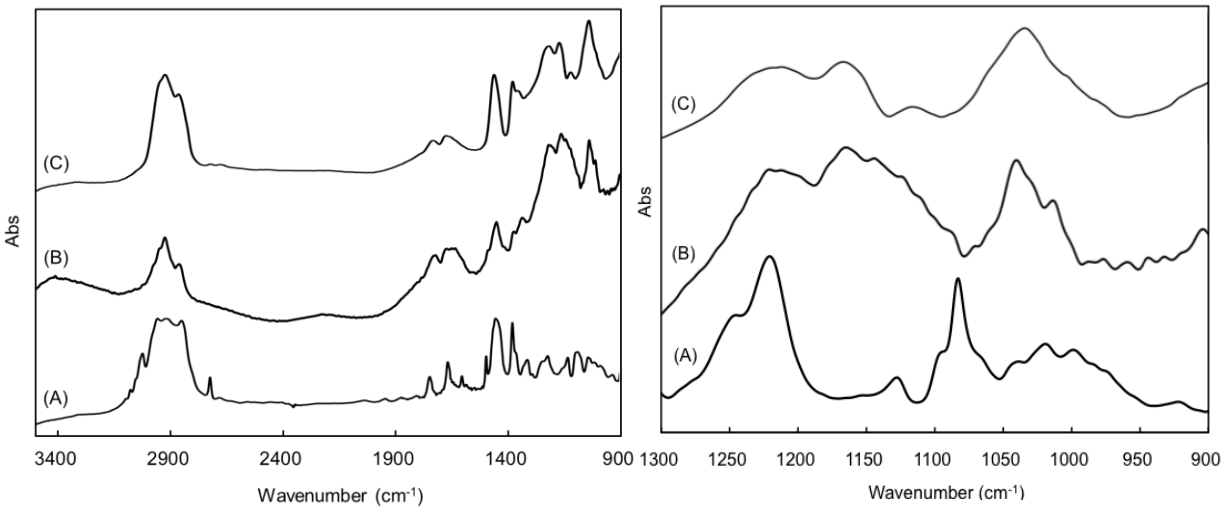

Figure 6-6 FT-IR spectra for (A) DPNR-*graft*-PS, (B) SDPNR-*graft*-PS and (C) sulfonated DPNR

Figure 6-7 shows the ^{13}C CP/MAS NMR spectra for DPNR-*graft*-PS, SDPNR-*graft*-PS, and sulfonated DPNR. In the spectrum of DPNR-*graft*-PS, five signals appeared at 24, 27, 33, 126 and 136 ppm, which were assigned to methyl, methylene, methylene, methine and quaternary carbons of *cis*-1,4-

isoprene units, respectively (Figure 6-7 (A)). Furthermore, signals at 41 and 147 ppm were assigned to methylene carbon and aromatic carbons of the styrene units, respectively. After sulfonation of DPNR-*graft*-PS (Figure 6-7(B)), new broad signals appeared at 120-150 ppm, which overlapped with the signals of olefinic carbon of *cis*-1,4-isoprene units and aromatic carbons of styrene units. In contrast, very broad signals appeared in the aliphatic region ranging from 10 ppm to 80 ppm. They also overlapped with many signals in the spectrum. The signals shown in Figure 6-7(B) were assigned by comparison with that of sulfonated DPNR as a model compound. In the spectrum of sulfonated DPNR (Figure 6-7(C)), two overlapping broad signals appeared at 10-80 ppm and 110-155 ppm, respectively. The broad signals appeared due to the presence of complicated structural units in the polymer after sulfonation of the DPNR. According to a previous study, the overlapping broad signals in the aliphatic region ranging from 10 ppm to 80 ppm were assigned to methyl and methylene carbons of cyclized *cis*-1,4-isoprene units, and that in the olefinic region ranging from 110 ppm to 155 ppm were assigned to the olefinic methine and trisubstituted carbons. [14] Thus, the broad signals in the ^{13}C CP/MAS NMR spectrum for the SDPNR-*graft*-PS were assigned to the cyclized *cis*-1,4-isoprene units and the sulfonated PS units.

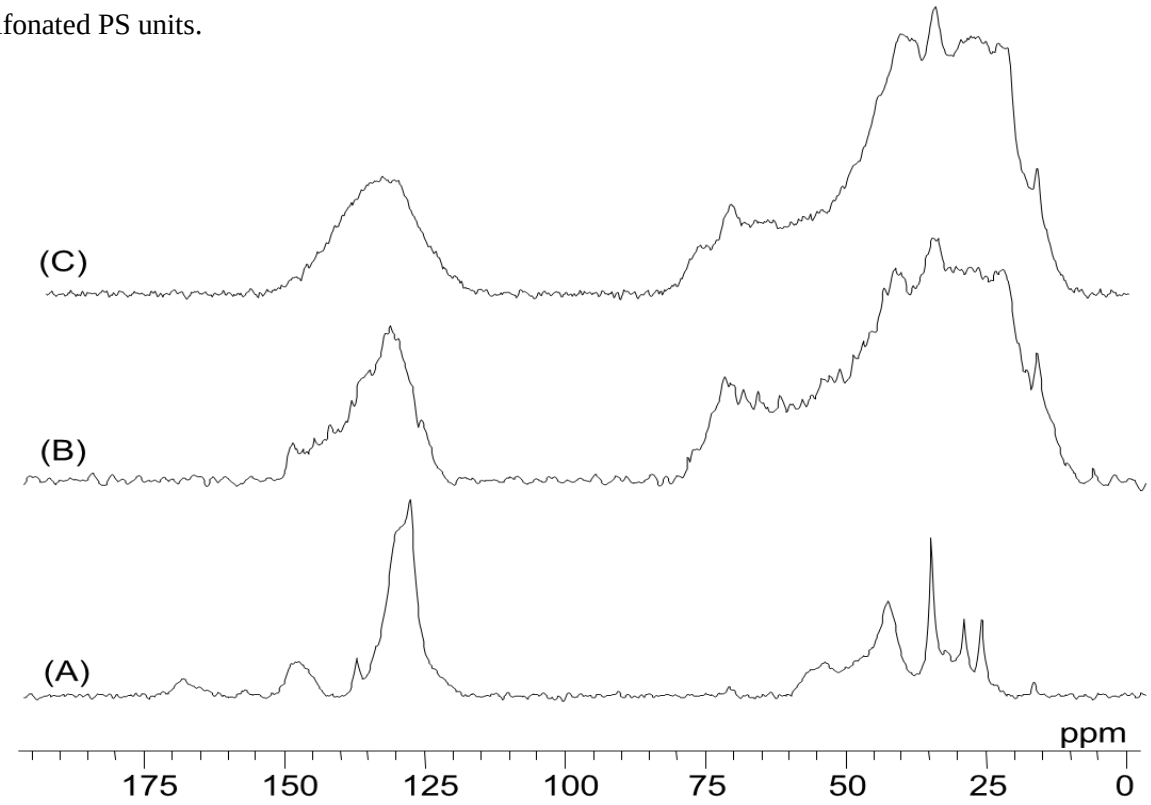

Figure 6-7 ^{13}C CP/MAS NMR spectra for (A) DPNR-*graft*-PS, (B) SDPNR-*graft*-PS, and (C) SDPNR

Figure 6-8 shows TEM images for SDPNR-*graft*-PS, which was prepared with a chloroform solution of 0.8 N chlorosulfonic acid. The bright domains represent natural rubber and the gloomy domains represent sulfonated PS, since the film specimen was stained with RuO_4. The dark sulfonated PS domains was found to form continuous nanomatrix, i.e. the nanomatrix channel, the thickness of which was about 60 nm. On the other hand, the bright natural rubber domains, which contained cyclized natural rubber, were dispersed in the nanomatrix. These demonstrate that the continuous nanomatrix channel is formed in chloroform solution without destroying the nanomatrix structure. This may be explained to be due to the difference in the molecular weight between natural rubber and PS. In the previous work, It was reported that the weight average molecular weight of PS of DPNR-*graft*-PS was approximately 15 thousand, which was significantly lower than that of natural rubber, i.e. about 2 million. In this case, lower molecular weight PS may be easily dissolved into chloroform, whereas higher molecular weight natural rubber may not. Thus, the PS nano-particles may be dissolved in to chloroform to form the continuous nanomatrix and, then, PS may react with chlorosulfonic acid. During this reaction, natural rubber particles may keep their shapes. The continuous nanomatrix channel, thus formed, may be useful to transport protons as a PEM.

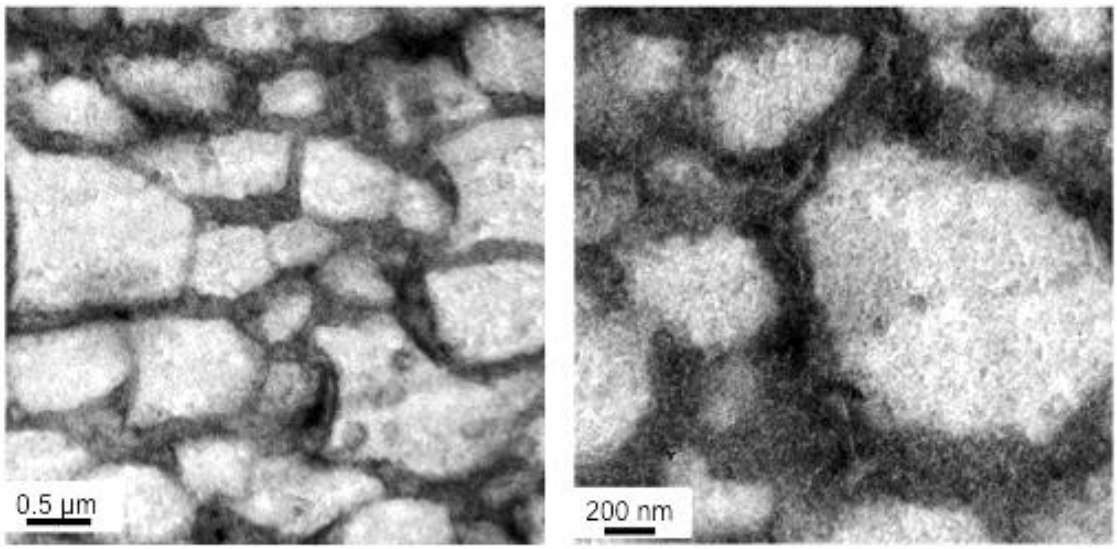

(A) (B)

Figure 6-8 TEM images of SDPNR-*graft*-PS: (A) ×5000, (B) ×20000

Table 6-2 Sulfur content, proton conductivity, IEC, and water uptake of DPNR, SDPNR, DPNR-*graft*-PS, SDPNR-*graft*-PS, and Nafion®117

Specimen	Sulfur content (wt%)	Conductivity[a)] (S/cm)	IEC (meq/g)	Water uptake (wt%)
DPNR	-	0.0	0.00	-
SDPNR	5.8	0.011	1.15	51.2
DPNR-*graft*-PS	-	0.0	0.00	-
SDPNR-*graft*-PS	10.2	0.29	1.44	66.5
Sulfonated PS	-	0.032	1.50	340.0
Nafion®117	-	0.055	1.02	18.6

[a)] measured at 323K

Table 6-2 shows the sulfur content, proton conductivity, IEC, and water uptake of DPNR, sulfonated DPNR, DPNR-*graft*-PS, SDPNR-*graft*-PS, and Nafion®117. The sulfur content was estimated, as in the following equation:

$$\mathrm{Sulfur\,content\,(wt\%)} = \frac{\mathrm{Weight\,of\,sulfur}}{\mathrm{Weight\,of\,sample}} \times 100 \qquad (6\text{-}4)$$

where weight of sulfur was determined from the results of an elemental analysis. The sulfur content of the sulfonated DPNR was 5.8 w/w% because the sulfonic acid group was incorporated into the DPNR, as shown in Figure 6-6(C). In contrast, the sulfur content of the SDPNR-*graft*-PS was 10.2 w/w%, which was twice as high as that of sulfonated DPNR. This may be explained to be due that nucleophilic sulfonation proceeded preferentially on the benzene ring of the polystyrene. On the other hand, a degree of sulfonation estimated from sulfur content was 276 mol%, suggesting that sulfonic acid group was incorporated into not only benzene ring of polystyrene but also natural rubber.

$$\mathrm{Degree\ of\ sulfonation\,(mol\%)} = \frac{\mathrm{mol\,of\ sulfur}}{\mathrm{mol\,of\ styrene\,unit}} \times 100 \qquad (6\text{-}5)$$

In table 6-2, the value of the proton conductivity of SDPNR-*graft*-PS was about 5 times as high as that of Nafion®117. It was about 10 times higher than the value of the proton conductivity of sulfonated PS, even though the amount of sulfonated PS contained in SDPNR-*graft*-PS was about 1/3, compared with sulfonated PS, itself. It is, consequently, rational to consider that the value of the proton conductivity of sulfonated PS present in SDPNR-graft-PS is 5 times as high as that of Nafion®117, when the proton conductive path was assigned to sulfonated PS phase. The 5 times higher value of the proton conductivity may correspond to the 10 times higher effective H^+ concentration. This is consistent with the fact that a part of the ion clusters present in Nafion®117 are connected to each other to transport H^+, but the others are not. Based on the results, it is possible to conclude that the nanomatrix channel of SDPNR-*graft*-PS plays an important role in the effective transport of the protons, by a factor of 10.

The IEC of the rubbers was investigated by titration method, in which the calculation was shown in the following equation:

$$\mathrm{IEC(wt\%)} = \frac{N_{\mathrm{NaOH}} \times V_{\mathrm{NaOH}}}{W_{\mathrm{dry}}} \times 100 \qquad (6\text{-}6)$$

where N_{NaOH}, V_{NaOH}, and W_{dry} are the normality of NaOH, the volume of NaOH solution consumed in the titration, and the weight of the dry membrane (g), respectively. The values of IEC of sulfonated DPNR and SDPNR-*graft*-PS were 1.15 meq/g and 1.44 meq/g, whereas those of DPNR and DPNR-*graft*-PS were 0.00 meq/g. This may be attributed to the effect of the incorporated sulfonic acid groups of the rubber on the IEC.

The proton conductivity of the rubbers was calculated as follows:

$$\text{Proton conductivity } (\mathrm{S/cm}) = \frac{\mathrm{d}}{R \times A} \times 100 \qquad (6\text{-}7)$$

where d is the sample thickness, *R* is the membrane resistance, and *A* is surface

e area of the membranes. The proton conductivity of DPNR was 0 S/cm due to the absence of sulfonic acid group in the DPNR. In contrast, that of sulfonated DPNR was 1.1×10^{-2} S/cm. This may reflect to an incorporation of sulfonic acid group into DPNR. It is worthy of note that the proton conductivity of SDPNR-*graft*-PS was 9.8×10^{-2} S/cm, which was significantly higher than that of Nafion®117 (8.0×10^{-2} S/cm) and sulfonated DPNR (1.1×10^{-2} S/cm). This was attributed to an increase in the sulfur content and to the formation of continuous nanomatrix channel, as shown in Figure 6-8.

The water uptake of the rubbers was calculated through the following equation:

$$\text{Wateruptake}(\text{wt}\%) = \frac{W_{\text{wet}} \times W_{\text{dry}}}{W_{\text{dry}}} \times 100 \qquad (6\text{-}8)$$

where W_{wet} is the weight of swollen membrane and W_{dry} is the weight of the dry membrane. The water uptake of SDPNR-*graft*-PS was 66.5 wt%, which was similar to that of sulfonated DPNR. This is significantly distinguished from the water uptake of sulfonated PS, i.e. 340.0 wt%, even though the IEC of sulfonated PDNR-*graft*-PS was similar to that of sulfonated PS. The chemical linkages between sulfonated PS and DPNR may prevent swelling DPNR-*graft*-PS with water to reduce the water uptake.

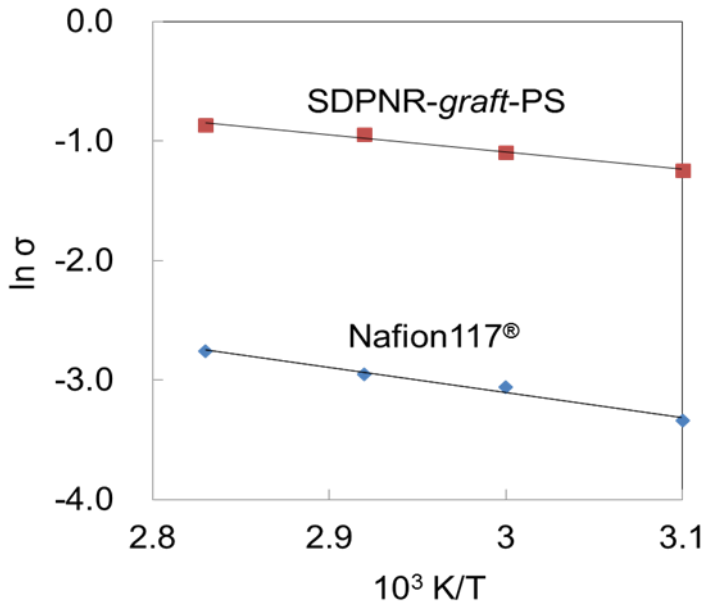

Figure 6-9 Arrhenius plot for proton conductivity, σ, of SDPNR-*graft*-PS and Nafion®117

Consequently, the nanomatrix channel was found to play an important role in high proton conductivity and low water uptake.

Figure 6-9 shows Arrhenius plot for proton conductivity, σ, of SDPNR-*graft*-PS and Nafion®117. The proton conductivity of SDPNR-*graft*-PS and Nafion®117increased with increasing temperature. The apparent activation energy of SDPNR-*graft*-PS and Nafion®117 was estimated from the slope of the plot, as in the following expression:

$$\sigma(T) = \sigma_0 \exp\left[-B/(T - T_0)\right] \times 100 \quad = \mathrm{A}T^{-1/2} \exp\left[-B/T - T_0\right] \tag{6-9}$$

where σ_0 is σ at T_0, A the effective H^+ concentration and B the Activation energy of H^+. The estimated values of the apparent activation energy were 12 kJ/mol for SDPNR-*graft*-PS and 17 kJ/mol for Nafion®117, respectively. The value of the activation energy for SDPNR-*graft*-PS was less than that for Nafion®117 and it was quite lower than the reported value of the activation energy for sulfonated polystyrene, i.e. about 30 kJ/mol.[15] From the results, it is expected that the proton-transport of SDPNR-*graft*-PS with nanomatrix channel and Nafion®117 occurs in a manner of Grotthuss mechanism, in which the proton-jump from one sulfonic acid to the other may takes place. In this case, the effective H^+ concentration for proton-transport may be compared between SDPNR-graft-PS and Nafion®117. In equation (6-9), T_0 of SDPNR-*graft*-PS may be assumed to be similar to that of Nafion®117, since SDPNR-*graft*-PS and Nafion®117 are floating in water in use. Furthermore, the slopes in Figure 6-9 may be approximated to be similar to each other. Under these circumstances, thus, the gap between the proton conductivities of SDPNR-*graft*-PS and Nafion®117 are directly proportional to the difference in the effective H^+ concentration estimated from intercept of the Arrhenius plot. The effective H^+ concentration of SDPNR-*graft*-PS was found to be about 10 times as high as that of Nafion®117, as shown in Figure 6-9.

6.4 Conclusion

SDPNR--*graft*-PS was prepared by graft-copolymerization of styrene onto DPNR followed by the sulfonation using chlorosulfonic acid. The proton conductivity, IEC, sulfur content, and water uptake were 9.8×10^{-2} S/cm, 1.41 meq/g, 10.2 w/w%, and 66.5 w/w%, respectively. TEM observation of the SDPNR-*graft*-PS revealed the formation of a continuous nanomatrix channel, which is effective to transport a lot of proton. The activation energy of SDPNR-*graft*-PS and Nafion®117 was 12 kJ/mol and 17 kJ/mol, respectively. The proton-transport in SDPNR-*graft*-PS with nanomatrix channel and Nafion®117was found to occur mainly via Grotthuss mechanism, since the activation energy of the membranes was less than 40 kJ/mol. The low value of the apparent activation energy and high value of the effective proton concentration for SDPNR-*graft*-PS demonstrated that the nanomatrix channel of SDPNR-*graft*-PS contributed to the effective transport of the protons.

6.5 References

1. Hsu, W. Y. ; Gierke T. D. *J. Membr. Sci*. **1983**, 13, 307.
2. Kawahara, S.; Suksawad, P.; Yamamoto, Y.; Kuroda H. *Macromolecules* **2009**, 42, 8557.
3. Suksawad, P.; Kosugi, K.; Yamamoto, Y.; Akabori, K.; Kuroda, H.; Kawahara, S. *J. Appl. Polym. Sci*. **2011**, 122, 2403.
4. Wu, X.; Scott, K. *Fuel Cells* **2013**, 13, 1138.
5. Jetsrisuparb, K.; Ben youcef, H.; Wokaun, A.; Gubler, L. *J. Membrane Sci*. **2014**, 450, 28.
6. Fimrite, J.; Struchtrup, H.; Djilali, N. J. *Electrochem. Soc*. **2005**, 152, 1804.
7. Schmidt-Rohr, K.; Chen, Q. *Nature* **2008**, 7, 75.
8. Sata, T. Ion Exchange Membranes, Preparation, Characterization, Modification and Application; The Royal Society of Chemistry: London, **2004**.
9. Yeo, R. *Electrochem.* S. *Sci. Technol.* **1983**, 130, 533.
10. Zhong S.; Cui, X.; Dou, S.; Luo, Y.; Cui, W.; Zhao S.; Zhu, H.; Liu, W. *Solid State Ionics* **2010**, 181, 1499.

11. Kato, M.; Ito, T.; Aoyama, Y.; Sawa, K.; Kaneko, T.; Kawase, N.; Jinnai, H. *J. Polym. Sci.*: Part B: *Polym. Phys*. **2007**, 45, 677.

12. Kawahara, S.; Yamamoto, Y.; Fujii, S.; Isono, Y.; Niihara, K.; Jinnai, H.; Nishioka, H.; Takaoka, A. *Macromolecules* **2008**, 44, 4510

13. Kim, J.; Kim, B.; Jung, B. *J. Membr. Sci*. **2002**, 207, 129.

14. Patterson, D. J.; Koenig, J. L. *Makromol. Chem*. **1987**, 188, 2325.

15. Carretta, N.; Tricoli, V.; Picchioni, F. *J. Membr. Sci*. **2000**, 166, 189.

Chapter7

General Conclusion

The nanomatrix structure, formed by graft-copolymerization of styrene onto natural rubber followed by preparation of film, was observed by 3D imaging techniques, i.e., TEMT method and FIB-SEM. The 3D images, thus obtained, revealed that the nanomatrix structure was comprised of natural rubber particles of about 1 μm in average diameter and PS nano-particles of about 5 nm in diameter. The PS nano-particles gathered to form the nanomatrix, in which the natural rubber particles were well dispersed, and the distance between the PS nano-particles were about 5 nm. The outstanding mechanical properties of natural rubber with the nanomatrix structure were closely related to the discontinuous nanomatrix densely aligned structure of the PS nano-particles. The increase in the proton-conductivity was also associated with the continuous nanomatrix.

The protein free natural rubber and the leached natural rubber gloves were prepared under various conditions. The extractable protein content and nitrogen content were 0.0 μg/g and 0.000 w/w% for the protein free natural rubber and they were 86 μg/g and 0.175 w/w% for the leached natural rubber glove. It was found that two times centrifugation was needed for the preparation of the protein free natural rubber. The nanomatrix of the non-rubber components disappeared after removal of the proteins.

Graft-copolymer of natural rubber with PS, which had the nanomatrix structure, was prepared by graft-copolymerization of styrene onto DPNR and fresh DPNR with *tert*-butyl hydroperoxide / tetraethylenepentamine as an initiator in latex stage. The highest styrene conversion of 98 mol% and the grafting efficiency of 80 mol% were achieved at 1.5 mol/kg-rubber of styrene and 3.3×10^{-2} mol/kg-rubber of initiator. The nanomatrix structure was observed in TEM photographs of the fresh DPNR-*graft*-PS. The values of the stress at break of DPNR-*graft*-PS and fresh DPNR-*graft*-PS was 18 MPa and 21 MPa, respectively, in spite of no crosslinking.

TEM and TEMT observations of the ultra-thin sections prepared by FIB processing were made for the DPNR-*graft*-PS with the nanomatrix structure. The dimension of the ultra-thin section

prepared by FIB processing was about 6 μm×9 μm×54 nm, which was extremely smaller than that prepared with the cryo-microtome. It was demonstrated by TEM and TEMT observations that the FIB processing was superior in non-destructive nature to prepare the ultra-thin section; that is, the spatial position of the nanomatrix structure was maintained by the FIB processing due to no physical contact, whereas it was distorted with the cryo-microtome due to the physical contact with the glass knife. The nanomatrix structure was found to be the complexly hieratical structure comprising of the natural rubber micro-particles and the nanomatrix of PS nano-particles / natural rubber. In the nanomatrix, the PS nano-particles of about 5 nm in diameter were closely dispersed, whose distance was about 5 nm. The FIB processing was proved to be indispensable for the TEMT observation of the nano strucutre, i.e. the nanomatrix structure of DPNR-*graft*-PS.

TEMT method, FIB-SEM and synchrotron scattering techniques were applied to DPNR-*graft*-PS with the nanomatrix structure to elucidate the relationship between morphology and mechanical properties. The nanomatrix structure was found to consist of natural rubber particles of about 1 μm in average diameter and polystyrene nano-particles of 5.6 nm in diameter, in which the PS nano-particles were densely packed in the nanomatrix. The increase in the tensile strength and frequency independent loss tangent at plateau region were attributed to the discontinuous nanomatrix structure. DPNR-*graft*-PS with the nanomatrix structure was pressed at 303 K and 7 MPa, in order to make the nanomatrix continuous. The frozen anisotropic rubber particles were obtained in conjunction with the continuous PS-nanomatrix. The increase in the stress at strain of 1 and 35 times increase in the storage modulus (*G*') as well as frequency dependent loss tangent (tanδ) were attributed to the continuous nanomatrix structure.

SDPNR-*graft*-PS was prepared by graft-copolymerization of styrene onto DPNR followed by sulfonation using chlorosulfonic acid. The proton conductivity, IEC, sulfur content, and water uptake were 9.8×10^{-2} S/cm, 1.41 meq/g, 10.2 w/w%, and 66.5 w/w%, respectively. TEM observation of the SDPNR-*graft*-PS revealed the formation of a continuous nanomatrix channel, which is effective to transport a lot of proton. The activation energies of SDPNR-*graft*-PS and Nafion®117 were 12

kJ/mol and 17 kJ/mol, respectively. The proton-transport in SDPNR-*graft*-PS with nanomatrix channel and nafion®117 was found to occur mainly *via* Grotthuss mechanism, since the activation energy of the membranes was less than 40 kJ/mol. The low value of the apparent activation energy and high value of the effective proton concentration for SDPNR-*graft*-PS demonstrated that the nanomatrix channel of SDPNR-*graft*-PS contributed to the effective transport of the protons.

It was concluded that the 3D imaging techniques, i.e., TEMT techniques and FIB-SEM, played an important role to relate the nanomatrix structure with not only the mechanical properties but also the proton-conductivity.

Symbol Table

symbol	unit	parameter
A		the effective H^+ concentration
A		surface area of the membranes
a		b/6 b: unit of monomer distance
B		activation energy of H^+
$< d >$		distance between PS nano-particles
d		sample thickness
E*i	Pa	complex modulus of i component
E_{NR}	Pa	values of storage moduli of natural rubber
E_{PS}	Pa	values of storage moduli of PS
G’	Pa	storage modulus (at plateau region)
G’’	Pa	loss modulus (at plateau region)
I	q	intensity
IEC	meq/g	ion exchange capacity
N		molecular weight
N_{NaOH}		normality of NaOH
q		scattering vector
q_{max}		q at the peak top
R		membrane resistance
R		end-to-end distance
R_g		radius of gyration
tanδ		loss tangent (at plateau region)
T_g	wt%	sulfur content
V_2		volume fraction of phase 2
V_{NaOH}		volume of NaOH
W_{dry}	g	weight of the dry membrane
W_{wet}		weight of swollen membrane
γ		shearing starin
λ		parameters relating to the volume fraction
ν	Hz	frequency
σ	MPa	stress
σ_0		σ at T_0,
ϕ		mixing state of materials
ω	s^{-1}	displacement frequency

List of Publications

Chapter 2

1. タンパク質を除去することによる精製天然ゴムの調製
   福原吏奈、宮野快、山本祥正、石井宏幸、河原成元
   高分子論文集 **2015**, 72, No.1,1-6
2. Removal of Proteins from Natural Rubber
   Fukuhara, L.; Miyano, K.; Yamamoto, Y.; Nghia, P. T.; Ishii, H.; Kawahara, S.
   Kautschuk Gummi Kunststoffe **2015**, 3-15, 24-29

Chapter 3

3. Nanomatrix Structure Formed by Graft-copolymerization of Styrene onto Fresh Natural Rubber
   Fukuhara, L.; Kado, N.; T. Thuong, N.; Loykulant, S.; Suchiva, K.; Kosugi, K.; Yamamoto, Y.; Ishii, H.; Kawahara, S.
   Rubber Chem. Technol. **2015**, 88, No. 1, 117-124.

Chapter 4

4. FIB Processing for Natural Rubber with Nanomatrix Structure
   Fukuhara, L.; Kosugi, K.; Yamamoto, Y.; Jinnai, H.; Nishioka, H.; Ishii, H.; Kawahara, S.
   Polymer **2015**, 57, 143-149.

Chapter 5

5. Frozen Non-equilibrium Structure for Anisotropically Deformed Natural Rubber with Nanomatrix Structure Observed by 3D FIB-SEM and TEMT Techniques
   Fukuhara, L.; Kosugi, K.; Yamamoto, Y.; Jinnai, H.; Nishioka, H.; Ishii, H.; Fukuda, M.; Kawahara, S.
   Colloid and Polymer Science, in press

Chapter 6

6. Preparation of Polymer Electrolyte Membrane with Nanomatrix Channel through Sulfonation of Natural Rubber Grafted with Polystyrene
   Fukuhara, L.; Kado, N. ; Kosugi, K.; Suksawad, P. ; Yamamoto, Y.; Ishii, H.; Kawahara, S.
   Solid State Ionics **2014**, 268, Part A, 191–197.

Presentations

1. FIB Processing for Natural Rubber with Nanomatrix Structure
   14th International Seminar on Elastomer, Bratislava, Slovakia, Aug. 24-28th, 2014.

2. FIB Processing for Natural Rubber with Nanomatrix Structure
   11th Fall Rubber Colloquium, Hannover, Germany, Nov. 26-28th, 2014.

3. Nanomatrix Structure of Natural Rubber
   10th SPSJ International Polymer Conference (IPC 2014), Tsukuba, Japan, Dec.3-5th, 2014.

Acknowledgements

This thesis was based on research works which were accomplished under supervisions of Professor Dr. Hiroyuki Ishii of Tokyo National College of Technology, Associate Professor Dr. Yoshimasa Yamamoto of Tokyo National College of Technology and Associate Professor Dr. Seiichi Kawahara of Nagaoka University of Technology

The author would like to thank Professor Hiroyuki Ishii and Associate Professor Yoshimasa Yamamoto of Tokyo National college of Technology for their constant guidance in all phase of this work. The author learned methodology and philosophy in study from them.

The author would like to express her sincere thanks to Associate Professor Seiichi Kawahara of Nagaoka University of Technology for enlightening discussion and his valuable suggestion on rubber chemistry and technology.

The author would like to thank Professor Hiroshi Jinnai of Kyushu University and Professor Masao Fukuda Nagaoka University of Technology for their advices.

Thanks are given to Professor Kazuhisa Maeda and Professor Masashi Shibata of Tokyo University of Technology of Tokyo and Professor Mitsuo Takahashi of National college of Technology for their valuable advice and useful comments.

The author thanks Mr. Masahito Hayashi of Shiseido Co. Ltd. for their advice.

The author would like to thank all laboratory members: particularly, Mr. Kai Miyano of Tokyo National College of Technology and, Dr. Kenichiro Kosugi, Mr. Noriyuki Kado, Dr. Patjaree Suksawad and Ms. Nghiem Thi Thuong of Nagaoka University of Technology for their kind teaching, assistance, collaboration and friendship.

Finally, the author would like to express her hearty gratitude to her parents and her family for their continuous supports and encouragements.

Lina Fukuhra

June, 2015